Overlapping and Distinct Mechanisms of Effective Neoantigen Cancer Vaccines and Immune Checkpoint Therapy

Sunita Keshari[1], Alexander S. Shavkunov[1], Qi Miao[2], Akata Saha[1], Charmelle D. Williams[1], Anna M. Highsmith[1], Josué E. Pineda[1], Elise Alspach[3], Kenneth H. Hu[1,4,5], Kristen E. Pauken[1], Ken Chen[2], Matthew M. Gubin[1,4#]

1. Department of Immunology, The University of Texas MD Anderson Cancer Center, Houston, TX, USA

2. Department of Bioinformatics and Computational Biology, The University of Texas MD Anderson Cancer Center, Houston, TX, USA

3. Department of Molecular Microbiology and Immunology, Saint Louis University School of Medicine, St. Louis, MO, USA

4. The Parker Institute for Cancer Immunotherapy, The University of Texas MD Anderson Cancer Center, Houston, TX, USA

5. The James P. Allison Institute, The University of Texas MD Anderson Cancer Center, Houston, TX, USA

#Corresponding author:

Matthew M. Gubin, PhD
Department of Immunology
The University of Texas MD Anderson Cancer Center
7455 Fannin St., Unit 901
Houston, TX 77054
Phone (713) 713-745-9790
Email mgubin@mdanderson.org

Highlights

- Neoantigen vaccines utilize distinct cellular mechanisms from anti-CTLA-4 or anti-PD-1 immune checkpoint therapy.
- Neoantigen vaccines preferentially induce PD-1+ TCF1+ stem-like and proliferating neoantigen-specific CD8 T cells
- Anti-PD-1 expands PD-1+ TCF-7- NeoAg-specific Teff/Tex, with combination anti-PD-1 + anti-CTLA-4 ICT inducing robust expansion of Bhlhe40hi PD-1+ TCF-7- NeoAg-specific Teff/Tex.
- Anti-CTLA-4 promotes Th1-like ICOS+ Bhlhe40+ CD4 T cells, while combination anti-CTLA-4 and anti-PD-1 ICT induces a small subset of Th2-like CD4 T cells
- Neoantigen vaccines induce partially distinct intratumoral macrophage remodeling from immune checkpoint therapy
- Neoantigen vaccines in combination with anti-CTLA-4 or anti-PD-1 provides enhanced tumor protection equivalent to or even exceeding protection seen with combination anti-CTLA-4 and anti-PD-1

SUMMARY

The goal of therapeutic cancer vaccines and immune checkpoint therapy (ICT) is to eliminate cancer by expanding and/or sustaining intratumoral T cells with enhanced anti-tumor capabilities. However, whether therapeutic cancer vaccination and ICT achieve enhanced anti-tumor immunity by distinct or somewhat overlapping immunological mechanisms remains unclear. Considering increasing interest in combining these two types of treatment to improve efficacy rates, a better understanding of how these treatments are similar and different is needed. Here, we compared effective therapeutic tumor-specific mutant neoantigen (NeoAg) cancer vaccines with anti-PD-1, anti-CTLA-4, or anti-CTLA-4 plus anti-PD-1 combination ICT in preclinical models. We found that both NeoAg vaccines and anti-CTLA-4 and/or anti-PD-1 ICT induced robust expansion of intratumoral NeoAg-specific CD8 T cells, though the degree of

expansion and acquisition of effector activity was more substantial following NeoAg vaccine compared to ICT. Further, we found that NeoAg vaccines are particularly adept at inducing proliferating and stem-like NeoAg-specific CD8 T cells. Additionally, anti-CTLA-4 notably induced ICOS^{+} Th1-like CD4 T cells expressing the transcription factor Bhlhe40 and, interestingly, when combined with anti-PD-1 a small subset of Th2-like CD4 T cells was observed. Conversely, we observed a more divergent effect on certain subsets of intratumoral macrophages induced by NeoAg vaccines as compared to ICT. Although effective NeoAg vaccines or ICT expanded M1-like iNOS^{+} macrophages, NeoAg vaccines expanded rather than suppressed (as observed with ICT) distinct subpopulations of M2-like CX3CR1^{+} CD206^{+} macrophages, associated with the poly I:C adjuvant used in the vaccine. Considering the similarities and difference we identified in how NeoAg vaccines versus ICT reshaped the TME, we hypothesized that combining ICT with NeoAg vaccines would expand the therapeutic window for efficacy in these preclinical models. Indeed, we found the combination NeoAg vaccine plus ICT induced superior anti-tumor control compared to either therapy in isolation, highlighting the utility of combining these modalities to eliminate cancer.

INTRODUCTION:

For cancer immunotherapies such as ICT, T cell recognition of tumor antigens is critical for efficacy[1]. In contrast to aberrantly expressed non-mutant antigens, tumor-specific neoantigens (NeoAgs) formed from somatic alterations in cancer cells are not subject to immune tolerance and are exclusively expressed in cancer cells, making them favorable cancer vaccine targets[2-4]. Significant progress has been made in the field of NeoAg cancer vaccine development, showing promise in early-phase clinical trials[5-11]. Despite this progress, many fundamental questions regarding NeoAg vaccines remain unclear[5,6,10,12], including how to best combine therapeutic vaccines with other T cell-directed therapeutic modalities including ICT to promote optimal outcomes in cancer patients. A more refined understanding of how NeoAg vaccines impact the immune tumor microenvironment (TME) in comparison to other immunotherapies like anti-PD-1 and anti-CTLA-4 ICT can inform rational use of NeoAg vaccines and combinatorial immunotherapies.

To address this, we developed preclinical models to interrogate potential synergies between the mechanisms of action of NeoAg cancer vaccines and ICT. We previously used immunogenomic/mass spectrometry approaches to identify NeoAgs and subsequently demonstrated that therapeutic NeoAg cancer vaccines could provoke tumor rejection in methylcholanthrene (MCA)-induced sarcoma models[4,13]. Others have used similar approaches to identify immunogenic NeoAgs[4,6,7,14-16]. We further showed that NeoAgs are major targets of T cells reactivated by ICT and that anti-PD-1 and anti-CTLA-4 administered either alone or in combination induces changes in both CD4 and CD8 T cells within the TME[13,17-20], consistent with findings from others[21,22]. While both conventional CD4 and CD8 T cells drive immunotherapeutic responses to cancer, cytotoxic CD8 T cells are typically the most potent direct inducers of tumor cell death. In both cancer patients and preclinical models, intratumoral

CD8 T cells that express activation markers including inhibitory receptors such as PD-1, LAG-3, and TIM-3 often exist in a terminally differentiated state and may display a range of functional capabilities from short-lived CD8 T effector cells with potent cytotoxicity and cytokine production to dysfunctional or exhausted CD8 T cells that exist in a state of limited or restrained functional capabilities[23]. These dysfunctional or exhausted CD8 T cells also exist on a spectrum of intermediate to terminally dysfunctional/exhausted with progression to terminally dysfunctional/exhausted characterized by high, sustained expression of inhibitory receptors, reduced function, and unique transcriptional and epigenetic profiles, differentiating them from memory T cells and T cells displaying stem-like properties (often referred to as progenitor/precursor exhausted CD8 T cells). These distinct states are driven by key transcription factors, including TCF-1, which promotes stemness or memory-like attributes[24], and TOX, which plays a crucial role in establishing terminal dysfunction/exhaustion[25-27]. Although TOX is induced in an NFAT-dependent manner upon T cell activation, chronic antigen exposure and/or signals within the TME promote maintenance of NFAT-independent TOX expression and establishment of a fixed epigenetic landscape in terminal dysfunctional/exhausted CD8 T cells[28]. The increased presence of PD-1^{hi} TOX^{+} TCF-1^{-} CD8 T cells in tumor biopsies correlates with a poorer prognosis in patients treated with ICT and these cells likely do not drastically gain effector function following PD-1/PD-L1 blockade. Instead, stem-like PD-1^{+} Tim-3^{-} TCF-1^{+} CD8 T cells within tumors and lymph nodes expand and differentiate into PD-1^{+} Tim-3^{+} CD8 T effector-like cells in response to anti-PD-1/PD-L1 ICT[29,30].

While T cells are the major target of NeoAg vaccines and ICT, myeloid cells are a critical component of the TME[31]. Macrophages are amongst the most abundant myeloid cell population within tumors and may comprise both embryonically-derived tissue-resident macrophages and monocyte-derived macrophages[32-35]. Although macrophages can exhibit anti-

49 tumor effects, macrophages often promote tumor growth. We previously observed major
50 complexity in the ICT-induced changes occurring in the intratumoral macrophage
51 compartment[18-20]. These included remodeling from M2-like CX3CR1$^+$ CD206$^+$ macrophages in
52 progressively growing tumors to M1-like iNOS$^+$ macrophages in tumors that go on to reject in
53 response to ICT. Further, blockade of TREM2 expressed on macrophages using Fc-mutated anti-
54 TREM2 monoclonal antibody (mAb) induced a decline in CX3CR1$^+$ CD206$^+$ macrophages and
55 induced iNOS$^+$ macrophages and subsets of macrophages expressing immunostimulatory
56 molecules, with anti-TREM2 dampening tumor growth and augmenting anti-PD-1 efficacy[36].
57 While tumor immune cell compositions clearly play a major role in response to
58 immunotherapy[33,37], the heterogeneity and dynamics of immune infiltrates in response to
59 immunotherapies such as NeoAg cancer vaccines is not thoroughly characterized. Further,
60 although much progress has been made towards defining the mechanisms behind ICT efficacy,
61 our understanding is still incomplete and direct comparisons between cancer vaccines and
62 different ICTs used alone or in combination are largely lacking.

63 Here, we systematically compared different immunotherapies that lead to tumor
64 rejection, including NeoAg cancer vaccines, anti-PD-1, anti-CTLA-4, and anti-PD-1 + anti-CTLA-4
65 ICT using mouse melanoma models expressing defined NeoAgs. NeoAg vaccines induced robust
66 expansion of polyfunctional NeoAg-specific CD8 T cells, including proliferating and stem-like
67 CD8 T cells. Anti-CTLA-4 and/or anti-PD-1 ICT increased the frequency and effector function of
68 intratumoral NeoAg-specific CD8 T cells, with anti-CTLA-4 containing treatments also
69 dramatically altering the CD4 T cell compartment. Both NeoAg vaccines and ICT resulted in an
70 expansion of M1-like iNOS$^+$ macrophages. Whereas ICT reduced the frequency of intratumoral
71 CX3CR1$^+$ CD206$^+$ M2-like macrophages, NeoAg vaccine treated mice instead displayed a higher
72 frequency of CX3CR1$^+$ CD206$^+$ macrophages. Thus, effective NeoAg cancer vaccines reshape the

TME, leading to overlapping as well as distinct alterations when compared to different ICT treatments. To investigate whether the unique impacts of NeoAg vaccines and ICT combine for enhanced tumor control, we tested the efficacy of NeoAg vaccination in combination with either anti-CTLA-4 or anti-PD-1 and found that the window of therapeutic efficacy was extended by combination treatments, further supporting the rationale of combining NeoAg vaccines with ICT.

RESULTS:

NeoAg vaccines and ICT induce T cell-dependent long-term tumor protection

For this study, we modified the *Braf*^{V600E} *Pten*$^{-/-}$ *Cdkn2a*$^{-/-}$ YUMM1.7 mouse melanoma line to express different combinations of MHC-I and MHC-II NeoAgs[38]. While GEMMs recapitulate many features of human cancers, GEMM-derived tumors generally nonimmunogenic and lack NeoAgs; however, they can be engineered to express NeoAgs to study tumor-immune interactions[19,39-43]. To generate a YUMM1.7 cell line expressing known tumor antigens, we engineered it to express minigenes encoding the G1254V mutation in Laminin subunit alpha 4 (mLama4^{MHC-I}), the A506T mutation in Alpha-1,3-glucosyltransferase (mAlg8^{MHC-I}), and the N710Y mutation in Integrin beta 1 (mItgb1^{MHC-II}) NeoAgs in various combinations **(Figure S1A)**. We generated YUMM1.7 lines expressing minigenes for mLama4^{MHC-I} + mItgb1^{MHC-II} (Y1.7LI) or mAlg8^{MHC-I} + mItgb1^{MHC-II} (Y1.7AI). Consistent with prior observations[38,44], the parental YUMM1.7 melanoma line was insensitive to ICT, even anti-PD-1 and anti-CTLA-4 combination ICT **(Figure S1B)**. In contrast, enforced expression of mLama4^{MHC-I} or mAlg8^{MHC-I} NeoAg along with mItgb1^{MHC-II} NeoAg rendered YUMM1.7 melanoma lines (Y1.7LI and Y1.7AI) sensitive to anti-CTLA-4 ICT **(Figure 1A)**.

96 We next asked whether therapeutic cancer vaccines composed of 10 µg of the SLP
97 containing the minimal MHC-I NeoAg epitope and 50 µg of the adjuvant poly:IC (pI:C) could induce
98 regression of the Y1.7LI and Y1.7AI NeoAg-expressing lines. Tumor bearing mice treated with pI:C
99 alone displayed outgrowth of Y1.7LI or Y1.7AI melanoma, whereas vaccines composed of relevant
100 NeoAg SLP + pI:C (neo VAX) induced complete rejection or delayed outgrowth of both Y1.7 NeoAg
101 expressing variants **(Figure 1B)**. Here the NeoAg vaccine-induced tumor rejection was dependent
102 upon specific NeoAg expression, as vaccinating the Y1.7LI (mLama4-expressing) tumor bearing
103 mice with the mAlg8 SLP + pI:C was not able to lead to tumor rejection and vice versa with the
104 Y1.7AI (mAlg8-expressing) tumors **(Figure 1B)**. Mice that rejected Y1.7AI or Y1.7LI tumors upon
105 anti-CTLA-4 or neo VAX were rechallenged with the same tumors at least 60 days after rejection
106 of primary tumors in the absence of any additional treatment. Upon secondary challenge, no
107 detectable tumor was observed indicating long-term protection against rechallenge with the
108 same tumor line **(Figure S1C)**. In contrast, both Y1.7-NeoAg expressing lines grew out when
109 injected in control naïve WT mice in the absence of treatment, indicating cell line preparations
110 used in rechallenge experiments were capable of tumor formation. Additionally, when mice
111 that previously rejected Y1.7LI tumors in response to anti-CTLA-4 or neo VAX therapy were
112 rechallenged with the YUMM1.7 parental line, progressive tumor growth was observed **(Figure**
113 **S1D)**, indicating that long-term immunity was likely tumor NeoAg-specific.
114 We next used peptide-MHC (pMHC) tetramers to detect intratumoral CD8 T cells
115 recognizing the mLama4 or mAlg8 NeoAg presented on H-2K^b. Tumors from anti-CTLA-4 treated
116 mice contained greater frequencies of mAlg8- or mLama4-specific CD8 T cells compared to the
117 frequency of these cells in tumors from mice receiving control mAb **(Figures 1C and S1E)**. Whereas
118 pI:C alone had little effect on the NeoAg-specific CD8 T cell frequency, neo VAX induced an over 5-
119 fold increase in the frequency of NeoAg-specific CD8 T cells **(Figures 1C and S1E)**. This was

120 particularly notable with the Y1.7LI tumor treated with NeoVAX, where over 14% of CD8 T cells
121 were specific for mLama4. Neo VAX significantly increased the frequency of NeoAg-specific CD8 T
122 cells co-expressing the inhibitory receptors PD-1 and TIM-3 **(Figure S1F)**. Although PD-1 and TIM-3
123 are associated with dysfunction/exhaustion, their co-expression alone does not indicate reduced
124 function and may be indicative of antigen stimulation and T cell activation state[45,46].

125 To expand on these observations, we focused on the Y1.7LI line, delayed treatment
126 initiation until day 7, and evaluated anti-CTLA-4 and/or anti-PD-1. As expected, Y1.7LI tumor
127 bearing mice treated with control mAb or control VAX (irrelevant mAlg8 SLP + pI:C) starting on day
128 7 post-transplant displayed progressive tumor outgrowth **(Figure 1D)**. In contrast, anti-CTLA-4,
129 anti-PD-1, combination anti-PD-1 plus anti-CTLA-4, or neo VAX induced tumor rejection in a
130 majority of mice. ICT- and neo VAX-induced tumor rejection was dependent on both CD4 and CD8
131 T cells, as mAb depletion of either T cell subset completely abolished ICT efficacy **(Figure S2A)**.
132 Mice that rejected Y1.7LI tumors upon anti-PD-1 and/or anti-CTLA-4 or neo VAX initiated on day
133 7 were rechallenged with Y1.7LI at least 60 days after rejection of primary tumors in the
134 absence of any additional treatment. Upon secondary challenge, no detectable tumor was
135 observed under any of the conditions **(Figure S2B)**. In contrast, Y1.7LI grew out when injected in
136 control naïve WT mice in the absence of treatment.

137

138 **scRNAseq analysis of tumor microenvironment remodeling induced by NeoAg vaccines and**
139 **ICT**

140 We next used an unbiased approach to assess whether effective tumor-specific NeoAg
141 vaccines induced TME alterations that are distinct or overlapping with different forms of ICT.
142 Groups of Y1.7LI tumor bearing WT mice were treated with (1) control mAb, (2) anti-CTLA-4, (3)
143 anti-PD-1, (4) anti-CTLA-4 + anti-PD-1, (5) control VAX (irrelevant SLP + pI:C), or (6) neo VAX

144 (mLama4 SLP + pI:C) beginning on day 7 **(Figure 2A)**. Tumors were harvested on day 15 (a critical
145 timepoint prior to tumor rejection during ICT or neo VAX in this model) and live $CD45^+$ cells were
146 sorted and processed for 10X single cell 5' library generation and sequencing for scRNAseq. We
147 performed unsupervised graph-based clustering and noted clusters of myeloid cells and
148 lymphocytes (**Figures 2B and 2C)**. scRNAseq and flow cytometry both indicated that
149 immunotherapy altered the proportions of different myeloid and lymphoid subsets and in some
150 cases these alterations were dependent upon the specific treatment employed **(Figure S3A)**.
151 To gain more insights into how the different immunotherapies altered T cells in the TME,
152 we chose clusters containing activated T cells for subclustering and identified multiple clusters of
153 conventional CD4 and CD8 T cells, $Foxp3^+$ $CD4^+$ T regulatory cells (Tregs), gamma delta T cells (γδT),
154 and innate lymphoid cells (ILCs) **(Figures 2D, S3B-S3D, S4, and S5)**. Specific clusters of CD4 and CD8
155 T cells were annotated based on expression of select transcripts **(Figures 2E, S4, and S5)**. We
156 identified 5 exclusively CD8 T cell clusters, although this analysis did not distinguish their antigen
157 specificity **(Figures 2D, 2E, S4, S5, and S6A-S6F)**. Overall, these clusters of CD8 T cells spanned a
158 range of activation states including proliferating ($Cd8_{Cycling}$), $CD69^{hi}$ IFN stimulated [$Cd8_{iSTIM}$
159 (interferon STIMulated)], PD-1^+ $TCF7^+$ plastic/stem-like or progenitor exhausted ($Cd8_{PE}$), and PD-1^+
160 $TCF7^-$ terminal effectors or dysfunctional/exhausted CD8 T cells ($Cd8_{Eff/Ex}$) **(Figures 2E, S4, S5, and**
161 **S6A-S6F)**.
162
163 **NeoAg vaccines and ICT induce CD8 T cells with proliferative transcriptional signature**
164 While most clusters contained either CD4 or CD8 T cells, cluster $Cd4/8_{cycling}$ contained a mix
165 of Tregs, CD4 T cells, and CD8 T cells and displayed a cell proliferation transcript signature **(Figures**
166 **2D-2F S4 and S5)**. Not only did tumors from neo VAX, anti-PD-1, or anti-CTLA-4 treated mice have
167 a greater frequency of cells within $Cd4/8_{Cycling}$, but the ratio of cycling conventional CD4 and CD8 T

168 cells to Tregs was higher as compared to control mAb or control VAX **(Figures 2G-2K)**. Anti-CTLA-4
169 with or without anti-PD-1 reduced proliferating Tregs and expanded CD4 T cells within Cd4/8$_{Cycling}$,
170 while the ratio of proliferating CD8 T cells to Tregs or CD4 T cells was higher with anti-PD-1.
171 Interestingly, neo VAX contained the greatest ratio of cycling CD8 T cells to other T cells in this
172 cluster.

173 Cd8$_{Cycling}$ also exhibited features of proliferation/cycling but was exclusively composed
174 of CD8 T cells which displayed a more activated phenotype compared to Cd4/8$_{Cycling}$, along with
175 enrichment in gene sets associated with glycolysis, oxidative phosphorylation (OXPHOS), and fatty
176 acid metabolism were enriched as manifested by Gene Set Enrichment Analysis (GSEA) **(Figures S4,**
177 **S5, S6A, and S6B)**. Whereas the percentage of Cd8$_{Cycling}$ cells increased modestly with anti-CTLA-4
178 or anti-PD-1 ICT, neo VAX drove ~2-fold increase in the frequency of cells within this cluster **(Figure**
179 **S6B)**. These results suggest that while either neo VAX or ICT induce proliferating CD8 T cells, neo
180 VAX more robustly expands subsets of proliferating CD8 T cells.

181 Cluster Cd8$_{Eff/Ex}$ displayed little detectable *Tcf7* (encoding TCF-1) expression and elevated
182 transcript expression of multiple inhibitory receptors and other genes associated with T cell
183 activation, effector function, and also exhaustion/dysfunction including *Tox* **(Figures S5, S6A, and**
184 **S6C)**. Cd8$_{PE}$ expressed *Pdcd1* (PD-1), but to less of an extent than Cd8$_{Eff/Ex}$, and additionally
185 expressed *Slamf6* and *Tcf7,* indicating a phenotype consistent with progenitor/precursor
186 exhausted T cells that display plastic/stem-like properties **(Figures S5, S6A, and S6D)**. neo VAX or
187 monotherapy with anti-CTLA-4 or anti-PD-1 reduced the frequency of cells within Cd8$_{Eff/Ex}$ and
188 Cd8$_{PE}$, whereas combination anti-CTLA-4 plus anti-PD-1 stood out as the only treatment to not
189 decrease the frequency of Cd8$_{Eff/Ex}$ **(Figures S6C and S6D)**.

190 Within Cd8$_{Cycling}$, Cd8$_{PE}$, Cd8$_{iSTIM}$, and Cd8$_{Ccr7}$, the highest expression of *Lag3*, *Cd39*, and
191 *Gzmb* within each respective cluster was observed with combination anti-CTLA-4 + anti-PD-1 ICT

192 **(Figures S5, S6A, S6B, and S6D-S6F)**. Additionally, *Prf1* was most robustly induced by combination
193 ICT in all CD8 clusters, except for $Cd8_{Ccr7}$, where neo VAX induced the highest expression **(Figures**
194 **S5 and S6A-S6F)**. Further, a pattern emerged within CD8 T cells whereby in each cluster, anti-CTLA-
195 4 (alone or in combination with anti-PD-1), as well as neo VAX to some extent, drove higher
196 expression of *Cd226* encoding the co-activating receptor CD226/DNAM-1. CD226 counteracting
197 the actions of the inhibitory receptor TIGIT by competing for binding to ligands such as CD155[47].
198 Expression of *Tigit* followed an inverse pattern as *Cd226* with anti-CTLA-4 containing treatments
199 and neo VAX reducing *Tigit* expression within clusters expressing the highest levels of *Tigit*
200 ($Cd8_{Eff/Ex}$, $Cd8_{Cycling}$, $Cd8_{Ccr7}$) **(Figures S5, S6A, S6B, S6C, and S6F)**.
201

202 **Anti-PD-1 expands PD-1^{+} TCF7^{-} NeoAg-specific Teff/Tex, with combination anti-PD-1 + anti-CTLA-**
203 **4 ICT inducing robust expansion of Bhlhe40^{hi} PD-1^{+} TCF7^{-} NeoAg-specific Teff/Tex**

204 We and others have demonstrated that tumor antigen-specific CD8 T cells have unique
205 features as compared to bystander CD8 T cells and that immunotherapy primarily affects tumor
206 antigen-specific versus bulk CD8 T cells[13,17,48-50]. Therefore, we monitored CD8 T cells specific
207 for the mLama4 NeoAg in the setting of neo VAX or ICT **(Figure 3A)**. neo VAX, anti-CTLA-4, anti-
208 PD-1, or combination ICT all increased the overall frequency of intratumoral CD8 T cells **(Figure**
209 **3B)**. Anti-CTLA-4 alone or in combination with anti-PD-1 drove a significant increase in the
210 frequency of mLama4-specific CD8 T cells **(Figures 3C, 3D, and S7A)**. Although anti-PD-1 did not
211 alter mLama4-specific CD8 T cells as a percentage of CD8 T cells **(Figures 3C and S7A)**, mLama4-
212 specific CD8 T cells were significantly increased with anti-PD-1 when analyzed as a percentage
213 of CD45^{+} cells **(Figure 3D)**. Notably, neo VAX drove the greatest increase in mLama4-specific
214 CD8 T cells from less than 2% of CD8 T cells in control mAb or control VAX to over 20% in mice
215 treated with neo VAX, which corresponds to over 4% of all intratumoral CD45^{+} cells in mice

treated with neo VAX **(Figures 3C, 3D, and S7A)**. Since the scRNAseq profiling of intratumoral CD45^{+} cells did not distinguish NeoAg-specific CD8 T cells from other CD8 T cells, we profiled NeoAg-specific CD8 T cells by sorting intratumoral mLama4 tetramer positive CD8 T cells from mice treated with control mAb, anti-CTLA-4, anti-PD-1, anti-CTLA-4 plus anti-PD-1, control VAX, or neo VAX **(Figure 3E)**. We profiled between 937 to 1762 mLama4-specific CD8 T cells for each of the different ICT treatment conditions and 4459, 6723, and 7646 mLama4-specific CD8 T cells for control mAb, control VAX, and neo VAX, respectively. The two smallest clusters contained contaminating stromal cells, with the remaining clusters expressing transcripts consistent with CD8 T cells (**Figure 3F, 3G, S7B, S7C, and S8**). Apart from these two small clusters, this analysis uncovered multiple clusters of NeoAg-specific CD8 T cells that enabled us to distinguish features that were not evident when profiling bulk CD8 T cells.

Clusters nAg.Cd8$_{Eff/Ex}$ and nAg.Bhlhe40^{Hi}Cd8 both highly expressed *Pdcd1, Havcr2, Lag3, Tigit,* and *Ccl5* as well as effector transcripts (*Nkg7*, *Gzmb*, *Gzmk*, *Prf1, Cxcr6*) and *Tox* and exhibited little to no detectable expression of *Tcf7* **(Figures 3G-3I, 4A, S7B and S7C)**. neo VAX most notably reduced the proportion of nAg.Cd8$_{Eff/Ex}$ cells, whereas the proportion of cells in this cluster increased with anti-PD-1 alone or in combination with anti-CTLA-4 **(Figure 4B)**. The top defining marker of cluster nAg.Bhlhe40^{Hi}Cd8 was *Bhlhe40* **(Figures 3G, 3H, and S8)**, which we previously demonstrated was upregulated in tumor-specific T cells and required for CD4 and/or CD8 T cell effector function and response to ICT[20]. In addition to *Bhlhe40* (as well as *Pdcd1, Havcr2,* and *Lag3*) this cluster also expressed other transcripts induced by TCR activation, including *Ctla4, Cd69,* as well as *Nr4a1* (Nur77) and *Nr4a3* suggesting recent activation and/or TCR stimulation **(Figures 3H, 4A, and S7B)**. nAg.Bhlhe40^{Hi}Cd8 displayed the highest expression of *Tbx21* and *Ifng* amongst all the mLama4-specific CD8 T cell**s (Figure S7B)**. As compared to control mAb treatment, all other conditions (including control VAX) displayed a higher frequency of cells within this cluster, with the

240 frequency of nAg.Bhlhe40^{Hi}Cd8 increased from 2.4% of mLama4-specific CD8 T cells under control
241 mAb conditions to 6.2% under anti-PD-1 treatment conditions **(Figure 4B)**. Strikingly, anti-CTLA-4
242 and anti-PD-1 combination ICT increased this cluster to over 28% of mLama4-specific CD8 T cells.
243

244 **Anti-CTLA-4 alone or in combination with anti-PD-1 reduces expression of *Tox* and inhibitory**
245 **receptors and promotes *Il7r* expression in PD-1^{+} TCF7^{-} Teff/Tex NeoAg-specific CD8 T cells**

246 In addition to increasing the frequency of cells within PD-1^{+} TCF7^{-} Teff/Tex clusters
247 (nAg.Cd8$_{Eff/Ex}$ and nAg.Bhlhe40^{Hi}Cd8), combination ICT increased expression of *Bhlhe40, Fasl, Il7r,*
248 *Icos,* and *Cd28*, while decreasing *Tox*, *Pdcd1, Lag3, Entpd1,* and *Tigit* expression within both of
249 these clusters **(Figures 4A, S7B, and S7C)**. Further, combination ICT decreased expression on
250 *Havcr2* and increased expression of *Cd69* within nAg.Bhlhe40^{Hi}Cd8. While some of the features
251 observed in combination ICT were distinct from either anti-CTLA-4 or anti-PD-1, within both these
252 clusters the decrease in *Tox*, *Pdcd1, Lag3, Entpd1,* and *Tigit* (and *Havcr2* in nAg.Bhlhe40^{Hi}Cd8) with
253 combination ICT was also observed with anti-CTLA-4 ICT (but not with anti-PD-1) **(Figures 4A, S7B,**
254 **and S7C)**, suggesting that these specific changes included by combination therapy were primarily
255 driven by anti-CTLA-4. In contrast, increased expression of *Bhlhe40* was most prominently
256 observed in the presence of anti-PD-1. Other features (e.g., increased *Icos*, *Cd28,* and *Fasl*
257 expression) were unique to the anti-CTLA-4 and anti-PD-1 combination ICT treatment conditions.
258

259 **NeoAg vaccination preferentially increases NeoAg-specific stem-like PD-1^{+} TCF7^{+} CD8 T cells and**
260 **proliferating NeoAg-specific CD8 T cells**

261 Amongst the most prominent NeoAg vaccine-driven features observed, NeoAg vaccines
262 drove an over 3-fold increase in the frequency of mLama4-specific CD8 T cells within cluster
263 nAg.PD-1^{+} TCF7^{+} Cd8 as compared to control mAb and over 8-fold increase as compared to control

264 VAX **(Figure 4B)**. Cluster nAg.PD-1^{+} TCF7^{+} Cd8 displayed high expression of *Slamf6* and *Pdcd1*
265 amongst others; low to moderate expression of *Ifng*, *Gzmk*, *Prf1*, and *Cd226*; and no detectable
266 expression of *Havcr2* (TIM-3) or *Entpd1* (CD39) **(Figures 3G, 3H, 4A, and S7B)**. nAg.PD-1^{+} TCF7^{+} Cd8
267 also expressed transcripts encoding molecules related to T cell homing such as *Ccr7*, as well as
268 *Bach2*[51] and *Tcf7*. These features are consistent with CD8 T cells with plastic or stem-like
269 properties or progenitor exhausted CD8 T cells. While NeoAg vaccines promoted this population,
270 the proportion of NeoAg-specific CD8 T cells within this cluster was largely unchanged with anti-
271 CTLA-4, reduced slightly with anti-PD-1, and even further reduced with combination anti-CTLA-4
272 and anti-PD-1 **(Figure 4B)**. Anti-CTLA-4 containing treatments displayed decreased expression of
273 *Pdcd1*, *Lag3*, *Tigit* and increased expression of transcripts encoding molecules related to T cell
274 quiescence and homing such as *S1pr1, Sell* (Cd62l), and *Klf2*, as well as the IL-7 receptor transcript
275 *Il7r* **(Figures 4A, S7B, and S7C)**.
276 We annotated 5 clusters of NeoAg-specific CD8 T cells as "cycling". NeoAg vaccination
277 increased the frequency of cells in all 5 cycling NeoAg-specific CD8 T cell clusters displaying a
278 range of activation states and proliferation signatures **(Figures 4A, S7B, S7C, and S8)**. Each of the 5
279 cycling clusters also displayed a greater frequency of cells under control VAX conditions as
280 compared to control mAb **(Figure 4B)**. This suggests that although far more NeoAg-specific CD8 T
281 cells are observed within tumors treated with neo VAX as compared to control VAX **(Figures 3C**
282 **and 3D)**, within NeoAg-specific CD8 T cells, pI:C contained in both control VAX and neo VAX likely
283 promotes cycling of tumor-specific CD8 T cells. These 5 cycling clusters together represented
284 20.9% of all mLama4-specific CD8 T cells under control mAb treatment, 54.1% under control
285 VAX treatment, and 61.3% under neo VAX treatment **(Figure 4C)**. Within nAg.Cd8$_{Cycling}$_1,
286 nAg.Cd8$_{Cycling}$_2, and nAg.Cd8$_{Cycling}$_6, either control VAX or neo VAX increased the frequency of
287 NeoAg-specific CD8 T cells to about the same level **(Figure 4B)**. In contrast, nAg.Cd8$_{Cycling}$_3

288 represented 10.6% of NeoAg-specific CD8 T cells under control VAX conditions, whereas under
289 neo VAX conditions, the frequency of cells within this cluster increased to 19.2% of NeoAg-
290 specific CD8 T cells **(Figure 4B)**. As compared to the other cycling clusters, nAg.Cd8$_{Cycling}$_3
291 expressed higher *Xcl1*, *Tnfrsf4* (OX40), *Tnfrsf9* (4-1BB), *Prf1*, and *Ifng* **(Figures 4A, S7B and S8)**.
292 The frequency of total cells within cycling clusters was modestly increased by anti-CTLA-4 or
293 anti-PD-1 ICT, whereas anti-CTLA-4 plus anti-PD-1 combination ICT decreased the frequency by
294 almost half.
295

296 **NeoAg vaccines induce robust expansion of NeoAg-specific IFN-γ$^+$ CD8 T cells expressing PD-1**
297 **and LAG-3 and/or TIM-3**

298 Since we noted that mice treated with neo VAX displayed a greater frequency of PD-1$^+$
299 TIM-3$^+$ NeoAg-specific CD8 T cells as compared to other treatments when treatment was initiated
300 on d. 3 post-tumor transplant **(Figure S1F)**, we assessed surface expression of PD-1, TIM-3, and
301 additionally LAG-3 on intratumoral mLama4 NeoAg-specific CD8 T cells from mice when treatment
302 initiation occurred on d. 7 post-transplant (as in our scRNAseq experiments). As expected, a
303 majority of NeoAg-specific CD8 T cells expressed PD-1, with similar frequencies of PD-1$^+$ TIM-3$^+$ or
304 PD-1$^+$ LAG-3$^+$ NeoAg-specific CD8 T cells observed between control mAb, control VAX, and the
305 different ICT treatment conditions **(Figure 4D)**. However, the expression level of PD-1, TIM-3, and
306 LAG-3 on a per cell basis was lower in ICT treated groups. In contrast, a dramatic increase in the
307 percentage of PD-1$^+$ TIM-3$^+$ or PD-1$^+$ LAG-3$^+$ mLama4-specific CD8 T cells was observed in mice
308 treated with neo VAX and amongst PD-1$^+$, TIM-3$^+$, or LAG-3$^+$ NeoAg-specific CD8 T cells, PD-1, TIM-
309 3, and LAG-3, respectively, was expressed higher in the neo VAX treated group (**Figure 4D**). These
310 results were consistent with the discordance between effective NeoAg vaccines and ICT in PD-1
311 and TIM-3 surface expression on NeoAg-specific CD8 T cells observed when treatment was

312 initiated on day 3 **(Figure S1F)**. Intracellular cytokine staining (ICS) on isolated intratumoral CD8 T
313 cells restimulated with the mLama4 NeoAg peptide revealed anti-CTLA-4 increased the frequency
314 of IFN-γ^+ or TNFα^+ CD8 T cells, while neo VAX induced the greatest expansion of more than 5-fold
315 of IFN-γ^+ or TNFα^+ CD8 T cells **(Figures 4E and 4F)**. Amongst IFN-γ^+ CD8 T cells, expression of IFN-γ
316 on a per cell basis increased significantly with anti-CTLA-4 and/or anti-PD-1, with the most robust
317 increase occurring in mLama4 NeoAg-stimulated IFN-γ^+ CD8 T cells isolated from neo VAX treated
318 mice **(Figure 4E)**.
319
320 **Anti-CTLA-4 promotes IFNγ^+ Th1-like CD4 T cells expressing ICOS and Bhlhe40, while**
321 **combination anti-CTLA-4 and anti-PD-1 ICT induces a small subset of Th2-like CD4 T cells**
322 Since we observed that neo VAX or anti-CTLA-4/anti-PD-1 ICT required not only CD8 T cells,
323 but also CD4 T cells for efficacy **(Figure S2A)**, we examined CD4 T cells from our scRNAseq
324 performed on sorted CD45$^+$ cells **(Figure 2A)**. Conventional CD4 T cells and Tregs were significantly
325 altered by anti-CTLA-4, with anti-CTLA-4 inducing a higher frequency of CD4 T cells and reducing
326 the percentage of Tregs as assessed by both scRNAseq and flow cytometry (**Figures 2G-2I, 2K, S3A,**
327 **and S3B)**. Anti-CTLA-4 (+/- anti-PD-1) induced notable increases in proliferating CD4 T cells and a
328 decrease in proliferating Tregs within cluster Cd8/4$_{Cycling}$ **(Figures 2H, 2I, and 2K)**, further indicating
329 that anti-CTLA-4 containing treatments dramatically affect the intratumoral CD4 T cell
330 compartment. Most notably, anti-CTLA-4 (+/- anti-PD-1) induced subpopulations of Th1-like cells
331 expressing *Ifng* and *Bhlhe40*, including cluster ICOS^{hi} Bhlhe40^{hi} CD4$_{\mathbf{Th1}}$ that also highly expressed
332 *Icos* **(Figures 2E, 5A, 5B, S5 and S9A)**. ICOS^{hi} Bhlhe40^{hi} CD4$_{\mathbf{Th1}}$ expressed transcripts indicative of
333 highly activated T cells including high expression of *Pdcd1*, *Ctla4*, and the *Furin* transcript encoding
334 a proprotein convertase, whose expression is regulated by TCR signaling and IL-12 signaling
335 through STAT4[52] **(Figures 5A, S4, and S5**). This cluster also expressed *Cxcr6*, *Csf2*, *Fasl*, and *Tnfaip3*,

336 which encodes the A20 protein that regulates TCR/CD28-mediated NF-κB activation and TCR-
337 mediated survival[53] **(Figure S5)**. ICOS^{hi} Bhlhe40^{hi} CD4$_{\mathbf{Th1}}$ displayed enrichment in IL-2 STAT5 and IL-6
338 JAK STAT3 signaling, TNFa signaling via NF-κB, and IFN-γ response gene sets amongst others
339 **(Figure S9A)**. neo VAX also exhibited a greater frequency of cells within this cluster as compared to
340 control VAX **(Figure 5B)**. Bhlhe40^{+} Cd4$_{\mathbf{Th1}}$_a also expressed *Icos* and *Bhlhe40*, but to less of an
341 extent than ICOS^{hi} Bhlhe40^{hi} CD4$_{\mathbf{Th1}}$ (**Figures 5A and S5**). Bhlhe40^{+} Cd4$_{\mathbf{Th1}}$_a was further
342 distinguished from ICOS^{hi} Bhlhe40^{hi} CD4$_{\mathbf{Th1}}$ by lower *Csf2, Runx3, Tnfaip3, Cxcr6*, *Furin*, *Pdcd1,*
343 *Havcr2*, and *Lag3* expression and higher *Tbx21* (Tbet) expression. Anti-CTLA-4 dramatically
344 increased the frequency of Bhlhe40^{+} CD4$_{Th1}$_a, with anti-PD-1 also increasing cells within this
345 cluster **(Figure 5B)**. Likewise, neo VAX increased the frequency of Bhlhe40^{+} Cd4$_{Th1}$_a cells but to
346 much less of an extent **(Figure 5B)**. Although both clusters expressed glycolytic enzyme transcripts,
347 greater expression of several of these transcripts was seen in ICOS^{hi} Bhlhe40^{hi} CD4$_{Th1}$, while
348 Bhlhe40^{+} Cd4$_{Th1}$_a displayed gene set enrichment in Fatty Acid Metabolism **(Figures S5, S9A, and**
349 **S9B)**. Additionally, both clusters displayed significant enrichment in TGF beta signaling gene sets
350 **(Figures S9A and S9B)**. Cluster Bhlhe40^{+} CD4$_{Th1}$_b was the smallest cluster of Th1-like cells and
351 exhibited high *Ifng*, *Pdcd1*, *Tigit*, *Havcr2,* and *Lag3* expression **(Figures 5A, S5, and S9C)**. This
352 cluster also expressed the lowest level of *Icos* and the highest level of *Tox* amongst all CD4 clusters
353 **(Figures 5A and S5)**. While only subtle changes to the frequency of cells within this cluster were
354 seen with treatments apart from control VAX and combination anti-CTLA-4 and anti-PD-1, with the
355 latter displaying the highest frequency of cells within this cluster amongst all groups **(Figure 5B)**.
356 Amongst all treatment conditions, mice treated with anti-CTLA-4 alone or in combination
357 with anti-PD-1 displayed the highest expression of *Bhlhe40* and least expression of *Tnfrsf18* (*GITR*)
358 **(Figures 5A, S5, S9A-S9E, and S9G)**. As observed within CD8 T cell clusters, within multiple CD4

clusters, anti-CTLA-4 alone or in combination drove an increase in *Cd226* expression and a decrease in *Tigit* expression, with neo VAX also following this same pattern but to less of an extent.

The increase in IFN-γ expressing Th1-like cells most prominently induced by anti-CTLA-4 was reflected by ICS on isolated intratumoral CD4 T cells restimulated *ex vivo* with the mItgb1 MHC-II NeoAg peptide. Anti-CTLA-4 +/- anti-PD-1 induced the most dramatic increase in both the overall frequency of conventional CD4 T cells, with anti-CTLA-4 and/or anti-PD-1 increasing the frequency of IFN-γ^+ CD4 T cells upon restimulation with mItgb1 peptide **(Figures 5C and 5D)**. This is in contrast to neo VAX, where only subtle changes were observed. Altogether, these findings indicate that while mice treated with anti-CTLA-4, alone or in combination with anti-PD-1, display the most dramatic increase in IFN-γ-producing Th1-like CD4 T cells within the tumor, anti-PD-1 also provokes IFN-γ^+ CD4 T cells **(Figure 5D)**. This is supported by comparing the expression of *Ifng* transcript within *Ifng*$^+$ CD4 T cells clusters, where anti-PD-1 induced increased *Ifng* expression in these clusters, even those whose frequency was unaltered by anti-PD-1 (i.e., ICOS^{hi} Bhlhe40^{hi} Cd4$_{\mathbf{Th1}}$, Bhlhe40$^+$ Cd4$_{\mathbf{Th1}}$_b, Cd4$_{Tfh}$) (**Figures 5A, S5, and S9A-S9D**).

Interestingly, combination ICT induced a small population of cells found in Cd4$_{Th2}$, which also expressed *Icos* and *Bhlhe40*, but unlike the other ICOS$^+$ Bhlhe40$^+$ clusters the transcripts for *Ifng, Tim3,* and *Lag3* transcript were barely detectable **(Figures 5A, S5, and S9E)**. Amongst CD4 clusters, Cd4$_{Th2}$ expressed the highest level of *Cxcr6*, as well as *Tnfaip3* **(Figure S5)**. In addition to low *Ifng* expression, many cells within Cd4$_{Th2}$ expressed *Gata3*, *Il4*, *Il5*, and *Il13,* indicative of a Th2-like cluster (**Figures 5A, S5, and S9F**). Although cluster Cd4$_{Th2}$ expressed Th2 cytokine transcripts and *Gata3*, both Cd4$_{Th2}$ and ICOS^{hi} Bhlhe40^{hi} CD4$_{Th1}$ highly expressed *Furin* and *Bhlhe40* **(Figures 5A and S5).** ICOS^{hi} Bhlhe40^{hi} CD4$_{Th1}$ also displayed enrichment in TNFa signaling via NFkB and IFN-γ response gene sets, along with Kras signaling up, whereas Cd4$_{Th2}$ displayed enrichment in Kras signaling down **(Figures S9A and S9E)**.

To gain insight into the temporal dynamics of the observed changes in CD4 T cells, we used Monocle to analyze scRNAseq data[54]. Monocle suggested that the starting point for conventional CD4 T cells corresponds to cells within either the $Cd4_{Naive/Mem}$ cluster (expressing *Tcf7, Il7r,* and *S1pr1*, indicative of naïve or memory phenotype) or CD4 T cells within the $Cd4/8_{Cycling}$ cluster **(Figure 5E)** with $Cd4_{Tfh}$ connecting $Cd4/8_{Cycling}$ CD4 T cells to the main trajectory towards $Cd4_{Naive/Mem}$ and the branch to more activated, polarized CD4 T cells. Notably, a pseudotime trajectory branch point occurs whereby activated CD4 T cells occupy Th1-like $ICOS^{hi}Bhlhe40^{hi}Cd4_{Th1}$ driven by anti-CTLA-4 (+/- anti-PD-1) (and to a lesser extent by neo VAX) or encounter another branch whereby they assume one of two fates: they either become Th1-like CD4 T cells within $Bhlhe40^{+}Cd4_{Th1}$_a or become Th2-like $Cd4_{Th2}$, with $Bhlhe40^{+}$ $Cd4_{Th1}$_a being induced by anti-CTLA-4 and/or anti-PD-1 or neo VAX and $Cd4_{Th2}$ primarily being driven by combination anti-CTLA-4 + anti-PD-1.

Features of intratumoral Treg subpopulations during NeoAg vaccine or ICT treatment

We also identified three CD4 $Foxp3^{+}$ Treg clusters **(Figures S3B)**. Treg_1 and Treg_3 appeared to be the most activated with Treg_3 expressing the highest level of *Ctla4*, *Havcr2*, and *Klrg1* **(Figure S5)**. Mice treated with anti-CTLA-4 alone or in combination with anti-PD-1 experienced a decrease in frequency of Treg_1 and Treg_3 **(Figures S3B)**, which is consistent with previous results that the anti-CTLA-4 mAb we used (mouse IgG2b; clone 9D9) partially depletes Tregs, especially those highly expressing CTLA-4[55]. Treg_2 expressed lower amounts of *Ctla4, Havcr2, Tigit*, and *Klrg1* with the frequency of these Tregs not being affected by anti-CTLA-4, whereas anti-PD-1 with or without anti-CTLA-4, control VAX, or neo VAX displaying a greater frequency of cells in this cluster **(Figure S3B)**. As compared to control VAX, the cellular density of Treg_1 and Treg_2 decreased in tumors from mice treated with neo VAX **(Figures S3B)**. Further,

407 transcript expression of *Foxp3* in Treg_2 was lower in the neo VAX group **(Figure S3B)**. These
408 alterations to the overall frequency of Tregs most prominently observed in the presence of anti-
409 CTLA-4 are also corroborated by flow cytometry analysis **(Figure S3A)**.
410

411 **Intratumoral myeloid cell compartment during NeoAg vaccines or ICT treatment**

412 We first noted that neutrophils represented a small proportion of the overall immune
413 infiltrate as more reliably shown by flow cytometry **(Figures 2B and S3A)**. Consistent with previous
414 observations in sarcoma models[18], anti-CTLA-4 (+/- anti-PD-1) increased the proportion of
415 neutrophils to just under 1.5% of $CD45^+$ intratumoral cells **(Figure S3A)**. To comprehensively
416 characterize the signatures of intratumoral macrophages and DCs, we subclustered the myeloid
417 component excluding the single neutrophil cluster **(Figure S10A)**. In addition to a cluster of
418 plasmacytoid DCs (pDCs), four other DC clusters were identified ($CD103^+$ cDC1, $CD63^+$ $Ccr7^+$ cDC,
419 $Ccr7^+$ cDC, and $Mgl2^+$ DC) **(Figures S10A-S10G)**. Cluster $CD103^+$ cDC1 expressed multiple classical
420 DC (cDC) 1 transcripts including *Itgae* (*Cd103*), *Xcr1*, and *Clec9a* **(Figures S10A and S10B)**. $CD63^+$
421 $Ccr7^+$ cDC and $Ccr7^+$ cDC expressed *Ccr7*, *Cd1d1*, *Cd200*, *Fscn1*, *Cd274* (PD-L1), and *Pdcd1lg2* (PD-
422 L2). These two migratory cDC clusters are likely composed of mregDCs, which describes a
423 maturation state of cDC1s and cDC2s upon uptake of tumor antigen and although they express
424 immunoregulatory molecules, they are not necessarily immunosuppressive[56,57] **(Figures S10B,**
425 **S10D and S10E)**. $CD63^+$ $Ccr7^+$ cDC expressed higher *Cd63, Cd40, Cd70,* and *Btla* as compared to
426 $Ccr7^+$ cDC **(Figures S10B and S10D)**.
427

428 **Distinct Macrophage Remodeling Induced by NeoAg Vaccines and ICT**

429 We observed multiple intratumoral monocyte/macrophage clusters in Y1.7LI displaying a
430 range of phenotypic states[58,59] (**Figures 6A, 6B, and S11**). $Ccr2^+$ M_c1 displayed transcripts

431 consistent with monocytes, including *Ccr2* and *Chil3*, and the frequency of cells within this cluster
432 only increased slightly with anti-PD-1 or neo VAX **(Figures 6B, 6C, and S11)**. *Chil3*$^{+}$ monocytes were
433 previously shown to be reduced by a NeoAg vaccine in preclinical models[60]; however, the NeoAg
434 vaccine and adjuvant used in that setting differed from ours.

435 We previously demonstrated that anti-CTLA-4 and/or anti-PD-1 induces macrophage TME
436 remodeling characterized by a reduction in M2-like macrophages co-expressing the fractalkine
437 receptor (CX3CR1) and the CD206 pattern recognition receptor and an increase in M1-like iNOS^{+}
438 macrophages in mouse MCA sarcoma models[18,20]. We noted a similar ICT-induced remodeling
439 trend in the Y1.7LI melanoma model. Whereas a slight decrease in the frequency of CX3CR1^{+}
440 CD206^{hi} M_c2 cells expressing high levels of *Cx3cr1*, *Mrc1 (Cd206)*, *Trem2*, *Vcam1*, *Cd63,* and
441 *Cd72* was observed with anti-CTLA-4 and/or anti-PD-1 ICT, expression of *Cx3cr1* and frequency of
442 *Cx3cr1*$^{+}$ macrophages within this cluster was notably decreased under all ICT treatment conditions
443 **(Figures 6B-6D)**. The frequency of cells expressing *Cx3cr1* within this cluster under control VAX
444 treatment was equal to or higher than with control mAb **(Figure 6D)**. neo VAX reduced the
445 proportion of cells within this cluster expressing *Cx3cr1* **(Figure 6D)**. CX3CR1^{+} CD206^{+} M_c3 also
446 expressed *Cx3cr1*, as well as *Mrc1* (*Cd206*), *Trem2*, *Vcam1*, and *Cd72* with the latter transcripts
447 being expressed less than in CX3CR1^{+} CD206^{hi} M_c2. CX3CR1^{+} CD206^{+} M_c3 also displayed a cell
448 proliferation transcript signature that included high expression of *Mki67* and exhibited lower
449 *Mertk* expression as compared to CX3CR1^{+} CD206^{hi} M_c2 **(Figure 6B)**. Anti-CTLA-4 alone reduced
450 the frequency of CX3CR1^{+} CD206^{+} M_c3 **(Figures 6C and 6D)**. Although the aforementioned two
451 clusters expressed the highest levels of *Cx3cr1* and *Mrc1*, M_c8 and M_c9 macrophages also
452 expressed *Cx3cr1* and *Mrc1* under control mAb conditions with ICT reducing expression of *Cx3cr1*
453 within these clusters **(Figures 6B and 6D)**. Comparable expression levels of *Cx3cr1* was observed in
454 M_c8 under control VAX and neo VAX conditions, with neo VAX increasing the frequency of cells

455 within this cluster **(Figures 6B, 6C, and 6D)**. Under either control VAX or neo VAX conditions,
456 M_c11 expressed both *Cx3cr1* and *Mrc1* and the frequency of cells within this cluster dramatically
457 increased in mice treated with either control VAX or neo VAX, with ICT reducing this population
458 **(Figures 6B-6D)**. Overall, cells within all monocyte/macrophage clusters from mice treated with
459 control VAX and neo VAX displayed higher expression of *Cx3cr1* as compared to ICT groups, with
460 neo VAX also displaying similar expression of *Mrc1* as control mAb **(Figure 6E)**.

461 Several monocyte/macrophage clusters expressed high levels of *Nos2* (iNOS); other
462 clusters expressed varying levels of *Nos2*, with expression of *Nos2* being highly correlated with ICT
463 treatment as well as neo VAX, but to less of an extent **(Figures 6B and 6F)**. Further, expression of
464 *Cd274* (PD-L1) also correlated with expression of *Nos2* within macrophage clusters, in particular
465 under ICT treatment conditions **(Figure 6B)**. While the overall frequency of these iNOS^{+} M1-like
466 clusters often only modestly increased with ICT, the frequency of cells within these clusters
467 expressing *Nos2* and/or *Nos2* expression on a per cell basis dramatically increased under all ICT
468 conditions **(Figures 6B, 6C, and 6F)**. Nos2^{hi}M_c4 and Nos2^{hi} M_c6 both manifested high expression
469 of *Nos2*, *Il1a*, *Il1b*, *Cxcl2*, *Inhba,* and *Nfkb1,* signatures of inflammatory macrophages[61] **(Figure 6B)**.
470 While Nos2^{hi}M_c4 displayed classic features of M1-like macrophages including low *Mrc1*
471 expression, Nos2^{hi} M_c6 moderately expressed *Mrc1* as well as higher *F13a1, Trem2,* and *Il1a*[58,62],
472 along with lower *Il1r2* compared to Nos2^{hi}M_c4 **(Figure 6B)**. Nos2^{hi}M_c4 displayed high expression
473 of *Cxcl9* and *Spp1*, with expression of the latter diminished with ICT or neo VAX. Higher expression
474 of *CXCL9* and lower *SPP1* expression was found to be correlated with macrophage prognostic
475 score in cancer patients[63]. Nos2^{hi}M_c5 highly expressed *Nos2* in the presence of ICT, with ICT also
476 increasing the frequency of macrophages within this cluster (**Figures 6B, 6C, and 6F**). This cluster
477 also expressed moderate levels of *Mki67* and other cell cycle related transcripts, indicative of
478 iNOS^{+} macrophages with proliferative capabilities **(Figure 6B)**. Nos2^{hi} M_c7 was the smallest iNOS^{+}

479 macrophage cluster and in addition to *Nos2* expression, displayed highest expression of interferon-
480 stimulated genes (ISGs) and also expressed high levels of *Cxcl9*, *Cxcl10*, *Cd274*, *Cd72*, *Cd81,* and
481 *Ms4a4c* **(Figures 6B and 6F)**. Although M_c8 and M_c9 expressed modest levels of *Cx3cr1* under
482 control mAb conditions, its expression was reduced by ICT along with induction of *Nos2* expression
483 within these clusters **(Figures 6B, 6D, and 6F)**. These same overall patterns were manifested at the
484 protein level where in anti-CTLA-4 and/or anti-PD-1 treated mice, the frequency of intratumoral
485 CX3CR1$^+$ CD206$^+$ macrophages decreased with a concomitant increase in iNOS$^+$ macrophages
486 induced by ICT **(Figures 6G and 6H)**. In contrast, while neo VAX treated mice also displayed a
487 greater frequency of iNOS$^+$ macrophages, CX3CR1$^+$ CD206$^+$ macrophages were only slightly
488 reduced by neo VAX as compared to control VAX, but nonetheless were maintained at a similar
489 frequency as seen in control mAb treated mice **(Figures 6F and 6G)**. Since the frequency of
490 CX3CR1$^+$ CD206$^+$ macrophages in both control VAX and neo VAX treated mice were similar or even
491 greater than in control mAb treated mice, induction or maintenance of this macrophage
492 subpopulation was likely linked to the pI:C adjuvant used in both control Vax and neo VAX. These
493 results reveal that despite a relatively a similar abundance of M2-like CX3CR1$^+$ CD206$^+$
494 macrophages that were previously associated with progressively growing tumors in untreated or
495 control mAb treated mice[18,20], tumors in mice treated with neo VAX regress equivalently to ICT
496 treated mice.
497

498 **ICT Broadens Therapeutic Window for Neoantigen Vaccines**

499 We noted changes that were not only shared between treatment conditions, but also
500 distinct depending upon which treatment strategy was employed. Principle Component
501 Analysis (PCA) further illustrated that neo VAX induces distinct changes to the immune TME as
502 compared to anti-CTLA-4 and/or anti-PD-1 **(Figure S12)**. This, together with our findings that

503 neo VAX induces robust expansion of NeoAg-specific CD8 T cells that produce IFN-γ and appear
504 functional, yet highly express PD-1/TIM-3/LAG-3 **(Figures 3C, 3D, 4D, 4E, and S7A)**, prompted us
505 to asked whether neo VAX could synergize with ICT. While neo VAX or ICT led to robust
506 rejection of Y1.7LI when initiated on d. 7 post-transplant, a majority of tumor bearing mice
507 displayed tumor outgrowth when treatment with anti-CTLA-4, anti-PD-1, or neo VAX was
508 initiated on d. 12 post-transplant. We therefore used a d. 12 treatment start timepoint to
509 assess whether combining neo VAX with anti-CTLA-4 or anti-PD-1 improved efficacy **(Figure 7A)**.
510 Mice treated with neo VAX in combination with anti-CTLA-4 or anti-PD-1 displayed enhanced
511 tumor control as compared to control VAX (irrelevant SLP + pI:C) + anti-PD-1 or control VAX +
512 anti-CTLA-4 **(Figure 7A)**. Further, neo VAX used in combination with anti-CTLA-4 or anti-PD-1
513 provided superior tumor growth inhibition compared to combination anti-CTLA-4 and anti-PD-1
514 ICT. To extend our findings to a distinct tumor model, we assessed our vaccine protocol and
515 combination treatment using the MC38 tumor model, which has several known endogenous
516 MHC-I tumor NeoAgs[16,64,65]. Since it has been reported that expression of these NeoAgs varies
517 depending on the source of the MC38 cell line, we previously confirmed in our MC38 line the
518 presence of point mutations that form NeoAgs (mAdpgk, mRpl18, and mDpagt1)[16,64]. We
519 assessed combinatorial treatments in MC38 tumor bearing mice by choosing an injection dose
520 of cells (see Methods) and treatment schedule where monotherapy with anti-CTLA-4, anti-PD-1,
521 or neo VAX alone is largely ineffective **(Figure 7B)**. PBS, control VAX, or neo VAX was
522 administered to MC38 tumor bearing mice on d. 12 and 19 post-transplant with or without anti-
523 CTLA-4 or anti-PD-1 given on d. 12, 15, 18, and 22. Similar to results in the Y1.7LI model, neo
524 VAX in combination with anti-CTLA-4 or anti-PD-1 provided superior protection versus
525 monotherapy **(Figure 7B)**. These findings in two distinct models complement ongoing NeoAg
526 vaccine clinical trials and further support the rationale for combination NeoAg-based therapies.

527

528 **Discussion**

529 In this study, we compared different immunotherapies that lead to tumor rejection (NeoAg
530 SLP vaccines, anti-CTLA-4, anti-PD-1, anti-CTLA-4 + anti-PD-1, or NeoAg SLP cancer vaccines) and
531 pertinent control treatments where tumor progression occurs using mouse melanoma models
532 expressing defined NeoAgs and melanoma-relevant gain-of-function and loss-of-function genetic
533 perturbations[38]. Although prior studies have examined NeoAg vaccines[60], few (if any) studies
534 have performed extensive comparisons between anti-PD-1, anti-CTLA-4, combination ICT, and
535 NeoAg vaccines in the same robust experimental system. Further, while the focus of most prior
536 studies involving ICT or NeoAg vaccines was on either lymphoid or myeloid cells[21,66], our work
537 has provided insights into both categories of cells and how different immunotherapies
538 differentially affect these cells within the TME. Our treatment schedule and analyses were
539 initially performed so that the NeoAg cancer vaccines or ICT we used lead to complete tumor
540 rejection in a majority of mice; thus, we could compare and contrast the molecular and cellular
541 changes that occur as a consequence of NeoAg vaccines or different forms of ICT and link them to
542 outcomes. We specifically chose to study an SLP NeoAg vaccine as SLP vaccines are highly relevant
543 with many clinical trials employing SLPs usually in combination with the adjuvant polyIC:LC
544 vaccines are being conducted[7,9,67].

545 The current study makes several key observations. First, NeoAg vaccines and ICT work by
546 several overlapping mechanisms related to the CD8 T cell response, with key differences in the
547 overall magnitude of the response and phenotype of NeoAg-specific CD8 T cells observed. NeoAg
548 vaccines induce the greatest expansion of functional intratumoral NeoAg-specific CD8 T cells
549 including proliferating T cells and PD-1^{+} TCF-1^{+} stem-like CD8 T cells and require not only CD8 T
550 cells, but also CD4 T cells for efficacy. However, anti-CTLA-4 and/or anti-PD-1 also increased the

551 frequency of intratumoral CD8 T cells, including NeoAg-specific CD8 T cells with enhanced
552 production of IFN-γ. Anti-PD-1 alone, or most dramatically when administered in combination with
553 anti-CTLA-4 ICT, induced a subset of Bhlhe40^{hi} NeoAg-specific CD8 T cells also display high
554 expression of *Tbx21* and *Ifng.* Additionally, this subset expressed *Ctla4, Cd69,* as well as *Nr4a1*
555 (Nur77) and *Nr4a3,* which suggest recent activation and/or TCR stimulation due to their known
556 pattern of rapid and transient expression following T cell stimulation. Interestingly, a recent study
557 identified Bhlhe40 as modulating a key differentiation point between progenitor and intermediate
558 subsets of exhausted T cells in an in vitro exhaustion model and chronic LCMV infection[68]. While
559 some of the features observed with combination ICT were distinct from either anti-CTLA-4 or anti-
560 PD-1, the decrease in *Tox*, *Pdcd1, Lag3, Havcr2, Entpd1,* and *Tigit* with combination ICT was also
561 observed with anti-CTLA-4 ICT, whereas the increased expression of Bhlhe40 within several
562 NeoAg-specific CD8 T cell subsets was often more akin to the level of increase observed with anti-
563 PD-1. These findings add to the accumulating evidence that the enhanced anti-tumor activity of
564 combination anti-CTLA-4 and anti-PD-1 ICT is likely mediated by not only additive effects, but also
565 through mechanisms distinct from the monotherapies[18,22]. In addition to modulating the CD8 T cell
566 compartment, ICT notably impacted the CD4 T cell compartment as well. Anti-CTLA-4 reduced the
567 frequency of Tregs and induced ICOS^{+} Th1-like conventional CD4 T cells displaying high expression
568 of Bhlhe40, a transcription factor that we previously documented regulates T cell effector function
569 during ICT[20]. Interestingly, subsets of Th1-like CD4 T cells with high expression of Bhlhe40 were
570 previously found to be enriched in patients with microsatellite instability (MSI) colorectal cancer,
571 who display favorable outcomes in response to anti-CTLA-4[69-71]. Further, studies in both preclinical
572 models and human melanoma patients have revealed that anti-CTLA-4 induces ICOS^{+} CD4 T cells
573 expressing IFN-γ[70,72]. Anti-PD-1 also increased the frequency of overall IFN-γ^{+} Th1-like CD4 T cells,
574 but to less of an extent as compared to anti-CTLA-4. Combination anti-CTLA-4 and anti-PD-1 ICT

575 induced a small, but significant subpopulation of Th2-like CD4 T cells ($Cd4_{Th2}$) expressing *Il4*, *Il13*,
576 *Gata3*.

577 While vaccines targeting MHC-I NeoAgs predominately affected CD8 T cells, we found that
578 these MHC-I NeoAg vaccines require CD4 T cells for efficacy. In MHC-II positive tumors, cytotoxic
579 CD4 T cells have been show to directly kill tumor cells[73]; however, even with tumors lacking MHC-II
580 expression, CD4 T cells are often required for anti-tumor immunity[19,42,74]. The importance of CD4 T
581 cells may be due to their ability to produce cytokines such as IFN-γ and IL-2 and also likely stems
582 from their ability to and their ability to be primed by cDC1s presenting tumor antigens and their
583 CD40-dependent licensing of cDC1s that is critical for priming and activation of CD8 T cells[75,76].
584 Further, CD4 T cell reprogramming of the myeloid compartment towards IFN-activated, iNOS-
585 expressing tumoricidal and antigen-presenting phenotypes has also been implicated in tumor
586 destruction[77,78]. The detailed mechanisms regarding the contribution of CD4 T cells in NeoAg
587 vaccines targeting MHC-I NeoAgs remains to be fully elucidated by future studies and may entail
588 multiple functions of CD4 T cells within both the lymph nodes and tumor. Although MHC-II NeoAgs
589 are critical components of anti-tumor immunity, we specifically chose to utilize an SLP vaccine
590 against a single MHC-I NeoAg in order to definitively link the MHC-I NeoAg vaccine to specific
591 defined NeoAgs. Further, since MHC-II NeoAgs are more difficult to predict than MHC-I NeoAgs,
592 we wanted to study the effects of an MHC-I NeoAg vaccine and whether this NeoAg vaccine
593 approach in combination with anti-CTLA-4 or anti-PD-1 ICT could provoke rejection of larger,
594 established tumors. SLPs offer several advantages over short peptides including the ability to
595 specifically target professional APCs, stability, and the capacity to provoke both CD4 and CD8 T
596 cells responses[79-81]; however, most immunogenic NeoAgs are either MHC-I or MHC-II NeoAgs,
597 even when using SLPs. In our study, the SLP NeoAgs (mAlg8 or mLama4) provoked only NeoAg-
598 specific CD8 T cell responses. Recent work revealed that physically linked MHC-I and MHC-II SLP

599 vaccines provoked tumor growth inhibition in a preclinical squamous cell tumor model[82].
600 Determining whether incorporating an MHC-II NeoAg such as mItgb1 or even a shared, non-
601 mutant antigen will enhance the efficacy of MHC-I NeoAg vaccines in our models is of future
602 interest.

603 Beyond the T cell compartment, we noted a more divergent impact of NeoAg vaccines on
604 the myeloid compartment than ICT. Both ICT and neo VAX increased M1-like iNOS$^+$ macrophages,
605 while ICT exclusively reduced the frequency of intratumoral CX3CR1$^+$ CD206$^+$ M2-like
606 macrophages. Although less than in control VAX (irrelevant SLP + pI:C) treated mice, neo VAX
607 (NeoAg SLP + pI:C) treated mice displayed a greater frequency of CX3CR1$^+$ CD206$^+$ macrophages as
608 compared to control mAb or ICT treated mice. The detailed mechanisms by which control VAX
609 and NeoAg vaccines induce CX3CR1$^+$ CD206$^+$ macrophages and the ability of NeoAg vaccines to
610 provoke tumor regression in an environment that is partially distinct from that exhibited with
611 ICT is yet to be fully delineated. In MCA sarcoma models, we previously found that intratumoral
612 macrophage subpopulations displayed the spectrum of activation states ranging from an M2-
613 like CX3CR1$^+$ CD206$^+$ phenotype in progressively growing tumors to a proinflammatory iNOS$^+$
614 phenotype in tumors that will reject in response to ICT[18], consistent with findings herein.
615 Whereas induction of iNOS$^+$ macrophages was dependent upon IFN-γ, ICT-driven depletion of
616 CX3CR1$^+$ CD206$^+$ macrophages was partially independent of IFN-γ[18]. In our vaccine setting, we
617 hypothesize that neo VAX comprising MHC-I NeoAg SLP and p:IC favors the induction of T cell-
618 derived IFN-γ and other signals that drives monocyte polarization to iNOS$^+$ macrophages upon
619 entering the tumor, but other signals promote expansion or induction of CX3CR1$^+$ CD206$^+$
620 macrophages as well. These details of these signals are yet unknown but are likely induced by
621 the pI:C (contained in both the control VAX and neo VAX), which acts as a TLR3 agonist in the
622 endosome to potently induce a type I IFN response and can also activate RIG-I/MDA-5 in the

623 cytosol to promote IL-12 production[83,84]. Although we and others use the term "M1-like" and
624 "M2-like" to describe features that at least partially overlap with M1 or 'classically' activated
625 and M2 or 'alternatively' activated macrophages, this is an oversimplification due to the
626 complexity of activation and functional states of intratumoral macrophages[58]. Further, it is also
627 important to note that although CX3CR1^{+} CD206^{+} macrophages display expression patterns
628 consistent with immunosuppressive macrophages, CD206 alone is not sufficient to distinguish
629 macrophages as immunosuppressive[59], as we observed CD206 expression on some
630 macrophages expressing iNOS. Nevertheless, it is tempting to speculate that combining NeoAg
631 vaccines that maintain or promote CX3CR1^{+} CD206^{+} macrophages expressing high levels of
632 *Trem2* with treatments targeting this macrophage population might enhance the efficacy of
633 NeoAg vaccines.

634 Lastly, in both the Y1.7LI melanoma model and MC38 model, neo VAX combined with
635 either anti-CTLA-4 or anti-PD-1 enhanced anti-tumor efficacy. Our rationale for assessing these
636 combinations resulted from our observation that while some of the changes induced by neo VAX,
637 as well as by ICT overlapped, distinct alterations were also noted. The unique features of each
638 immunotherapy therefore prompted us to assess combining anti-CTLA-4 or anti-PD-1 with neo
639 VAX and comparing efficacy to monotherapy or combination anti-CTLA-4 and anti-PD-1 ICT. We
640 now find that combining anti-CTLA-4 or anti-PD-1 with neo VAX leads to better anti-tumor immune
641 responses than even combination anti-CTLA-4 and anti-PD-1. While up to 20-30% of patients
642 treated with anti-CTLA-4 or anti-PD-1 may experience durable cancer control, ~50% of
643 metastatic melanoma patients treated with the combination of anti-CTLA-4 plus anti-PD-1
644 experience durable cancer control; however, immune related adverse events remain a
645 problem[85,86]. As NeoAg vaccines have demonstrated favorable safety profiles thus far,
646 combining NeoAg vaccines with single agent ICT may yield robust anti-tumor immunity with less

toxicity than anti-CTLA-4 and anti-PD-1 combination ICT. While we find that anti-CTLA-4 or anti-PD-1 can synergize with neo VAX in different tumor models when we give the first NeoAg vaccine and ICT mAb at the same time, the timing of treatment may impact the response in different settings, as it has been shown that blockade of PD-1 in sub-primed CD8 T cells provokes PD-1^{+} CD38^{+} T cells that contribute to resistance to anti-PD-1 in other models and vaccine settings[87]. Although our approach of targeting a single NeoAg has revealed important insights, it is likely that targeting multiple NeoAgs and possibly even shared, non-mutant antigens will be required in patients due to tumor heterogeneity and therapy induced-immunoediting, with at least some of the antigens targeted by the vaccine needing to be clonal NeoAgs[88,89].

This study provides key insights into the transcriptional, molecular, and functional changes that occur within major immune cell populations within the TME following different forms of cancer immunotherapy and compliments ongoing human clinical studies of NeoAg vaccines. Although we did not fully elaborate on every specific immune cell population we profiled, our analyses were designed to interrogate the entire immune TME, and thus our study should additionally provide an important resource. Therefore, the myeloid and lymphoid cell subsets and potential biomarkers we have described herein should inform the development of improved personalized NeoAg vaccines and combinatorial therapies in human patients.

STAR Methods

Key resources Table S1

Mice

All mice used were on a C57BL/6 background. WT C57BL/6J mice were purchased from Jackson Labs. All *in vivo* experiments used 8- to 12-week-old male or female mice (to match the sex and strain of the tumors). All mice were housed in a specific pathogen-free animal facility. All animal studies were performed in accordance with, and with the approval of the Institutional Animal Care and Use Committee (IACUC) of The University of Texas MD Anderson Cancer Center (Houston, TX).

Plasmids

Gene blocks for mAlg8, mItgb1, or mLama4 were purchased from Integrated DNA Technologies. Minigene constructs were cloned into the BglII site of pMSCV-IRES GFP (mAlg8 and mItgb1) or pMSCV (mLama4 and mItgb1) using the Gibson Assembly method (New England Biolabs). To generate neoantigen-expressing Y1.7 melanoma cell lines, constructs were transiently transfected into Phoenix Eco cells using Fugene (Promega). After 48 hours, viral supernatants were filtered and subsequently used for transfection of Y1.7 melanoma cell line. Y1.7 mLama4 $^{MHC\text{-}I}$.mItgb1 $^{MHC\text{-}II}$ (Y1.7LI) and Y1.7 mAlg8 $^{MHC\text{-}I}$.mItgb1 $^{MHC\text{-}II}$ (Y1.7AI) were sorted based on GFP positivity and clones were verified for neoantigen expression.

Tumor cell lines

The *Braf*^{V600E} *Cdkn2a*$^{-/-}$ *Pten*$^{-/-}$ YUMM1.7 parental line was originally generated in a male GEMM on the C57BL/6 background as described[38]. Parental YUMM1.7 was purchased from ATCC (CRL-

3362) and was modified to generate NeoAg-expressing Y1.7 lines. The MC38 line was obtained from B. Schreiber (Washington University in St. Louis School of Medicine). All tumor cell lines were found to be free of common mouse pathogens and Mycoplasma as assessed by IDEXX IMPACT I mouse pathogen testing [PCR evaluation for: Corynebacterium bovis, Corynebacterium sp. (HAC2), Ectromelia, EDIM, Hantaan, K virus, LCMV, LDEV, MAV1, MAV2, mCMV, MHV, MNV, MPV, MTV, MVM, Mycoplasma pulmonis, Mycoplasma sp., Polyoma, PVM, REO3, Sendai, TMEV]. Tumor cell lines from the same cryopreserved stocks that were used in this study tested negative for Mycoplasma and were authenticated and found to be free of non-mouse cells as assessed by mouse cell STR profiling (IDEXX CellCheck mouse 19 plus Mycoplasma spp. testing).

Tumor transplantation

The *Braf*^{V600E} *Cdkn2a*$^{-/-}$ *Pten*$^{-/-}$ YUMM1.7 parental melanoma line, Y1.7LI or Y1.7AI melanoma line, and the MC38 colorectal cancer line cells were propagated in R-10 plus BME media [RPMI media (HyClone) supplemented with 1% l-glutamine, 1% penicillin–streptomycin, 1% sodium pyruvate, 0.5% sodium bicarbonate, 0.1% 2-mercaptoethanol, and 10% heat-inactivated fetal calf serum (FCS) (HyClone) upon thawing, tumor lines were passaged 3 to 6 times before experimental use. Prior to injection, cells were washed extensively, resuspended at a concentration of 0.5×10^6 cells (for YUMM1.7, Y1.7LI, and Y1.7AI) or 1.5×10^6 cells (for MC38) in 150 µL of endotoxin-free PBS and 150 µL was injected subcutaneously into the flanks of recipient mice. Tumor cells were >90% viable at the time of injection as assessed by Trypan blue exclusion. Tumor growth was quantified by caliper measurements and expressed as the average of two perpendicular diameters. Lack of survival was defined as mouse death or mean tumor diameter size of 15 mm.

Tumor rechallenge

For tumor rechallenge, mice that rejected primary tumors after treatment with anti-CTLA-4, anti-PD-1, anti-CTLA-4 + anti-PD-1, or NeoAg vaccines were then rechallenged with same number of cells used in primary challenge with either the same tumor line used in the primary tumor challenge or a different tumor line as indicated at least 60 days after complete rejection of the primary tumor.

***In vivo* antibody treatments**

For ICT treatment, YUMM1.7 parental, Y1.7LI, or Y1.7AI tumor-bearing mice were treated intraperitoneally with 200 µg of anti-CTLA-4 and/or anti-PD-1 on d. 3, 6, 9, 12, 18, and 22 or d. 7, 10, 13, 16, 22, and 28; or d. 12, 15, 18, 21, 27 and 33 post-tumor transplant. For controls, mice were injected with 200 µg of IgG2a isotype control antibodies. MC38 tumor-bearing mice were treated intraperitoneally with 200 µg of anti-CTLA-4 and/or anti-PD-1 on d. 12, 15, 18, and 22 post-transplant. For antibody depletion studies, 250 µg of control mAb, anti-CD4, or anti-CD8a was injected intraperitoneally into mice at d. −1 and every 7 days thereafter until day 20. CD4 and CD8 depletion was verified by flow cytometry analysis of surface-stained peripheral blood monocytes (PBMC) and intratumoral immune cells. For *in vivo* experiments, "*In vivo* Platinum"-grade antibodies that were verified to be free of mouse pathogens (IDEXX IMPACT I mouse pathogen testing) were purchased from Leinco Technologies: anti-PD-1 (rat IgG2a clone RMP1–14), anti-CTLA-4 (murine IgG2b clone 9D9), anti-CD4 (rat IgG2b clone GK1.5), anti-CD8a (rat IgG2b clone YTS169.4), and isotype controls (rat IgG2a clone 1–1, mouse IgG2a clone OKT3, or rat IgG2b clone 1–2).

Peptides

Mutant Lama4 8-mer (VGFNFRTL), mutant Lama4 SLP (QKISFFDGFEVGFNFRTLQPNGLLFYYT), mutant Adpgk SLP (HLELASMTNMELMSSIVHQ), mutant Rpl18 SLP (KAGGKILTFDRLALESPK), mutant Dpagt1 SLP (EAGQSLVISASIIVFNLLELEGDYR), mutant Alg8 8-mer (ITYTWTRL), OVA-$I_{257–264}$ (SIINFEKL), mutant Itgb1 SLP (DDCWFYFTYSVNGYNEAIVHVVETPDCP), and OVA-$II_{323–339}$ (ISQAVHAAHAEINEAGR) peptides were custom ordered from Peptide 2.0. All peptides were HPLC purified to >95% purity.

Vaccination

Y1.7LI or Y1.7AI tumor bearing male mice were vaccinated subcutaneously with 10 µg mLama4 or mAlg8 synthetic long peptide (SLP) in combination with 50 µg of VacciGrade™ high molecular weight Polyinosinic-polycytidylic acid (pI:C) (InvivoGen) in a total volume of 150 µL diluted in endotoxin-free PBS on d. 3, 9, and 15 or d. 7, 13, and 19 or on d. 12, 18, and 24 post tumor transplant. MC38 tumor bearing female mice were vaccinated subcutaneously with 20 µg of mAdpgk SLP plus 20 µg of mRpl18 SLP plus 20 µg of mDpagt1 plus 50 µg pI:C adjuvant or control vaccine composed of 40 µg of irrelevant HPV SLP + 50 µg of pI:C on d. 12 and 19 post-tumor transplant. For SLP, peptide sequence used for mLama4; QKISFFDGFEVGFNFRTLQPNGLLFYYT (epitope underlined), for mAlg8; AVGITYTWTRLYASVLTGSLV (epitope underlined), for mAdpgk; HLELASMTNMELMSSIVHQ, for mRpl18; KAGGKILTFD***R***LALESPK and for mDpagt1; EAGQSLVISASIIVFNLLELEGDYR. mLama4 SLP served as a relevant SLP for the Y1.7LI line and an irrelevant SLP for the Y1.7AI line. mAlg8 served as a relevant SLP for the Y1.7AI line and an irrelevant SLP for the Y1.7LI tumor.

766 **Tetramers**

767 OVA-I (SIINFEKL)-H-2K^b (irrelevant control tetramer), mutant Alg8-H-2K^b, and mutant Lama4-H-2K^b

768 tetramers conjugated to PE or APC fluorophores, were obtained from the Baylor College of

769 Medicine MHC Tetramer Production Facility.

770

771 **Tumor and spleen harvest**

772 Established tumors were excised from mice, minced, and treated with 1 mg/mL type IA

773 collagenase (Sigma-Aldrich) in HBSS (Hyclone) for 45 minutes at 37°C. Cells were washed thrice.

774 Red blood cells were lysed using ACK lysis buffer (Gibco). To remove aggregates and clumps, cells

775 were passed through a 40-µm strainer. Spleens were harvested, crushed, and vigorously

776 resuspended to make single-cell suspensions. To remove aggregates and clumps, cells were passed

777 through a 70-µm strainer and subsequently through a 40-µm strainer.

778

779 **TIL peptide restimulation**

780 For peptide and PMA/ionomycin T-cell stimulation, cells from tumors, isolated as described above

781 (see tumor and spleen harvest section), stained, and CD4 and CD8 T cells were sorted. For sorting

782 CD4 and CD8 T cells, tumor cells were stained for 5 min at room temperature with 500 ng of Fc

783 block (anti-CD16/32) and then stained with antibodies to CD45, CD3ε, CD4 or CD8α and Zombie

784 NIR Viability dye in 100 µl of staining buffer. Cells were incubated for 30 minutes at 4°C. Live

785 CD45$^+$Cd3ε$^+$CD4$^+$ and live CD45$^+$Cd3ε$^+$CD8α$^+$ were then sorted on a BD FACSAria II (BD

786 Biosciences). Splenocytes harvested from naive mice and 100,000 splenocytes were then pulsed

787 with 1 µM of various 8- or 9- or 17- or 28-mer peptides or simulated with 10 ng/mL of PMA

788 (MilliporeSigma) and 1 µg/mL of ionomycin (Fisher) and 100,000 CD4 or CD8 TIL were

789 subsequently added and incubated at 37 °C. Naive splenocytes added with or without CD4 or CD8

790 TIL, was included as control. After 1 h, BD GolgiPlug (BD Bioscience) was added in, and cells were
791 incubated for an additional 5 h at 37 °C.
792
793 **Tetramer staining**
794 For tetramer staining, cells were stained for 5 min at room temperature with 500 ng of Fc block
795 (anti-CD16/32). H-2K^b tetramers conjugated to PE (1:50) or APC (1:100) for mutated Alg8, mutated
796 Lama4, or SIINFEKL were added to cells and incubated for 20 min at 37°C. Tetramer-stained cells
797 were further stained with surface antibody for anti-CD45, anti-Thy1.2, anti-CD8α, anti-CD4, anti-
798 PD-1, anti-TIM-3, and anti-LAG-3 antibody for 20 min at 4 °C.
799
800 **Flow cytometry**
801 For flow cytometry, cells were stained for 5 minutes at room temperature with rat anti-mouse
802 CD16/32 (mouse BD Fc Block; clone 2.4G2, BD Biosciences) at 1 µg/million cells and then surface
803 stained with flow antibodies for 20 minutes at 4°C. Surface antibodies were diluted in FACS
804 staining buffer (PBS with 2% FCS, 2 mmol/L EDTA, and 0.05% NaN3; Sigma). Anti-mouse CD45-
805 BV605, CD90.2/Thy1.2-PE-Cy7, anti-mouse CD8α-BV786, anti-mouse CD4-BV711, anti-mouse
806 CD19-BV650, anti-mouse CD20-BV421, anti-mouse CD45R/B220-BBUV395, anti-mouse
807 Nkp46/CD335-FITC, anti-mouse γδ TCR-PE-Cy7, anti-mouse PD-1-BV421, anti-mouse TIM-3, anti-
808 mouse LAG-3-PerCP-Cy5.5, anti-mouse CD3ε-APC , anti-mouse CD64-BV421, anti-mouse Ly6G-
809 Alexa Fluor 700, anti-mouse CX3CR1-FITC, anti-mouse I-A/I-E-BV650, anti-mouse CD103-BV421,
810 anti-mouse CD24-BV711, anti-mouse CD11c-BV786, anti-mouse CD11b-APC, anti-mouse F4/80-
811 BUV395, anti-mouse CD64-APC, CD117-FITC, anti-mouse CD11b- PerCP-Cy5.5 , anti-mouse PDCA-
812 1/BST-2 BV650, anti-mouse CD172a APC, anti-mouse PDL1-PE, anti-mouse FcεRI-PE-Cy7 were

used for surface staining at the indicated dilutions. Zombie NIR Viability dye was added at 1:500 during surface staining.

For intracellular staining, surface-stained cells were fixed and permeabilized with Fixation/Permeabilization Solution Kit (BD Bioscience). Fixed and permeabilized cells were then stained with anti-mouse Mrc1 (CD206)-PE-Cy7 and anti-mouse iNOS/NOS2-PE for 30 minutes at 4°C.

For FOXP3 staining, surface-stained cells were fixed and permeabilized using the eBioscience FOXP3/Transcription Factor Staining Buffer Set. Fixed and permeabilized cells were then stained with anti-mouse FOXP3-FITC for 30 minutes at 4°C.

For intracellular cytokine staining of lymphocytes, tumor cells were isolated and CD4 and CD8 T cells were sorted and added to peptide pulsed or PMA+Ionomycin stimulated splenocytes and incubated at 37°C for 6 hours with GolgiStop (BD Bioscience). Cells were then washed and stained for 5 minutes at room temperature with Fc block at 1 µg/million cells and then surface stained for 30 minutes at 4°C, and then fixed and permeabilized with BD Fixation and Permeabilization Kit. Fixed and permeabilized cells were then stained with anti-mouse IFNγ-APC, anti-mouse TNF-PE-Cy7 and anti-mouse Granzyme B-PE for 30 minutes at 4°C. All flow cytometry was performed on an BD Fortessa X-20, BD LSR, BD Fortessa, and analyzed using FlowJo software. Gating strategy used is depicted in **Figure S13**.

scRNAseq

Antibody hashing

For analysis of NeoAg-specific CD8 T cells, cell and nuclei labeling were performed according to an adapted BioLegend cell hashing protocol (TotalSeq™-C Antibodies and Cell Hashing with 10x Single Cell 5' Reagent Kit v1.1 Protocol, BioLegend). Briefly, single cell suspensions of harvested

tumors from treated mice were resuspended in BioLegend Cell Staining Buffer containing Fc receptor block and stained with mLama4 PE and APC labelled tetramers for 20 min at 37°C. Tetramer-stained cells from control mAb, control VAX, and neo VAX treatment conditions were immediately surface stained by adding anti-CD90.2/Thy1.2-PE-Cy7 and anti-CD8a-BV786 antibodies and incubating for 20 min at 4°C. Tetramer-stained samples from anti-CTLA-4, anti-PD-1, and anti-CTLA-4 plus anti-PD-1 treated groups were incubated with mixture of surface stain (anti-CD90.2/Thy1.2-PE-Cy7 and anti-CD8a-BV786 antibodies) and barcoded antibodies with unique hashtags for each treatment condition [anti-CTLA-4: Hashtag 1 Total Seq™-C0301 anti-mouse Hashtag 1 Antibody; anti-PD-1: Hashtag 2 (Total Seq™-C0302 anti-mouse Hashtag 2 Antibody); anti-CTLA-4 + anti-PD-1 combination: Hashtag 3 (Total Seq™-C0303 anti-mouse Hashtag 3 Antibody)]. Hashtag antibodies were used at a concentration of 1 µg per 2 million cells. Staining with surface antibodies and hashtag antibodies was done for 30 min at 4°C. Cells were then washed 3X with BioLegend Cell Staining Buffer. Sorted mLama4 tetramer-specific CD8 T cells with unique hashtags (anti-CTLA-4, anti-PD-1, and anti-CTLA-4 + anti-PD-1 samples) were pooled for single-cell library generation and CITE-seq (cellular indexing of transcriptomes and epitopes by sequencing) through multiplexing. Separate libraries were generated for control mAb, control VAX, and neo VAX samples and, thus, these were not multiplexed.

scRNAseq library generation

Droplet-based 5′ end massively parallel scRNAseq was performed by encapsulating sorted live $CD45^+$ tumor-infiltrating cells into droplets and libraries were prepared using Chromium Next GEM Single-cell 5′ Reagent Kit v2 (10x Genomics) according to manufacturer's protocol. The generated scRNAseq libraries were sequenced using an Illumina NovaSeq6000 S2 flow cell.

scRNAseq alignment, barcode assignment, and unique molecular identifier counting

The Cell Ranger Single-Cell Software Suite available at https://support.10xgenomics.com/single-cell-gene-expression/software/overview/welcome was used to perform sample demultiplexing, barcode processing, and single-cell 5 counting. Cellranger mkfastq was used to demultiplex raw base call files from the NovaSeq6000 sequencer, into sample-specific fastq files. Files were demultiplexed with 81.9% to 97.1% perfect barcode match, and 90%+ q30 reads. Afterward, fastq files for each sample were processed with Cellranger count, which was used to align samples to mm10 genome, filtered, and quantified. For each sample, the recovered cells' parameter was specified as 10,000 cells that we expected to recover for each individual library.

Preprocessing analysis with Seurat package

The Seurat pipeline was applied to each dataset following tutorial specifications from https://satijalab.org/seurat/articles/archive; version 3.2 and https://hbctraining.github.io/scRNA-seq_online/. Data from all groups were merged into a single Seurat object, and integration was performed using the reciprocal principal component analysis (PCA) workflow to identify integration anchors. After integration, genes that were expressed in fewer than 3 cells and cells that contained fewer than 500 transcripts (unique molecular identifiers; UMI) were excluded. Cells with more than 10%) of mitochondrial transcripts were also excluded from analysis. The cutoffs used were set based on the characteristics of the cell population in each dataset. Data were normalized using LogNormalize method (counts for each cell divided by the total counts for that cell, multiplied by the scale factor of 10^4 and natural-log transformed using log1p). PCA was performed on about 4,000 genes with PCA function. A uniform manifold approximation and projection (UMAP) dimensional reduction was performed on the scaled matrix (with most variable genes only) using the first 30 PCA components to obtain a two-dimensional representation of the

cell states. For clustering, we used the function FindClusters that implements SNN (shared nearest neighbor) modularity optimization–based clustering algorithm on 30 PCA components, leading to 33 clusters.

Identification of cluster-specific genes and marker-based classification

To identify marker genes, the FindAllMarkers function was used with likelihood-ratio test for single-cell gene expression. To characterize clusters, we used ImmGen database. For heatmap representation, mean expression of markers inside each cluster was used. To compare gene expression for the clusters inside cohorts (e.g., T cells, macrophages) we used FindMarkers function to calculate average log2 fold change and identify differentially expressed genes between each pair of experimental conditions using a Wilcoxon rank-sum test for calculating P values and Bonferroni correction for Padj values.

T cell population analysis

To gain more insights into different immunotherapies-induced T cells remodeling in the TME, we subclustered activated T cells (excluding quiescent T cell clusters 10 and 12). Identification of most variable genes, PCA, UMAP, clustering, and marker selection analysis were performed as described above.

Gene set enrichment analysis (GSEA)

To identify if MSigDB hallmark gene sets are up-regulated or down-regulated between clusters and treatments, we performed gene set enrichment analysis. Fold-changes of gene expression between comparisons were calculated using Seurat R package v.4.3.0.1, and normalized

enrichment scores as well as p-values of given gene sets were then estimated using the gage R package v.2.46.1.

Pseudo time trajectory analysis

To determine the potential lineage differentiation within CD4 T cell subpopulations, we used the Monocle3 R package to construct CD4 differentiation trajectories after specifying the corresponding cells as root nodes. Subsequently, graph test was used to find the pseudo time trajectory difference genes, and the obtained genes were used to plot the heat map.

Statistical analysis

Samples were compared using an unpaired, two-tailed Student t test, two-way ANOVA, or log-rank (Mantel–Cox) test unless specified otherwise.

Data and software availability

Data files for the sequencing data reported in this article will be deposited in the Gene Expression Omnibus (GEO) database and made publicly available at the time of publication. Software used in this study is available online: current version of Cell Ranger: https://support.10xgenomics.com/single-cell-gene-expression/software/downloads/latest; Seurat 4.0: https://satijalab.org/seurat/; ggplot2 3.3.3: https://ggplot2.tidy verse.org/index.html; and ImmGen: https://www.immgen.org. All other data generated in this study are available within the article and its Supplementary Data files, will be provided upon request at the time of publication, and/or will made publicly available at the time of publication via deposition in appropriate databases.

Authors' Contributions

S. Keshari: Conceptualization, data curation, investigation, visualization, methodology, data analysis, writing–original draft, writing–review and editing. A.S. Shavkunov: Conceptualization, data curation, investigation, data analysis, writing–review and editing. Q. Miao: Conceptualization, data curation, investigation, visualization, data analysis, writing–review and editing. A. Saha: Data curation, investigation, visualization, writing–review and editing. C.D. Williams: data curation, investigation, visualization, writing–review and editing. A.M. Highsmith: data curation, investigation, visualization, writing–review and editing. J.E. Pineda: data curation, investigation, visualization, writing–review and editing. E. Alspach: Resources, formal analysis, investigation, visualization, writing–review and editing. K. Hu: Formal analysis, investigation, visualization, writing–review and editing. K.E. Pauken: Formal analysis, investigation, visualization, writing–review and editing. K. Chen: Resources, formal analysis, investigation, visualization, writing–review and editing. M.M. Gubin: Conceptualization, resources, data curation, formal analysis, supervision, validation, investigation, methodology, writing–original draft, writing–review and editing.

Acknowledgements

S. Keshari was a Balzan Postdoctoral Research Fellow supported by The International Balzan Prize Foundation. M.M. Gubin is a Cancer Prevention and Research Institute of Texas (CPRIT) Scholar in Cancer Research and an Andrew Sabin Family Fellow. This work was supported by CPRIT (Recruitment of First-Time Tenure-Track Faculty Members; RR190017), an Andrew Sabin Family Foundation Fellowship, Parker Institute for Cancer Immunotherapy (PICI) Bridge Scholar Award, University of Texas (UT) Rising Stars Award, and the University of Texas MD Anderson Cancer Center (MDACC) Support Grant (CCSG) New Faculty Award supported by the National Institutes of Health (NIH)/National Cancer Institute (NCI) (P30CA016672) to M.M. Gubin; and NIH/NCI

U01CA247760 to K. Chen. K.H. Hu is a CPRIT Scholar in Cancer Research and a PICI Bridge Scholar. K.E. Pauken is supported by an Andrew Sabin Family Foundation Fellowship, a Melanoma SPORE Developmental Research Program Grant, and a UT Rising STARs Award. The Flow Cytometry and Cellular Imaging Core Facility was supported in part by MDACC and NIH/NCI Core grant P30CA016672. scRNAseq was performed by the MDACC Advanced Technology Genomics Core (ATGC) Facility supported by an NCI Core grant [CA016672 (ATGC)]. We would like to thank David Pollock at MDACC ATGC Facility for assistance with scRNAseq. We would like to thank the Baylor College of Medicine MHC Tetramer Core and thank the core director, X. Lily Wang for production of MHC tetramers used in this study. We would like to thank Prachi Sao (MDACC) for assistance with deconvolution of multiplexed hashtagged scRNAseq samples. We would like to thank Mehdi Chaib, (MDACC) for providing feedback to the manuscript. The authors thank all members of the Gubin lab for helpful discussions and technical support.

Authors' Disclosures

K.H. Hu reports grants from Cancer Prevention and Research Institute of Texas (CPRIT), grants from Parker Institute for Cancer Immunotherapy (PICI). K. Chen reports grants from the NIH/NCI during the conduct of this study. M.M. Gubin reports grants from CPRIT (RR190017), PICI, and The University of Texas MD Anderson Cancer Center Support Grant (CCSG) New Faculty Award supported by the NIH/NCI (P30CA016672) during the conduct of the study; and a personal honorarium of $1000.00 USD per year from Springer Nature Ltd for his role as an Associate Editor for the journal Nature Precision Oncology. No disclosures were reported by the other authors.

REFERENCES:

1 Coulie, P. G., Van den Eynde, B. J., van der Bruggen, P. & Boon, T. Tumour antigens recognized by T lymphocytes: at the core of cancer immunotherapy. *Nat Rev Cancer* **14**, 135-146, doi:10.1038/nrc3670 (2014).

2 Heemskerk, B., Kvistborg, P. & Schumacher, T. N. The cancer antigenome. *The EMBO journal* **32**, 194-203, doi:10.1038/emboj.2012.333 (2013).

3 Schumacher, T. N. & Schreiber, R. D. Neoantigens in cancer immunotherapy. *Science* **348**, 69-74, doi:10.1126/science.aaa4971 (2015).

4 Gubin, M. M., Artyomov, M. N., Mardis, E. R. & Schreiber, R. D. Tumor neoantigens: building a framework for personalized cancer immunotherapy. *J Clin Invest* **125**, 3413-3421, doi:10.1172/JCI80008 (2015).

5 Carreno, B. M. *et al.* A dendritic cell vaccine increases the breadth and diversity of melanoma neoantigen-specific T cells. *Science*, doi:10.1126/science.aaa3828 (2015).

6 Sahin, U. *et al.* Personalized RNA mutanome vaccines mobilize poly-specific therapeutic immunity against cancer. *Nature* **547**, 222-226, doi:10.1038/nature23003 (2017).

7 Ott, P. A. *et al.* An immunogenic personal neoantigen vaccine for patients with melanoma. *Nature* **547**, 217-221, doi:10.1038/nature22991 (2017).

8 Keskin, D. B. *et al.* Neoantigen vaccine generates intratumoral T cell responses in phase Ib glioblastoma trial. *Nature* **565**, 234-239, doi:10.1038/s41586-018-0792-9 (2019).

9 Ott, P. A. *et al.* A Phase Ib Trial of Personalized Neoantigen Therapy Plus Anti-PD-1 in Patients with Advanced Melanoma, Non-small Cell Lung Cancer, or Bladder Cancer. *Cell* **183**, 347-362 e324, doi:10.1016/j.cell.2020.08.053 (2020).

10 Blass, E. & Ott, P. A. Advances in the development of personalized neoantigen-based therapeutic cancer vaccines. *Nat Rev Clin Oncol* **18**, 215-229, doi:10.1038/s41571-020-00460-2 (2021).

11 Rojas, L. A. *et al.* Personalized RNA neoantigen vaccines stimulate T cells in pancreatic cancer. *Nature* **618**, 144-150, doi:10.1038/s41586-023-06063-y (2023).

12 Sahin, U. *et al.* An RNA vaccine drives immunity in checkpoint-inhibitor-treated melanoma. *Nature* **585**, 107-112, doi:10.1038/s41586-020-2537-9 (2020).

13 Gubin, M. M. *et al.* Checkpoint blockade cancer immunotherapy targets tumour-specific mutant antigens. *Nature* **515**, 577-581, doi:10.1038/nature13988 (2014).

14 Robbins, P. F. *et al.* Mining exomic sequencing data to identify mutated antigens recognized by adoptively transferred tumor-reactive T cells. *Nat Med* **19**, 747-752, doi:10.1038/nm.3161 (2013).

15 Castle, J. C. *et al.* Exploiting the mutanome for tumor vaccination. *Cancer research* **72**, 1081-1091, doi:10.1158/0008-5472.CAN-11-3722 (2012).

16 Yadav, M. *et al.* Predicting immunogenic tumour mutations by combining mass spectrometry and exome sequencing. *Nature* **515**, 572-576, doi:10.1038/nature14001 (2014).

17 Fehlings, M. *et al.* Checkpoint blockade immunotherapy reshapes the high-dimensional phenotypic heterogeneity of murine intratumoural neoantigen-specific CD8(+) T cells. *Nat Commun* **8**, 562, doi:10.1038/s41467-017-00627-z (2017).

18 Gubin, M. M. *et al.* High-Dimensional Analysis Delineates Myeloid and Lymphoid Compartment Remodeling during Successful Immune-Checkpoint Cancer Therapy. *Cell* **175**, 1014-1030 e1019, doi:10.1016/j.cell.2018.09.030 (2018).

19 Alspach, E. *et al.* MHC-II neoantigens shape tumour immunity and response to immunotherapy. *Nature* **574**, 696-701, doi:10.1038/s41586-019-1671-8 (2019).

20 Salmon, A. J. *et al.* BHLHE40 Regulates the T-Cell Effector Function Required for Tumor Microenvironment Remodeling and Immune Checkpoint-Therapy Efficacy. *Cancer Immunol Res*, doi:10.1158/2326-6066.CIR-21-0129 (2022).

21 Wei, S. C. *et al.* Distinct Cellular Mechanisms Underlie Anti-CTLA-4 and Anti-PD-1 Checkpoint Blockade. *Cell* **170**, 1120-1133 e1117, doi:10.1016/j.cell.2017.07.024 (2017).

22 Wei, S. C. *et al.* Combination anti-CTLA-4 plus anti-PD-1 checkpoint blockade utilizes cellular mechanisms partially distinct from monotherapies. *Proc Natl Acad Sci U S A* **116**, 22699-22709, doi:10.1073/pnas.1821218116 (2019).

23 Miller, B. C. *et al.* Subsets of exhausted CD8(+) T cells differentially mediate tumor control and respond to checkpoint blockade. *Nat Immunol* **20**, 326-336, doi:10.1038/s41590-019-0312-6 (2019).

24 Chen, Z. *et al.* TCF-1-Centered Transcriptional Network Drives an Effector versus Exhausted CD8 T Cell-Fate Decision. *Immunity* **51**, 840-855 e845, doi:10.1016/j.immuni.2019.09.013 (2019).

25 Khan, O. *et al.* TOX transcriptionally and epigenetically programs CD8(+) T cell exhaustion. *Nature* **571**, 211-218, doi:10.1038/s41586-019-1325-x (2019).

26 Scott, A. C. *et al.* TOX is a critical regulator of tumour-specific T cell differentiation. *Nature* **571**, 270-274, doi:10.1038/s41586-019-1324-y (2019).

27 Philip, M. & Schietinger, A. CD8(+) T cell differentiation and dysfunction in cancer. *Nat Rev Immunol* **22**, 209-223, doi:10.1038/s41577-021-00574-3 (2022).

28 Martinez, G. J. *et al.* The transcription factor NFAT promotes exhaustion of activated CD8(+) T cells. *Immunity* **42**, 265-278, doi:10.1016/j.immuni.2015.01.006 (2015).

29 Jansen, C. S. *et al.* An intra-tumoral niche maintains and differentiates stem-like CD8 T cells. *Nature* **576**, 465-470, doi:10.1038/s41586-019-1836-5 (2019).

30 Yost, K. E. *et al.* Clonal replacement of tumor-specific T cells following PD-1 blockade. *Nat Med* **25**, 1251-1259, doi:10.1038/s41591-019-0522-3 (2019).

31 Goswami, S., Anandhan, S., Raychaudhuri, D. & Sharma, P. Myeloid cell-targeted therapies for solid tumours. *Nat Rev Immunol* **23**, 106-120, doi:10.1038/s41577-022-00737-w (2023).

32 Gabrilovich, D. I., Ostrand-Rosenberg, S. & Bronte, V. Coordinated regulation of myeloid cells by tumours. *Nat Rev Immunol* **12**, 253-268, doi:10.1038/nri3175 (2012).

33 Ren, X. *et al.* Insights Gained from Single-Cell Analysis of Immune Cells in the Tumor Microenvironment. *Annu Rev Immunol* **39**, 583-609, doi:10.1146/annurev-immunol-110519-071134 (2021).

34 DeNardo, D. G. & Ruffell, B. Macrophages as regulators of tumour immunity and immunotherapy. *Nat Rev Immunol* **19**, 369-382, doi:10.1038/s41577-019-0127-6 (2019).

35 Cassetta, L. & Pollard, J. W. A timeline of tumour-associated macrophage biology. *Nat Rev Cancer* **23**, 238-257, doi:10.1038/s41568-022-00547-1 (2023).

36 Molgora, M. *et al.* TREM2 Modulation Remodels the Tumor Myeloid Landscape Enhancing Anti-PD-1 Immunotherapy. *Cell* **182**, 886-900 e817, doi:10.1016/j.cell.2020.07.013 (2020).

37 Cassetta, L. *et al.* Human Tumor-Associated Macrophage and Monocyte Transcriptional Landscapes Reveal Cancer-Specific Reprogramming, Biomarkers, and Therapeutic Targets. *Cancer Cell* **35**, 588-602 e510, doi:10.1016/j.ccell.2019.02.009 (2019).

38 Meeth, K., Wang, J. X., Micevic, G., Damsky, W. & Bosenberg, M. W. The YUMM lines: a series of congenic mouse melanoma cell lines with defined genetic alterations. *Pigment Cell Melanoma Res* **29**, 590-597, doi:10.1111/pcmr.12498 (2016).

39 DuPage, M. *et al.* Endogenous T cell responses to antigens expressed in lung adenocarcinomas delay malignant tumor progression. *Cancer Cell* **19**, 72-85, doi:10.1016/j.ccr.2010.11.011 (2011).

40 DuPage, M., Mazumdar, C., Schmidt, L. M., Cheung, A. F. & Jacks, T. Expression of tumour-specific antigens underlies cancer immunoediting. *Nature* **482**, 405-409, doi:10.1038/nature10803 (2012).

41 Spranger, S., Bao, R. & Gajewski, T. F. Melanoma-intrinsic beta-catenin signalling prevents anti-tumour immunity. *Nature* **523**, 231-235, doi:10.1038/nature14404 (2015).

42 Cui, C. *et al.* Neoantigen-driven B cell and CD4 T follicular helper cell collaboration promotes anti-tumor CD8 T cell responses. *Cell* **184**, 6101-6118 e6113, doi:10.1016/j.cell.2021.11.007 (2021).

43 Burger, M. L. *et al.* Antigen dominance hierarchies shape TCF1(+) progenitor CD8 T cell phenotypes in tumors. *Cell* **184**, 4996-5014 e4926, doi:10.1016/j.cell.2021.08.020 (2021).

44 Park, J. *et al.* SLC45A2: A Melanoma Antigen with High Tumor Selectivity and Reduced Potential for Autoimmune Toxicity. *Cancer Immunol Res* **5**, 618-629, doi:10.1158/2326-6066.CIR-17-0051 (2017).

45 Legat, A., Speiser, D. E., Pircher, H., Zehn, D. & Fuertes Marraco, S. A. Inhibitory Receptor Expression Depends More Dominantly on Differentiation and Activation than "Exhaustion" of Human CD8 T Cells. *Front Immunol* **4**, 455, doi:10.3389/fimmu.2013.00455 (2013).

46 Speiser, D. E. *et al.* T cell differentiation in chronic infection and cancer: functional adaptation or exhaustion? *Nat Rev Immunol* **14**, 768-774, doi:10.1038/nri3740 (2014).

47 Chiang, E. Y. & Mellman, I. TIGIT-CD226-PVR axis: advancing immune checkpoint blockade for cancer immunotherapy. *J Immunother Cancer* **10**, doi:10.1136/jitc-2022-004711 (2022).

48 Oliveira, G. *et al.* Phenotype, specificity and avidity of antitumour CD8(+) T cells in melanoma. *Nature* **596**, 119-125, doi:10.1038/s41586-021-03704-y (2021).

49 Pauken, K. E. *et al.* Single-cell analyses identify circulating anti-tumor CD8 T cells and markers for their enrichment. *J Exp Med* **218**, doi:10.1084/jem.20200920 (2021).

50 Lowery, F. J. *et al.* Molecular signatures of antitumor neoantigen-reactive T cells from metastatic human cancers. *Science* **375**, 877-884, doi:10.1126/science.abl5447 (2022).

51 Yao, C. *et al.* BACH2 enforces the transcriptional and epigenetic programs of stem-like CD8(+) T cells. *Nat Immunol* **22**, 370-380, doi:10.1038/s41590-021-00868-7 (2021).

52 Pesu, M., Muul, L., Kanno, Y. & O'Shea, J. J. Proprotein convertase furin is preferentially expressed in T helper 1 cells and regulates interferon gamma. *Blood* **108**, 983-985, doi:10.1182/blood-2005-09-3824 (2006).

53 Duwel, M. *et al.* A20 negatively regulates T cell receptor signaling to NF-kappaB by cleaving Malt1 ubiquitin chains. *J Immunol* **182**, 7718-7728, doi:10.4049/jimmunol.0803313 (2009).

54 Trapnell, C. *et al.* The dynamics and regulators of cell fate decisions are revealed by pseudotemporal ordering of single cells. *Nat Biotechnol* **32**, 381-386, doi:10.1038/nbt.2859 (2014).

55 Salmon, A. J. *et al.* BHLHE40 Regulates the T-Cell Effector Function Required for Tumor Microenvironment Remodeling and Immune Checkpoint Therapy Efficacy. *Cancer Immunol Res* **10**, 597-611, doi:10.1158/2326-6066.CIR-21-0129 (2022).

56 Maier, B. *et al.* A conserved dendritic-cell regulatory program limits antitumour immunity. *Nature* **580**, 257-262, doi:10.1038/s41586-020-2134-y (2020).

57 Di Pilato, M. *et al.* CXCR6 positions cytotoxic T cells to receive critical survival signals in the tumor microenvironment. *Cell* **184**, 4512-4530 e4522, doi:10.1016/j.cell.2021.07.015 (2021).

58 Ma, R. Y., Black, A. & Qian, B. Z. Macrophage diversity in cancer revisited in the era of single-cell omics. *Trends Immunol* **43**, 546-563, doi:10.1016/j.it.2022.04.008 (2022).

59 Ray, A. *et al.* Critical role of CD206+ macrophages in organizing anti-tumor immunity. *bioRxiv*, doi:10.1101/2023.10.31.560822 (2023).

60 Baharom, F. *et al.* Systemic vaccination induces CD8(+) T cells and remodels the tumor microenvironment. *Cell* **185**, 4317-4332 e4315, doi:10.1016/j.cell.2022.10.006 (2022).

61 Kemp, S. B. *et al.* Pancreatic cancer is marked by complement-high blood monocytes and tumor-associated macrophages. *Life Sci Alliance* **4**, doi:10.26508/lsa.202000935 (2021).

62 Xiong, D., Wang, Y. & You, M. A gene expression signature of TREM2(hi) macrophages and gammadelta T cells predicts immunotherapy response. *Nat Commun* **11**, 5084, doi:10.1038/s41467-020-18546-x (2020).

63 Bill, R. *et al.* CXCL9:SPP1 macrophage polarity identifies a network of cellular programs that control human cancers. *Science* **381**, 515-524, doi:10.1126/science.ade2292 (2023).

64 Hos, B. J. *et al.* Identification of a neo-epitope dominating endogenous CD8 T cell responses to MC-38 colorectal cancer. *Oncoimmunology* **9**, 1673125, doi:10.1080/2162402X.2019.1673125 (2019).

65 Schrors, B. *et al.* MC38 colorectal tumor cell lines from two different sources display substantial differences in transcriptome, mutanome and neoantigen expression. *Front Immunol* **14**, 1102282, doi:10.3389/fimmu.2023.1102282 (2023).

66 Liu, L. *et al.* Concurrent delivery of immune checkpoint blockade modulates T cell dynamics to enhance neoantigen vaccine-generated antitumor immunity. *Nat Cancer* **3**, 437-452, doi:10.1038/s43018-022-00352-7 (2022).

67 Hu, Z. *et al.* Personal neoantigen vaccines induce persistent memory T cell responses and epitope spreading in patients with melanoma. *Nat Med* **27**, 515-525, doi:10.1038/s41591-020-01206-4 (2021).

68 Wu, J. E. *et al.* In vitro modeling of CD8(+) T cell exhaustion enables CRISPR screening to reveal a role for BHLHE40. *Sci Immunol* **8**, eade3369, doi:10.1126/sciimmunol.ade3369 (2023).

69 Ng Tang, D. *et al.* Increased frequency of ICOS+ CD4 T cells as a pharmacodynamic biomarker for anti-CTLA-4 therapy. *Cancer Immunol Res* **1**, 229-234, doi:10.1158/2326-6066.CIR-13-0020 (2013).

70 Chen, H. *et al.* Anti-CTLA-4 therapy results in higher CD4+ICOShi T cell frequency and IFN-gamma levels in both nonmalignant and malignant prostate tissues. *Proc Natl Acad Sci U S A* **106**, 2729-2734, doi:10.1073/pnas.0813175106 (2009).

71 Zhang, L. *et al.* Lineage tracking reveals dynamic relationships of T cells in colorectal cancer. *Nature* **564**, 268-272, doi:10.1038/s41586-018-0694-x (2018).

72 Fan, X., Quezada, S. A., Sepulveda, M. A., Sharma, P. & Allison, J. P. Engagement of the ICOS pathway markedly enhances efficacy of CTLA-4 blockade in cancer immunotherapy. *J Exp Med* **211**, 715-725, doi:10.1084/jem.20130590 (2014).

73 Oh, D. Y. & Fong, L. Cytotoxic CD4(+) T cells in cancer: Expanding the immune effector toolbox. *Immunity* **54**, 2701-2711, doi:10.1016/j.immuni.2021.11.015 (2021).

74 Kreiter, S. *et al.* Mutant MHC class II epitopes drive therapeutic immune responses to cancer. *Nature* **520**, 692-696, doi:10.1038/nature14426 (2015).

75 Ferris, S. T. *et al.* cDC1 prime and are licensed by CD4(+) T cells to induce anti-tumour immunity. *Nature* **584**, 624-629, doi:10.1038/s41586-020-2611-3 (2020).

76 Wu, R. *et al.* Mechanisms of CD40-dependent cDC1 licensing beyond costimulation. *Nat Immunol* **23**, 1536-1550, doi:10.1038/s41590-022-01324-w (2022).

77 Haabeth, O. A. W. *et al.* CD4(+) T-cell-Mediated Rejection of MHC Class II-Positive Tumor Cells Is Dependent on Antigen Secretion and Indirect Presentation on Host APCs. *Cancer research* **78**, 4573-4585, doi:10.1158/0008-5472.CAN-17-2426 (2018).

78 Kruse, B. *et al.* CD4(+) T cell-induced inflammatory cell death controls immune-evasive tumours. *Nature* **618**, 1033-1040, doi:10.1038/s41586-023-06199-x (2023).

79 Rosalia, R. A. *et al.* Dendritic cells process synthetic long peptides better than whole protein, improving antigen presentation and T-cell activation. *Eur J Immunol* **43**, 2554-2565, doi:10.1002/eji.201343324 (2013).

80 Melief, C. J., van Hall, T., Arens, R., Ossendorp, F. & van der Burg, S. H. Therapeutic cancer vaccines. *J Clin Invest* **125**, 3401-3412, doi:10.1172/JCI80009 (2015).

81 Saxena, M., van der Burg, S. H., Melief, C. J. M. & Bhardwaj, N. Therapeutic cancer vaccines. *Nat Rev Cancer* **21**, 360-378, doi:10.1038/s41568-021-00346-0 (2021).

82 Dolina, J. S. *et al.* Linked CD4+/CD8+ T cell neoantigen vaccination overcomes immune checkpoint blockade resistance and enables tumor regression. *J Clin Invest* **133**, doi:10.1172/JCI164258 (2023).

83 Alexopoulou, L., Holt, A. C., Medzhitov, R. & Flavell, R. A. Recognition of double-stranded RNA and activation of NF-kappaB by Toll-like receptor 3. *Nature* **413**, 732-738, doi:10.1038/35099560 (2001).

84 van den Boorn, J. G., Barchet, W. & Hartmann, G. Nucleic acid adjuvants: toward an educated vaccine. *Adv Immunol* **114**, 1-32, doi:10.1016/B978-0-12-396548-6.00001-9 (2012).

85 Sharma, P. *et al.* The Next Decade of Immune Checkpoint Therapy. *Cancer Discov* **11**, 838-857, doi:10.1158/2159-8290.CD-20-1680 (2021).

86 Wolchok, J. D. *et al.* Long-Term Outcomes With Nivolumab Plus Ipilimumab or Nivolumab Alone Versus Ipilimumab in Patients With Advanced Melanoma. *J Clin Oncol* **40**, 127-137, doi:10.1200/JCO.21.02229 (2022).

87 Verma, V. *et al.* PD-1 blockade in subprimed CD8 cells induces dysfunctional PD-1(+)CD38(hi) cells and anti-PD-1 resistance. *Nat Immunol* **20**, 1231-1243, doi:10.1038/s41590-019-0441-y (2019).

88 McGranahan, N. *et al.* Clonal neoantigens elicit T cell immunoreactivity and sensitivity to immune checkpoint blockade. *Science* **351**, 1463-1469, doi:10.1126/science.aaf1490 (2016).

89 Gubin, M. M. & Vesely, M. D. Cancer Immunoediting in the Era of Immuno-oncology. *Clin Cancer Res* **28**, 3917-3928, doi:10.1158/1078-0432.CCR-21-1804 (2022).

Figure Legends:

Figure 1. Therapeutic NeoAg Vaccines or ICT Inhibit Tumor Growth in Mice Bearing NeoAg-Expressing *Braf*^{V600E} *Pten*$^{-/-}$ *Cdkn2a*$^{-/-}$ Melanoma. (**A**) Tumor growth and percent tumor rejection in WT C57BL/6J mice transplanted with Y1.7 mA^{MHC-I}.mI^{MHC-II} (Y1.7AI) and Y1.7 mL^{MHC-I}.mI^{MHC-II} (Y1.7LI) melanoma cells and treated with control mAb or anti-CTLA-4 immune checkpoint therapy (ICT) starting on d. 3 post tumor-transplant, and subsequently on d. 6, 9, 12, 18, 24. (**B**) Tumor growth, cumulative mouse survival, and percent tumor rejection in WT C57BL/6J mice transplanted with Y1.7AI and Y1.7LI melanoma cells and treated with mAlg8 or mLama4 NeoAg synthetic long peptide (SLP) plus poly I:C (pI:C) vaccines or pI:C alone starting on d. 3 post tumor-transplant and given every 6 days for total 3 doses. (**C**) Representative graphs displaying mAlg8 or mLama4 tetramer-specific CD8 T cells in Y1.7AI and Y1.7LI tumors treated with control mAb, anti-CTLA-4, pI:C, mAlg8 SLP + pI:C NeoAg vaccine (for Y1.7AI) or mLama4 SLP + pI:C NeoAg vaccine (for Y1.7LI) as in **A** and **B** and harvested on d. 16 post-tumor transplant. mAlg8-H2-K^b, mLama4-H2-K^b, or SIINFEKL-H2-K^b (irrelevant control) tetramers were labeled with PE and APC. Dot plots are gated on live CD45$^+$ Thy1.2$^+$ CD8 T cells. (**D**) Tumor growth, cumulative mouse survival, and percent tumor rejection in WT C57BL/6J mice transplanted with Y1.7LI melanoma cells and treated with control mAb, anti-CTLA-4, anti-PD-1, anti-CTLA-4 + anti-PD-1, irrelevant (for Y1.7LI) mAlg8 SLP + pI:C (Control VAX), or relevant mLama4 SLP + pI:C (neo VAX) starting on d. 7 post tumor-transplant, and subsequently on d. 10, 13, 16, 22, 28 for ICT and d. 13, 19 for NeoAg vaccines. Tumor growth data in (**A**), (**B**), and (**D**) are presented as individual mouse tumor growth as mean tumor diameter and are representative of (**A**) five, (**B**) three, or (**D**) four independent experiments. Tumor rejection graphs display cumulative percentage of mice with complete tumor rejection from independent experiments. Cumulative survival curves and tumor rejection graphs include mice from three independent experiments (***P < 0.01*, ****P < 0.001*, log-rank (Mantel–Cox) test). Bar graphs in (**C**), display mean ± SEM and are representative of at least three independent experiments (**P* < 0.05, ***P* < 0.01, ****P* < 0.005, NS, not significant; unpaired, two-tailed Student's *t* test).

Figure 2. scRNAseq of Intratumoral Immune Cells from Y1.7LI Tumor Bearing Mice Treated with NeoAg Vaccines or ICT. (**A**) WT C57BL/6J mice were injected with Y1.7LI melanoma cells and subsequently treated beginning on d. 7 with control mAb, anti-CTLA-4, anti-PD-1, anti-CTLA-4 + anti-PD-1, irrelevant (for Y1.7LI) mAlg8 SLP + pI:C (Control VAX), or relevant mLama4 SLP + pI:C (neo VAX) and harvested on d. 15 post-tumor transplant. Intratumoral live CD45$^+$ cells were sorted and analyzed by scRNAseq. (**B**) UMAP plot from scRNAseq of intratumoral CD45$^+$ cells. Cell types were annotated based on lineage marker expression. (**C**) Feature plot showing lineage-specific transcripts defining lymphoid and myeloid cell types. (**D**) Feature plots displaying subclustering of activated T cell containing clusters and subclustered T cell/ILC cluster annotations (middle plot) and *Cd4* and *Cd8* expression (bottom plot). (**E**) Table showing select genes describing each CD8 and CD4 T cell cluster. (**F**) Gene set enrichment analysis (GSEA) displaying significantly enriched gene sets in cluster Cd4/8$_{Cycling}$. (**G**) Proliferating T cells in cluster Cd4/8$_{Cycling}$ by treatment condition represented as percentage of subclustered T cells. (**H**) Dot plot depicting expression level and percent of cells expressing *Foxp3*, *Cd4*, *Cd8*, *Ifng* in Cd4/8$_{Cycling}$ by treatment condition. (**I**) Percentage of Foxp3$^+$ CD4 Tregs, conventional CD4 T cells, or CD8 T cells in Cd4/8$_{Cycling}$ by treatment condition. (**J**) Graph displaying CD8 T cells from cluster Cd4/8$_{Cycling}$ represented as percentage of total subclustered T cells. (**K**) Graph displaying CD4 T cells from cluster Cd4/8$_{Cycling}$ represented as percentage of total subclustered T cells.

Figure 3. scRNAseq Profiling of mLama4 NeoAg-Specific CD8 T cells from Y1.7LI Tumor Bearing Mice Treated with NeoAg Vaccines or ICT. (**A**) WT C57BL/6J mice were injected with Y1.7LI melanoma cells and subsequently treated beginning on d. 7 with control mAb, anti-CTLA-4, anti-PD-1, anti-CTLA-4 + anti-PD-1, irrelevant (for Y1.7LI) mAlg8 SLP + pI:C (Control VAX), or relevant mLama4 SLP + pI:C (neo VAX) and harvested on d. 15 post-tumor transplant. single cell suspensions of harvested tumors from treated mice were stained with SIINFEKL or mLama4 PE and APC labelled tetramers and surface stained with flow antibodies. (**B**) Graph displaying CD8 T cells as a percentage of intratumoral live $CD45^+$ cells in Y1.7LI tumors treated with control mAb, anti-CTLA-4, anti-PD-1, anti-CTLA-4 + anti-PD-1, irrelevant (for Y1.7LI) mAlg8 SLP + pI:C (Control VAX), or relevant mLama4 SLP + pI:C (neo VAX) and harvested on d. 15 post-tumor transplant. Graph displaying, (**C**) mLama4 tetramer-specific CD8 T cells and **(D)** mLama4 tetramer-specific CD45+ cells in Y1.7LI tumors treated with control mAb, anti-CTLA-4, anti-PD-1, anti-CTLA-4 + anti-PD-1, irrelevant (for Y1.7LI) mAlg8 SLP + pI:C (Control VAX), or relevant mLama4 SLP + pI:C (neo VAX) and harvested on d. 15 post-tumor transplant. mLama4-H2-K^b or SIINFEKL-H2-K^b (irrelevant control) tetramers were labeled with PE and APC. **(E)** WT C57BL/6J mice were injected with Y1.7LI melanoma cells and subsequently treated beginning on d. 7 with control mAb, anti-CTLA-4, anti-PD-1, anti-CTLA-4 + anti-PD-1, irrelevant (for Y1.7LI) mAlg8 SLP + pI:C (Control VAX), or relevant mLama4 SLP + pI:C (neo VAX) and harvested on d. 15 post-tumor transplant. Sorted mLama4 tetramer positive CD8 T cells were analyzed by scRNAseq. **(F)** UMAP plot from scRNAseq of mLama4 NeoAg-specific CD8 T cells. Cell types were annotated based on transcriptional activation states of NeoAg-specific CD8 T cells. **(G)** Feature plots displaying expression of select subtype or functional state defining genes. **(H)** Violin plots denoting expression level of select genes per neoAg-specific CD8 T cell. **(I)** Table showing select genes describing each NeoAg-specific CD8 T cells cluster.

Figure 4. NeoAg Vaccines Promote Cycling and PD-1^+ TCF-7^+ Stem-Like NeoAg-Specific CD8 T Cells and Anti-CTLA-4 and/or Anti-PD-1 ICT Induce Distinct Effects on NeoAg-Specific CD8 T Cells. (A) Heat map displaying normalized expression of select genes in each NeoAg-specific CD8 T cell cluster by treatment condition. **(B)** Bar graphs displaying mLama4 NeoAg-specific CD8 T cells within each cluster by treatment condition. **(C)** The frequency of total mLama4 NeoAg-specific CD8 T cells within the combined 5 cycling clusters by treatment condition. **(D)** Representative flow cytometry plots displaying PD-1^+ and/or TIM-3^+/LAG-3^+ after gating on mLama4 tetramer positive CD8 T cells and graphs displaying percent of PD-1^+ TIM-3^+/LAG-3^+ or expression level of PD-1, TIM-3, or LAG-3 on PD-1^+, TIM-3^+, or LAG-3^+ mLama4-specific CD8 T cells in Y1.7LI tumors treated with control mAb, anti-CTLA-4, anti-PD-1, anti-CTLA-4 + anti-PD-1, Control VAX, or neo VAX and harvested on d. 15 post-tumor transplant. Graph displaying **(E)** IFNγ^+ mLama4-specific CD8 T cells and **(F)** TNFα^+ mLama4-specific CD8 T cells assessed by intracellular cytokine staining of CD8 T cells isolated from Y1.7LI tumors under different treatment conditions and harvested on d. 15 post-tumor transplant. Bar graphs in **(D)**, **(E)**, and **(F)** display mean ± SEM and are representative of at least three independent experiments (*$P < 0.05$, **$P < 0.01$, ***$P < 0.005$, **** $P < 0.0001$; NS, not significant, unpaired t test).

Figure 5. Anti-CTLA-4 Induces an ICOS$^+$ Bhlhe40$^+$ Th1-Like Subpopulation of CD4 T Cells and when Combined with Anti-PD-1, a Small Th2-Like Subpopulation. (A) Heat map displaying normalized expression of select genes in each CD4 T cell cluster. **(B)** Bar graphs depicting frequency of CD4 T cells within each cluster by treatment condition. **(C)** Graph displaying CD4 T cells as a percentage of intratumoral live CD45$^+$ cells as determined by flow cytometry in Y1.7LI tumors under different treatment conditions and harvested on d. 15 post-tumor transplant. **(D)** Graph displaying IFNγ$^+$ CD4 T cells as assessed by intracellular cytokine staining on CD4 T cells isolated from Y1.7LI tumors under different treatment conditions and harvested on d. 15 post-tumor transplant. **(E)** Monocle 3-Guided Cell Trajectory of CD4 T Cell Clusters. UMAP plot displaying exclusively CD4 T cell-containing clusters (left) of all experimental conditions, CD4 T cell trajectory graph overlaid on UMAP (middle) where the origin of the inferred pseudotime is indicated by the red arrow and assigned with pseudotime score 0, and geodesic distances and pseudotime score among other CD4 T cells are calculated from there based on transcripts associated cell states. CD4 T cell clusters overlaid on Monocle3 pseudotime plot (right). Bar graphs in **(C)** and **(D)** display mean ± SEM and are representative of at least three independent experiments (**P* < 0.05, ***P* < 0.01, ****P* < 0.005, *****P* < 0.0001, NS, not significant, unpaired t test).

Figure 6. NeoAg Vaccines Promote Partially Distinct Macrophage Remodeling from ICT. (A) UMAP displaying sub-clustering of select myeloid clusters from CD45$^+$ scRNAseq analysis (See Figure 2A). **(B)** Heatmap displaying normalized expression of select genes in each monocyte/macrophage cluster by treatment condition. **(C)** Percent monocytes/macrophages in each cluster by condition and treatment represented as percent of live CD45$^+$ cells. **(D)** Violin plots denoting expression level of *Cx3cr1* transcript per cell in each monocyte/macrophage cluster by treatment condition. **(E)** scRNAseq dot plot depicting expression level/percent of cells expressing *Mrc1* and *Cx3cr1* within all monocytes/macrophages clusters by treatment condition. **(F)** Representative flow cytometry plots and graph displaying CX3CR1$^+$CD206$^+$ macrophages in Y1.7LI tumors under different treatment conditions and harvested on d. 15 post-tumor transplant. **(G)** Violin plots denoting expression level of *Nos2* (iNOS) transcript per cell in each monocyte/macrophage cluster by treatment condition. **(H)** Representative flow cytometry plots and graph displaying iNOS$^+$ macrophages in Y1.7LI tumors under different treatment conditions and harvested on d. 15 post-tumor transplant. For flow cytometry analysis in **(F)** and **(H)**, dot plot displaying CX3CR1$^+$CD206$^+$ and iNOS$^+$ macrophages are gated on macrophages using a gating strategy previously described (39). Bar graphs in **(F)** and **(H)** display mean ± SEM and are representative of at least three independent experiments (***P* < 0.01, *****P* < 0.0001, NS, not significant, unpaired *t* test).

Figure 7. NeoAg Vaccines Broaden the Therapeutic Window for Anti-CTLA-4 or Anti-PD-1 ICT when Used in Combination Against Y1.7LI and MC38 Tumors. (A) Tumor growth and cumulative survival of WT C57BL/6J mice transplanted with Y1.7LI melanoma cells on d. 0 and treated beginning on d. 12 with different monotherapies: control mAb, anti-CTLA-4, anti-PD-1, irrelevant SLP + pI:C (Control VAX), or relevant mLama4 SLP + pI:C (neo VAX); or combination therapies: anti-CTLA-4 + anti-PD-1 combination ICT, anti-CTLA-4 + control VAX, anti-CTLA-4 + neo VAX, anti-PD-1 + control VAX, or anti-PD-1 + neo VAX. **(B)** Tumor growth and cumulative survival of WT C57BL/6J mice transplanted with MC38 cells on d. 0 and treated beginning on d. 12 with different monotherapies: control mAb, anti-CTLA-4, anti-PD-1, irrelevant HPV SLP + pI:C (Control VAX), or relevant mAdpgk SLP + mRpl18 SLP + mDpagt1 SLP + pI:C (neo VAX); or combination therapies: anti-CTLA-4 + anti-PD-1 combination ICT, anti-CTLA-4 + control VAX, anti-CTLA-4 + neo VAX, anti-PD-1 + control VAX, or anti-PD-1 + neo VAX. Tumor growth data in **(A)** and **(B)** are presented as individual mouse tumor growth as mean tumor diameter with fraction indicating # of mice rejecting tumor/# of mice used in experiment and are representative of three independent experiments. Cumulative survival curves in **(A)** and **(B)** include mice from three independent experiments (*$P < 0.01$, **$P < 0.05$, ***$P < 0.001$, log-rank (Mantel–Cox) test).

Figure Legends for Supplementary Figures:

Supplementary Figure 1. NeoAg Vaccines and ICT Induces Long-Term Tumor Protection in Y1.7AI and Y1.7LI Melanoma Models. (A) Depiction of minigene NeoAgs used to express NeoAgs in the parental *Braf*^{V600E} *Pten*$^{-/-}$ *Cdkn2a*$^{-/-}$ YUMM1.7 melanoma line. mLama4 or mAlg8 and mItgb1 NeoAgs were separated by 2A peptides that induce ribosomal skipping during translation. **(B)** Tumor growth in WT C57BL/6J mice transplanted with parental *Braf*^{V600E} *Pten*$^{-/-}$ *Cdkn2a*$^{-/-}$ YUMM1.7 melanoma cells and treated with control mAb, anti-CTLA-4, anti-PD-1 or anti-CTLA4 + anti-PD-1 combination immune checkpoint therapy (ICT) on d. 3, 6, 9, 12, 18, 24 post tumor-transplant. **(C)** WT C57BL/6J mice were transplanted with Y1.7 mA^{MHC-I}.mI^{MHC-II} (Y1.7AI) and Y1.7 mL^{MHC-I}.mI^{MHC-II} (Y1.7LI) melanoma cells and treated with control mAb or anti-CTLA-4 on d. 3, 6, 9, 12, 18, 24 or mAlg8 NeoAg (relevant for Y1.7AI) synthetic long peptide (SLP) + poly I:C (pI:C) or mLama4 NeoAg (relevant for Y1.7LI) synthetic long peptide (SLP) + pI:C on d. 3, 9, 15. mice were rechallenged with same tumor used for initial tumor challenge at least 60 days post-rejection of primary tumor. Naïve WT C57BL/6J mice transplanted with Y1.7AI or Y1.7LI tumor without any treatment was included as control indicating cell line preps used in rechallenge experiments were capable of tumor formation. **(D)** WT C57BL/6J mice were transplanted with Y1.7LI melanoma cells and treated with anti-CTLA-4 ICT on d. 3, 6, 9, 12, 18, 24 or with mLama4 NeoAg SLP + pI:C on d. 3, 9, 15. Mice were rechallenged with either with same tumor used for initial tumor challenge (Y1.7LI) or parental *Braf*^{V600E} *Pten*$^{-/-}$ *Cdkn2a*$^{-/-}$ YUMM1.7 at least 60 days post-rejection of primary tumor. Naïve WT C57Bl6J mice transplanted with either Y1.7 LI or parental *Braf*^{V600E} *Pten*$^{-/-}$ *Cdkn2a*$^{-/-}$ YUMM1.7 without any treatment was included as control indicating cell line preps used in rechallenge experiments were capable of tumor formation. **(E)** Representative flow cytometry plots displaying mAlg8 or mLama4 tetramer-specific CD8 T cells in Y1.7AI and Y1.7LI tumors treated with control mAb, anti-CTLA-4, pI:C, mAlg8 SLP + pI:C NeoAg vaccine (for Y1.7AI) or mLama4 SLP + pI:C NeoAg vaccine (for Y1.7LI) and harvested on d. 16 post-tumor transplant. mAlg8-H2-K^b, mLama4-H2-K^b, or SIINFEKL-H2-K^b (irrelevant control) tetramers were labeled with PE and APC. Dot plots are gated on live CD45$^+$ Thy1.2$^+$ CD8 T cells. **(F)** Co-expression of PD-1 and TIM-3 on mAlg8- or mLama4-specific CD8 T cells in Y1.7AI and Y1.7LI tumors treated with control mAb, anti-CTLA-4, pI:C, mAlg8 SLP + pI:C NeoAg vaccine (for Y1.7AI), or mLama4 SLP + pI:C NeoAg vaccine (for Y1.7LI). Tumor growth data in **(B)**, **(C)** and **(D)** are presented as individual mouse tumor growth as mean tumor diameter and are representative of three independent experiments.

Supplementary Figure 2. NeoAg Vaccines and ICT Induce Long-Term Tumor Protection in Y1.7LI Melanoma Models in a T Cell-Dependent Manner. (A) Y1.7LI tumor growth in WT C57BL/6J mice treated with control mAb, anti-CD4 or anti-CD8α mAbs on d. -1, 6, 13, 20 and anti-CTLA-4 or anti-PD-1 on d. 7, 10, 13, 16, 22, 28 or Irrelevant mAlg8 SLP + pI:C (Control VAX) or relevant mLama4 SLP + pI:C (neo VAX) on d. 7, 13, 19. **(B)** WT C57BL/6J mice transplanted with Y1.7LI melanoma cells and treated with control mAb, anti-CTLA-4, anti-PD-1, anti-CTLA-4 + anti-PD-1, irrelevant (for Y1.7LI) mAlg8 SLP + pI:C (Control VAX), or relevant mLama4 SLP + pI:C (neo VAX) starting on d. 7 post tumor-transplant, and subsequently on d. 10, 13, 16, 22, 28 for ICT and d. 13, 19 for NeoAg vaccines. Following post 60 days of primary tumor injection, mice were rechallenged with tumor used for initial tumor challenge. Naïve WT C57BL/6J mice transplanted with Y1.7 LI tumor without any treatment was included as control indicating cell line preps used in rechallenge experiments were capable

of tumor formation. Tumor growth data in **(A)** and **(B)** are presented as individual mouse tumor growth as mean tumor diameter and are representative of three independent experiments.

Supplementary Figure 3. scRNAseq Analysis of NeoAg Vaccines or ICT Induced Intratumoral Lymphoid and Myeloid Remodeling. (A) Graph of flow cytometry data displaying intratumoral lymphoid and myeloid cells as a percentage of intratumoral live or live $CD45^+$ cells in Y1.7LI tumors treated with control mAb, anti-CTLA-4, anti-PD-1, anti-CTLA-4 + anti-PD-1, irrelevant (for Y1.7LI) mAlg8 SLP + pI:C (Control VAX), or relevant mLama4 SLP + pI:C (neo VAX) beginning on d. 7 post-tumor transplant and harvested on d. 15. **(B)** Dot plot depicting expression level and percent of cells expressing *Foxp3, Ctla4, Icos, Tigit, Havcr2, Klrg1, Gzmb* and graph displaying frequency of regulatory T cell (Treg) clusters by treatment condition. **(C)** Graph displaying mixed T cell clusters represented as percentage of total subclustered T cells; GSEA displaying significantly enriched gene sets; and percentage of $Foxp3^+$ CD4 Tregs, conventional CD4 T cells, or CD8 T cells in clusters T_1, T_2; and T_3 by treatment condition. **(D)** Graph displaying γδ T cell clusters represented as percentage of total subclustered T cells by treatment condition. **(E)** Graph displaying ILC clusters represented as percentage of total subclustered T cells by treatment condition. Bar graphs in **(A)** display mean ± SEM and are representative of at least three independent experiments (**P* < 0.05, ***P* < 0.01, ****P* < 0.005, *****P* < 0.0001, NS, not significant, unpaired t test).

Supplemental Figure 4. Heatmap displaying normalized expression per cell of top 10 cluster-defining genes for each T cell/ILC Cluster (see Figure 2D).

Supplemental Figure 5. Heatmap displaying normalized expression of select genes in each T cell/ILC cluster by treatment condition.

Supplemental Figure 6. scRNAseq Analysis of Bulk CD8 T cells from Y1.7LI Tumor Bearing Mice Treated with NeoAg Vaccines or ICT. (A) Heat map displaying normalized expression of select genes in each bulk CD8 T cell clusters (see Figure 2A and 2D). **(B-F)** scRNAseq dot plot depicting expression level/percent of cells expressing select transcripts, GSEA displaying significantly enriched gene sets, and bar graphs depicting frequency of bulk CD8 T cells within each cluster by treatment condition.

Supplemental Figure 7. scRNAseq and Flow Cytometry Profiling of mLama4 NeoAg-Specific CD8 T cells from Y1.7LI Tumor Bearing Mice Treated with NeoAg Vaccines or ICT. (A) Representative flow cytometry plots displaying mLama4 tetramer-specific CD8 T cells in Y1.7LI tumors treated with control mAb, anti-CTLA-4, anti-PD-1, anti-CTLA-4 + anti-PD-1, irrelevant (for Y1.7LI) mAlg8 SLP + pI:C (Control VAX), or relevant mLama4 SLP + pI:C (neo VAX) and harvested on d. 15 post-tumor transplant. mLama4-H2-K^b or SIINFEKL-H2-K^b (irrelevant control) tetramers were labeled with PE and APC. Dot plots are gated on live $CD45^+$ $Thy1.2^+$ CD8 T cells. **(B)** Heatmap displaying normalized expression of select genes in each NeoAg-specific CD8 T cell clusters (see Figure 3E). **(C)** scRNAseq dot plot depicting expression level/percent of cells expressing select transcripts within each cluster by treatment condition.

Supplemental Figure 8. Heatmap displaying normalized expression per cell of top 10 cluster-defining genes for each NeoAg-specific CD8 T cells cluster (see Figure 3E).

Supplemental Figure 9. scRNAseq Profiling od CD4 T cells indicates Anti-CTLA-4 Induces an ICOS$^+$ Bhlhe40$^+$ Th1-Like Subpopulation of CD4 T Cells and when Combined with Anti-PD-1, a Small Th2-Like Subpopulation. (A-E and G) scRNAseq dot plots depicting expression level/percent of cells expressing select transcripts and GSEA displaying significantly enriched gene sets within each CD4 T cells cluster by treatment condition (see Figure 2D). **(F)** Violin plots denoting expression level of expression level of select genes per CD4 T cells.

Supplemental Figure 10. Dendritic Cell (DC) Changes Induced by ICT and NeoVAX in Y1.7LI Tumors. **(A)** UMAP displaying myeloid cell sub-clustering and DC annotations (See Fig. 2A and 6A). (**B**) Heatmap displaying normalized expression of select genes in each DC cluster. (**C-G)**
scRNAseq dot plot depicting expression level/percent of cells expressing select transcripts and bar graphs depicting frequency of DCs within each cluster by treatment condition.

Supplemental Figure 11. Heatmap displaying normalized expression of select genes in each monocyte/macrophage cluster by treatment condition.

Supplemental Figure 12. Principal Component Analysis of Subclustered T Cells/ILCs. Each dot represents individual sample from different treatment conditions (see Figure 2A and 2D).

Supplemental Figure 13. Gating Strategy for Identifying Intratumoral Immune Cells. Flow cytometry dot plots and gating of intratumoral myeloid and lymphoid populations.

Table S1:

REAGENT or RESOURCE	SOURCE	IDENTIFIER
***In vivo* Antibodies**		
Anti-CTLA-4 (clone 9D9)	Leinco	Cat# C2856, RRID: AB_2829611
Anti-CD279 (PD-1) (clone RMP1-14)	Leinco	Cat# RMP1-14, RRID: AB_2749820
Anti-mouse CD8 (clone YTS 169)	Leinco	Cat# C2442, RRID: AB_2829540
Anti-mouse CD4 (Clone GK1.5)	Leinco	Cat# C2838 RRID: AB_2829596
Mouse IgG2a Isotype.	Leinco	Cat# P381, RRID: AB_2831654
Flow Antibodies and reagents		
Anti-CD16/32 (clone 2.4G2)	BD Biosciences	Cat#553141, RRID: AB_394656
Anti-mouse CD45 BV605 (clone 30-F11) (1:800 dilution)	BioLegend	Cat#103140, RRID: AB_2562342
Anti-mouse CD90.2/Thy1.2-PE-Cy7 (clone 30-H12) (1:200 dilution)	BioLegend	Cat#105326, RRID: AB_2201290
Anti-mouse CD8a-BV786 (clone 53–6.7) (1:200 dilution)	BD Bioscience	Cat#563332, RRID: AB_2721167
Anti-mouse CD4-BV711(clone RM4–5) (1:200 dilution)	BioLegend	Cat#100550, RRID: AB_2562099
Anti-mouse CD19-BV650 (clone 1D3) (1:200 dilution)	BD Bioscience	Cat#563235, RRID: AB_2738085
Anti-mouse CD20-BV421 (clone SA275A11) (1:200 dilution)	BioLegend	Cat#150405, RRID: AB_2566540
Anti-mouse CD45R/B220-BUV395 (clone RA3-6B2) (1:200 dilution)	BD Bioscience	Cat# 563793, RRID: AB_2738427
Anti-mouse Nkp46/CD335-FITC (clone 29A1.4) (1:300 dilution)	BioLegend	Cat# 560756, RRID: AB_1727465
Anti-mouse γδ TCR-PE-Cy7 (clone GL3) (1:300 dilution)	BioLegend	Cat# 118124, RRID: AB_11204423
Anti-mouse PD-1-BV421 (clone 29F.1A12) (1:200 dilution)	BioLegend	Cat# 135218, RRID: AB_2561447
Anti-mouse TIM-3 (clone RMT3-23) (1:200 dilution)	BioLegend	Cat# 119727, RRID: AB_2716208
Anti-mouse LAG-3-PerCP-Cy5.5 (clone C9B7W) (1:200 dilution)	BioLegend	Cat# 125212, RRID: AB_2561517
Anti-mouse CD3e-APC (clone 145–2C11) (1:200 dilution),	BioLegend	Cat# 100312, RRID: AB_312677
Anti-mouse CD64-BV421 (clone X54–5/7.1) (1:200 dilution)	BioLegend	Cat# 139309, RRID: AB_2562694
Anti-mouse Ly6G-Alexa Fluor 700 (clone 1A8) (1:400 dilution)	BD Biosciences	Cat# 127622, RRID: AB_10643269
Anti-mouse CX3CR1-FITC (clone SA011F11) (1:1,000 dilution)	BioLegend	Cat# 149020, RRID: AB_2565703
Anti-mouse I-A/I-E-BV650 (clone M5/114.15.2) (1:3,000 dilution)	BD Bioscience	Cat# 563415, RRID: AB_2738192

Anti-mouse CD103-BV421 (clone 2E7) (1:200 dilution)	BioLegend	Cat# 121422, RRID: AB_2562901
Anti-mouse CD24-BV711 (clone M1/69) (1:500 dilution)	BD Bioscience	Cat# 563450, RRID: AB_2738213
Anti-mouse CD11c-BV786 (clone HL3) (1:400 dilution)	BD Biosciences	Cat# 563735, RRID: AB_2738394
Anti-mouse CD11b-APC (clone M1/70) (1:400 dilution)	BioLegend	Cat# 101212, RRID: AB_312795
Anti-mouse F4/80-BUV395 (clone T45–2342) (1:400 dilution)	BD Biosciences	Cat# 565614, RRID: AB_2739304
Anti-mouse CD64-APC (clone X54–5/7.1) (1:400 dilution)	BioLegend	Cat# 139306, RRID: AB_11219391
Anti-mouse CD117-FITC (clone ACK2) (1:100 dilution)	BioLegend	Cat# 135115, RRID: AB_2561633
Anti-mouse CD11b- PerCP-Cy5.5 (clone M1/70) (1:200 dilution)	BioLegend	Cat# 561114, RRID: AB_394002
Anti-mouse PDCA- 1/BST-2 BV650 (clone 927) (1:200 dilution)	BD Biosciences	Cat# 747605, RRID: AB_2744173
Anti-mouse CD172a APC (clone P84) (1:200 dilution)	BioLegend	Cat# 144014, RRID: AB_2564061
Anti-mouse CD274/PDL1-PE (clone MIH5) (1:200 dilution)	BD Biosciences	Cat# 558091, RRID: AB_397018
Anti-mouse FcεRI-PE-Cy7 (clone MAR-1) (1:200 dilution)	BioLegend	Cat# 134326, RRID: AB_2572064
Anti-mouse Mrc1 (CD206)-PE-Cy7 (clone C068C2) (1:400 dilution)	BioLegend	Cat# 141720, RRID: AB_2562248
Anti-mouse FOXP3-FITC (clone FJK-16s)	eBioscience™	Cat# 11-5773-82, RRID: AB_465243
Anti-mouse IFNγ-APC (Clone XMG1.2) (1:200 dilution)	BD Biosciences	Cat# 554413, RRID: AB_398551
Anti-mouse TNF -PE-Cy7 (Clone MP6-XT22) (1:200 dilution)	BD Biosciences	Cat# 561062, RRID: AB_398553
Anti-mouse Granzyme B-PE (Clone NGZB) (1:200 dilution)	eBioscience™	Cat# 12-8898-82, RRID: AB_10870787
Anti-mouse iNOS/Nos2 PE (clone CXNFT) (1:200 dilution)	eBioscience™	Cat# 12-5920-82, RRID: AB_2572642
Zombie Fixable Viability™ Sampler Kit	BioLegend	Cat# 423105
Chemicals, Peptides, and Gene blocks		
RPMI-1640	HyClone	Cat# SH30096.02
Trypsin	Genclone	Cat# 25200056
Defined fetal bovine serum	HyClone	Cat# SH30070.03HI
HBSS	Hyclone	Cat# SH30588.02
PBS	Gibco	Cat# 20012027
Sodium Bicarbonate	Gibco	Cat# 25080094

Sodium Pyruvate	Gibco	Cat# 11360070
L-Glutamine	Gibco	Cat# A2916801
ACK lysis buffer	Gibco	Cat# A1049201
Phorbol-12-myristate-13-acetate (PMA)	MilliporeSigma	Cat# 500582
Ionomycin	Fisher	Cat# BP2527-1
Fugene	Promega	Cat# E2311
pMSCV-IRES GFP	addgene	Cat# 20672
Collagenase Type IA	Sigma-Aldrich	Cat# C9891
Poly(I:C) HMW VacciGrade™	InvivoGen	Cat# vac-pic
Gibson Assembly® Cloning Kit	NEB	Cat# E5510S
Mutant Lama4 peptide, sequence VGFNFRTL	Peptide 2.0	Custom order
Mutant Alg8 peptide, sequence ITYTWTRL	Peptide 2.0	Custom order
Mutant Lama4 SLP, sequence QKISFFDGFEVGFNFRTLQPNGLLFYYT	Peptide 2.0	Custom order
Mutant Adpgk SLP, sequence HLELASMTNMELMSSIVHQ	Peptide 2.0	Custom order
Mutant Rpl18 SLP, sequence KAGGKILTFD***R***LALESPK	Peptide 2.0	Custom order
Mutant Dpagt1 SLP, sequence EAGQSLVISASIIVFNL***L***ELEGDYR	Peptide 2.0	Custom order
OVA-$I_{257–264}$ peptide, sequence SIINFEKL	Peptide 2.0	Custom order
Mutant Itgb1 SLP, sequence DDCWFYFTYSVNGY***N***EAIVHVVETPDCP	Peptide 2.0	Custom order
OVA-$II_{323–339}$, sequence ISQAVHAAHAEINEAGR	Peptide 2.0	Custom order
mAlg8-P2A-mItgb1 CTTCTCTAGGCGCCGGAATTCAGCCACCATGGCAGTG GGCATCACATACACCTGGACCAGGCTGTATGCTTCAGT GTTGACTGGCTCCCTTGTCGGCAGCGGCGCCACAAAC TTCTCTCTGCTAAAGCAAGCAGGTGATGTTGAAGAAAA CCCCGGGCCTGATGACTGCTGGTTCTATTTCACCTATTC AGTGAATGGCTACAATGAAGCTATCGTGCATGTTGTGG AGACTCCAGACTGTCCTTAATACGTAGCTAGCGGATCCCA	IDT	Custom order
mLama4-P2A-mItgb1 CTTCTCTAGGCGCCGGAATTCAGCCACCATGCAGAAAATA TCTTTCTTTGATGGCTTTGAAGTAGGCTTCAATTTCCGAAC ATTACAGCCAAATGGGTTACTATTCTACTACACAGGCAGCG GCGCCACAAACTTCTCTCTGCTAAAGCAAGCAGGTGATGT TGAAGAAAACCCCGGGCCTGATGACTGCTGGTTCTATTTCA CCTATTCAGTGAATGGCTACAATGAAGCTATCGTGCATGTTG	IDT	Custom order

TGGAGACTCCAGACTGTCCTTAATACGTAGCTAGCGGATCCCA		
Critical Commercial Assays		
Fixation/Permeabilization Solution Kit	BD Biosciences	Cat# 555028
Foxp3 / Transcription Factor Staining Buffer Set	eBioscience	Cat# 00-5523-00
Chromium Next GEM Single-cell 5 Reagent Kit v2	10x Genomics	Cat# 100263
TotalSeq Antibodies		
CD45 and H-2 MHC class Totalseq™-C0301 anti-mouse Hashtag 1, sequence	BioLegend	Cat# 155861, RRID: AB_2800693
CD45 and H-2 MHC class Totalseq™-C0302 anti-mouse Hashtag 2 Antibody	BioLegend	Cat# 155863, RRID: AB_2800694
CD45 and H-2 MHC class Totalseq™-C0303 anti-mouse Hashtag 3 Antibody	BioLegend	Cat# 155865, RRID: AB_2800695
Software and algorithms		
Flow jo_v10.8.1		
GraphPad Prism version 10		
Other		
Fortessa X-20	BD Biosciences	
LSR Fortessa	BD Biosciences	
BD FACSAria II	BD Biosciences	

Figure 1

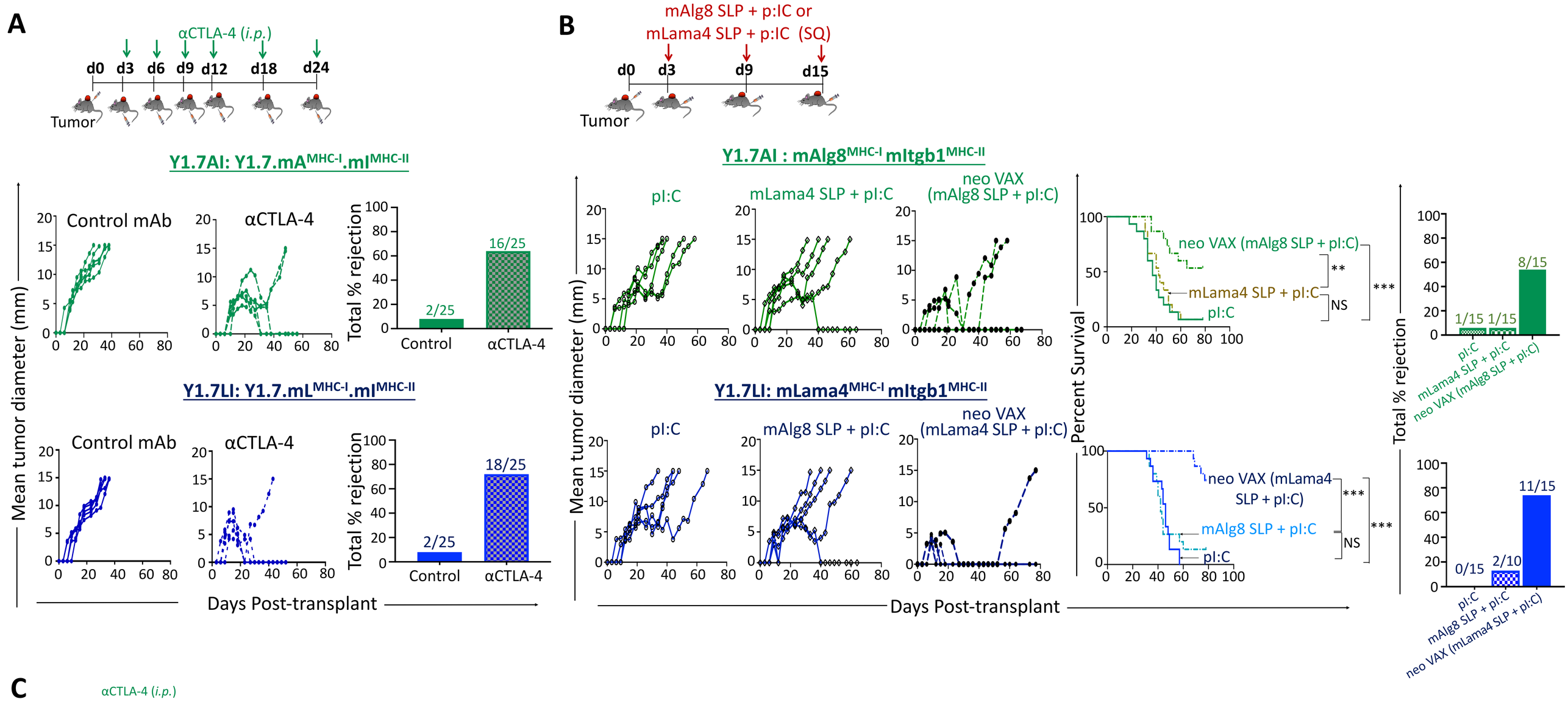
A
αCTLA-4 (i.p.)
d0 d3 d6 d9 d12 d18 d24
Tumor
Y1.7AI: Y1.7.mA^MHC-I.mI^MHC-II
Control mAb
αCTLA-4
Total % rejection
2/25
16/25
Control
αCTLA-4
Y1.7LI: Y1.7.mL^MHC-I.mI^MHC-II
Control mAb
αCTLA-4
Total % rejection
2/25
18/25
Control
αCTLA-4
Mean tumor diameter (mm)
Days Post-transplant
B
mAlg8 SLP + p:IC or
mLama4 SLP + p:IC (SQ)
d0 d3 d9 d15
Tumor
Y1.7AI : mAlg8^MHC-I mItgb1^MHC-II
pI:C
mLama4 SLP + pI:C
neo VAX
(mAlg8 SLP + pI:C)
Percent Survival
neo VAX (mAlg8 SLP + pI:C)
mLama4 SLP + pI:C
pI:C
**
NS
***
Total % rejection
1/15 1/15 8/15
pI:C
mLama4 SLP + pI:C
neo VAX (mAlg8 SLP + pI:C)
Y1.7LI: mLama4^MHC-I mItgb1^MHC-II
pI:C
mAlg8 SLP + pI:C
neo VAX
(mLama4 SLP + pI:C)
neo VAX (mLama4
SLP + pI:C)
mAlg8 SLP + pI:C
pI:C
***
NS
***
0/15 2/10 11/15
pI:C
mAlg8 SLP + pI:C
neo VAX (mLama4 SLP + pI:C)
Mean tumor diameter (mm)
Days Post-transplant

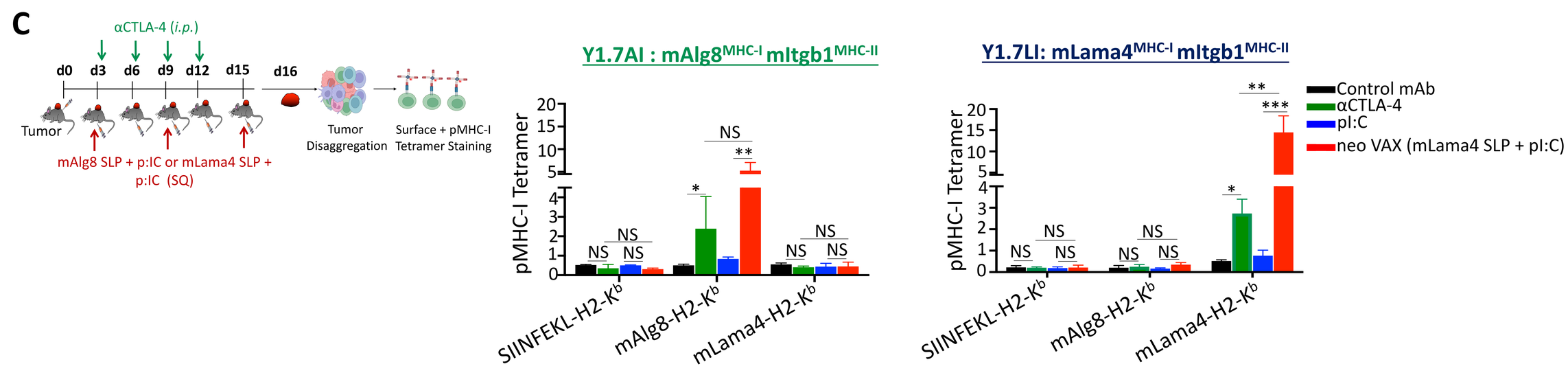
C
αCTLA-4 (i.p.)
d0 d3 d6 d9 d12 d15 d16
Tumor
mAlg8 SLP + p:IC or mLama4 SLP +
p:IC (SQ)
Tumor
Disaggregation
Surface + pMHC-I
Tetramer Staining
Y1.7AI : mAlg8^MHC-I mItgb1^MHC-II
Y1.7LI: mLama4^MHC-I mItgb1^MHC-II
pMHC-I Tetramer
NS
*
**
***
SIINFEKL-H2-K^b
mAlg8-H2-K^b
mLama4-H2-K^b
Control mAb
αCTLA-4
pI:C
neo VAX (mLama4 SLP + pI:C)

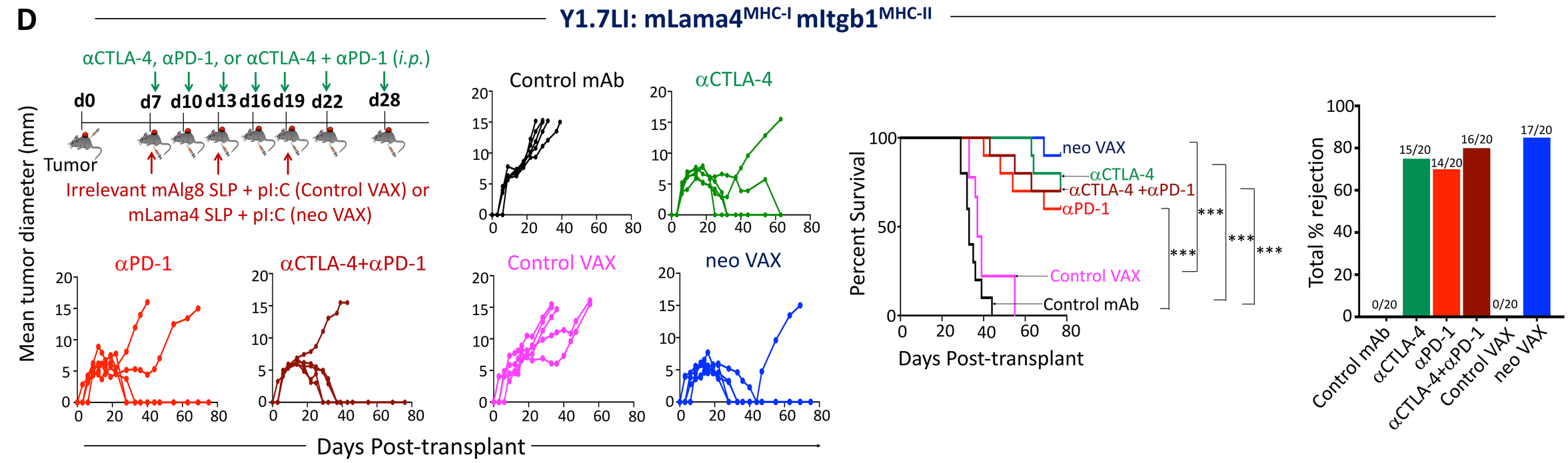
D
Y1.7LI: mLama4^MHC-I mItgb1^MHC-II
αCTLA-4, αPD-1, or αCTLA-4 + αPD-1 (i.p.)
d0 d7 d10 d13 d16 d19 d22 d28
Tumor
Irrelevant mAlg8 SLP + pI:C (Control VAX) or
mLama4 SLP + pI:C (neo VAX)
Control mAb
αCTLA-4
αPD-1
αCTLA-4+αPD-1
Control VAX
neo VAX
Mean tumor diameter (mm)
Days Post-transplant
Percent Survival
neo VAX
αCTLA-4
αCTLA-4 +αPD-1
αPD-1
Control VAX
Control mAb
***
Total % rejection
0/20 15/20 14/20 16/20 0/20 17/20
Control mAb
αCTLA-4
αPD-1
αCTLA-4+αPD-1
Control VAX
neo VAX

Figure 2

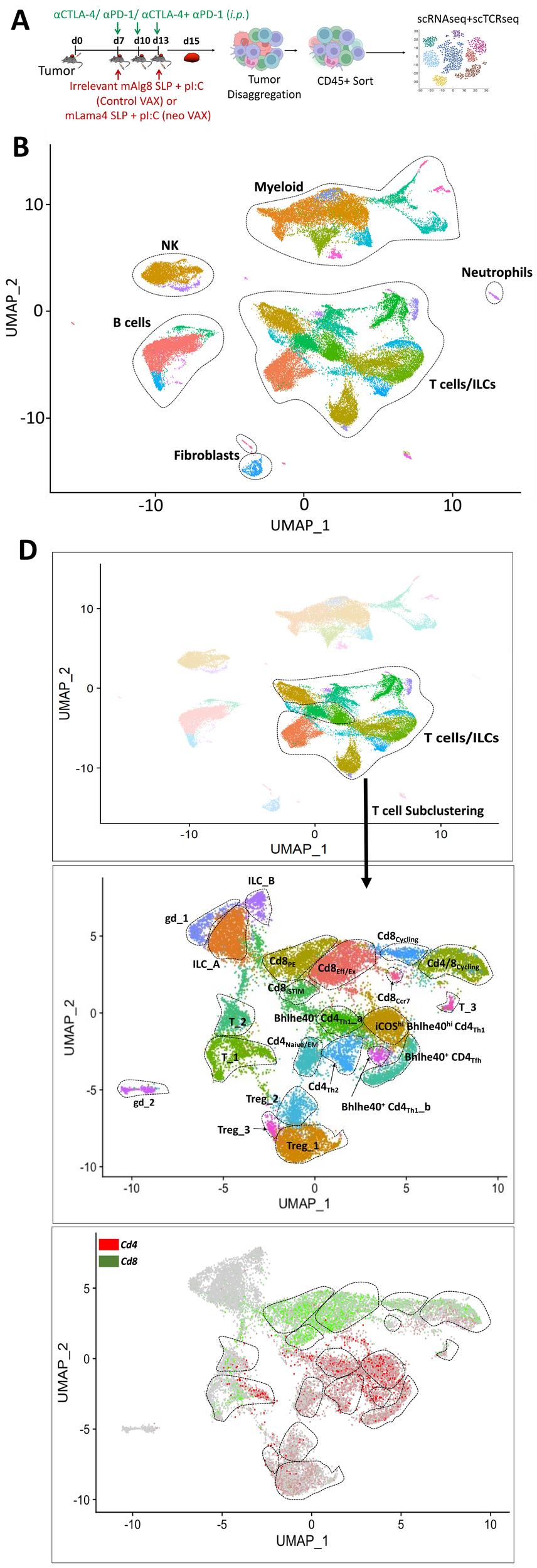

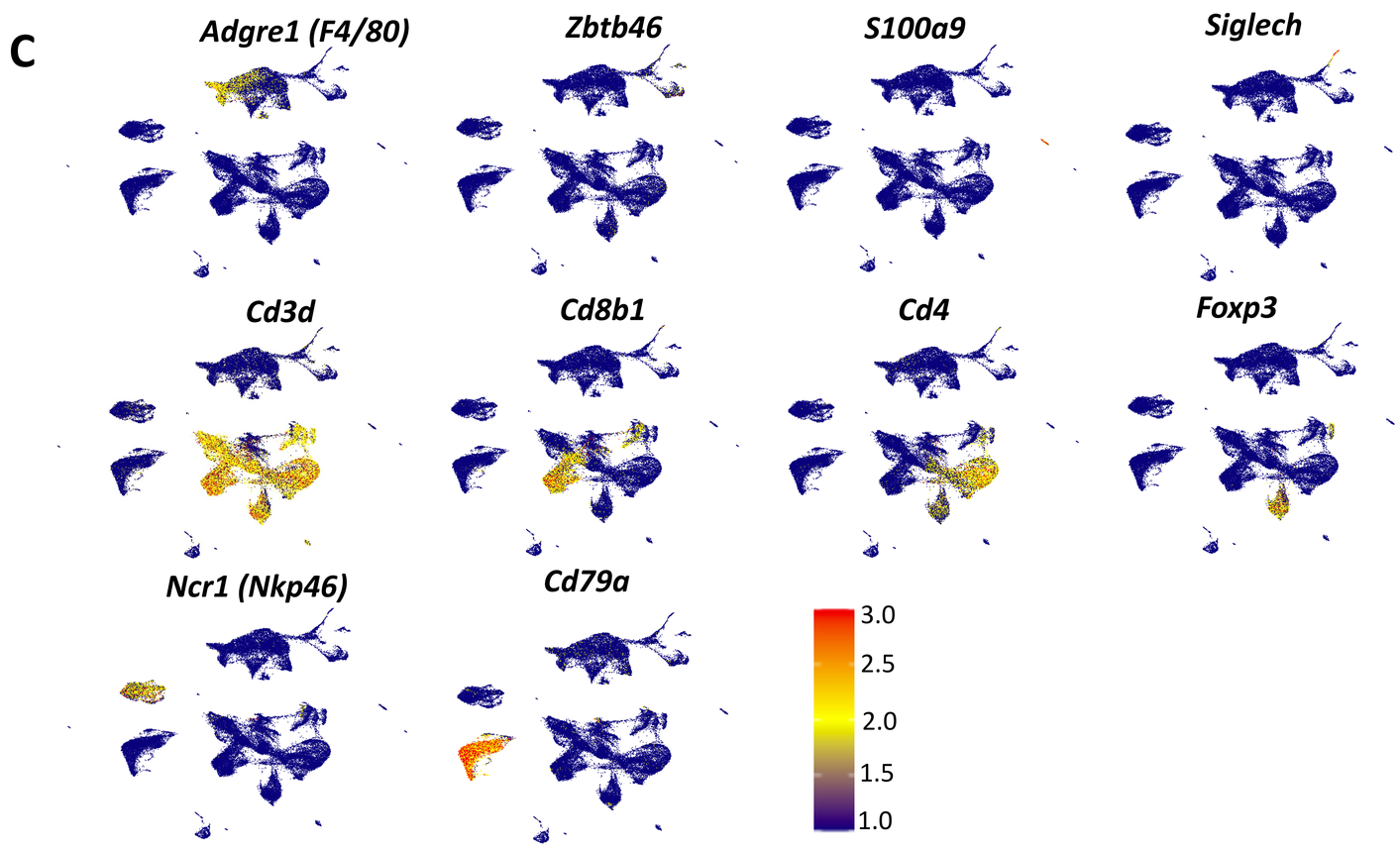

E

Cluster	Identifying Genes
$Cd4/8_{Cycling}$	**High:** *Mki67* **Low:** *Lag3, Pdcd1 (Pd-1), Havcr2 (Tim-3)*
$Cd8_{Cycling}$	**High:** *Mki67, Pdcd1, Havcr2, Prf1 (perforin), Eomes* **Low**: *Lag3, Tcf7, Tox*
$Cd8_{Eff/Ex}$	**High:** *Ifng, Tox, Lag3, Pdcd1, Havcr2, Nkg7, Gzmb, Gzmk, Prf1, Ccl5, Tbx21 (Tbet), Eomes, Bhlhe40*
$Cd8_{PE}$	**High**: *Ifng, Tox, Tcf7, Nkg7, Gzmk, Prf1, S1pr1, Il7r, Tbx21, Cxcr3, Ccl5, Eomes* **Low**: *Pdcd1, Lag3, Bhlhe40*
$Cd8_{iSTIM}$	**High:** *Ifng, Cd69, Stat1, Tcf7,* **Low:** *Lag3, Prf1, Sell (Cd62l), S1pr1*
$Cd8_{Ccr7}$	**High:** *Havcr2, Lag3, Gzmb, Prf1, Ccl3, Ccr7* **Low:** *Pdcd1*
$iCOS^{hi}$ $Bhlhe40^{hi}$ $Cd4_{Th1}$	**High:** *Ifng, Csf2, Icos, Bhlhe40, Pdcd1, Lag3, Havcr2, Tbx21*
$Bhlhe40^{+}$ $Cd4_{Th1}$_a	**High:** *Ifng, Bhlhe40, Tbx21* **Low:** *Icos, Pdcd1, Lag3*
$Bhlhe40^{+}$ $Cd4_{Th1}$_b	**High:** *Bhlhe40, Tbet, Tox, Lag3, Pdcd1, Havcr2*
$Bhlhe40^{+}$ $CD4_{Tfh}$	**High:** *Bhlhe40, Csf2, Cxcr5* **Low:** *Ifng, Tcf7, Tox, Nfkb1, Pdcd1, Lag3*
$Cd4_{Naive/Mem}$	**High:** *Tcf7, Il7r, S1pr1*
$Cd4_{Th2}$	**High:** *Il13, Il4, Il5, Gata3, Nfkb1, Bhlhe40, Icos*

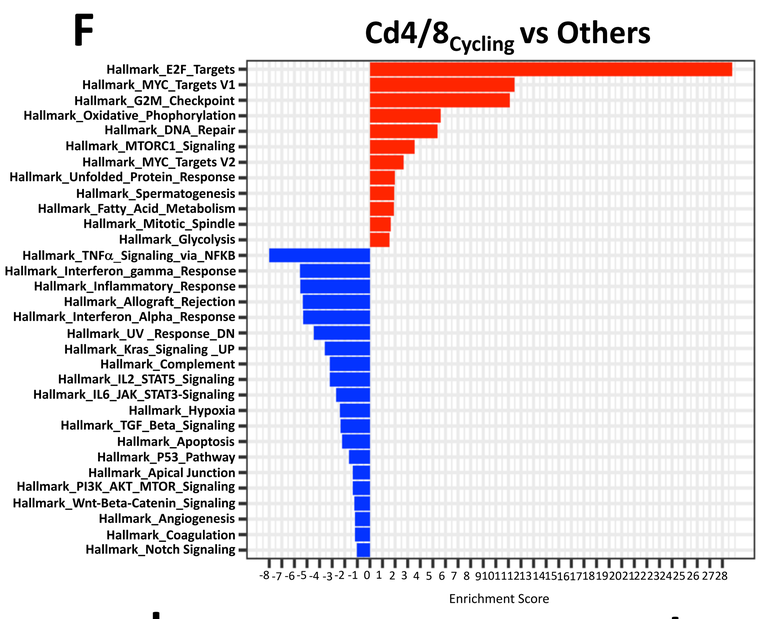

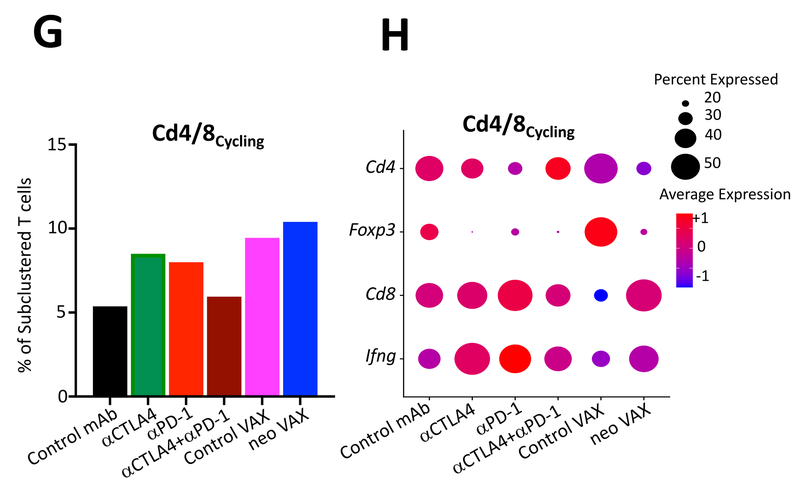

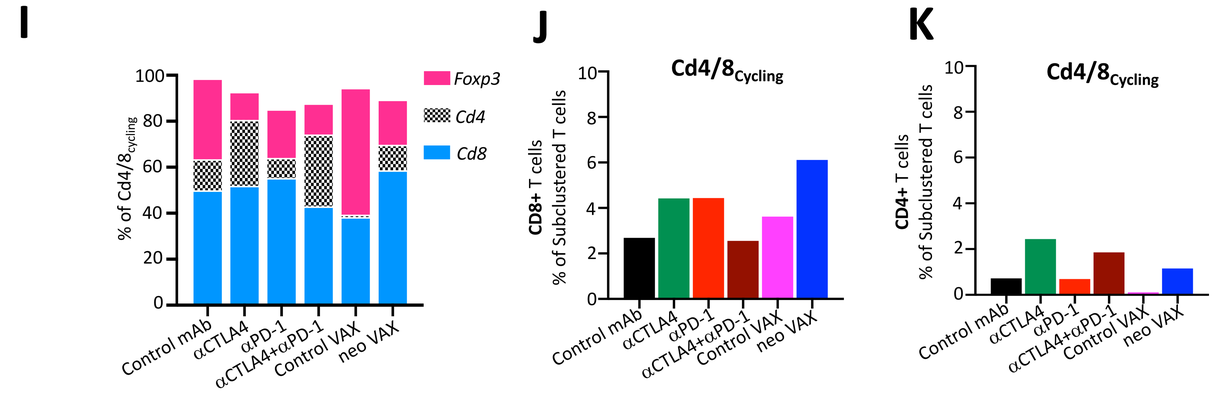

Figure 3

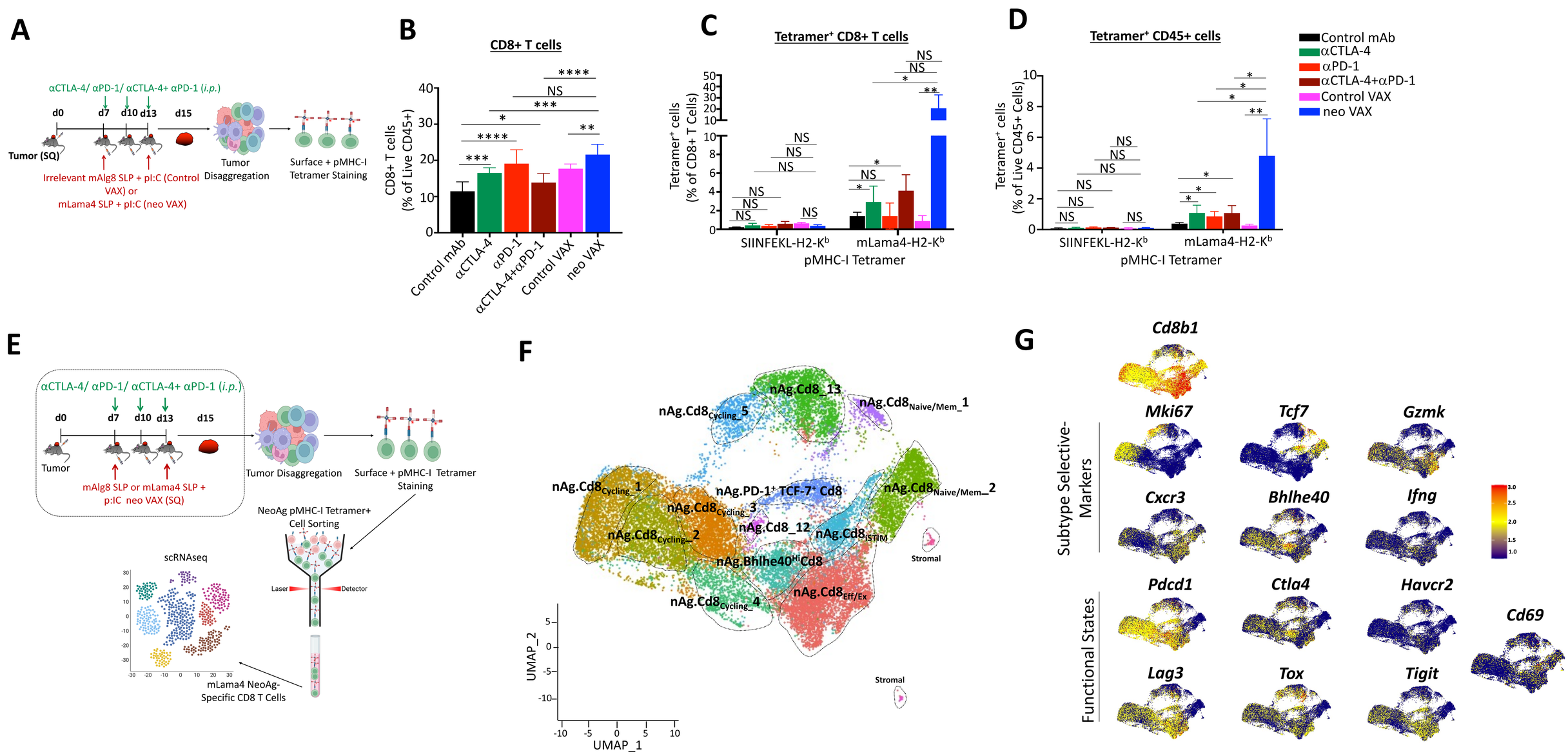

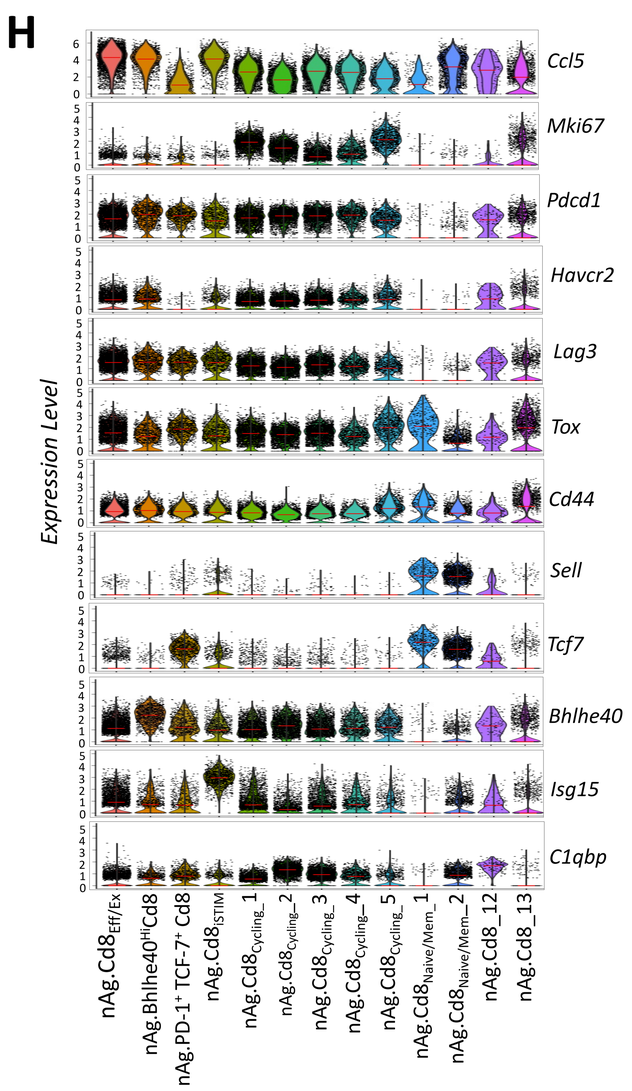

I

Cluster	Identifying Genes
nAg.Cd8$_{Eff/Ex}$	**High:** *Ifng, Tox, Lag3, Pdcd1 (Pd1), Havcr2 (Tim-3), Tigit, Entpd1 (Cd39), Klrd1, Cd160, Cd226, Nkg7, Gzmb, Gzmk, Prf1, Fasl, Cxcr3, Cxcr6, Ccl5*
nAg.Bhlhe40^{Hi}Cd8	**High:** *Bhlhe40, Hopx, Tnfaip3, Ifng, Lag3, Pdcd1, Havcr2, Klrd1, Cd160, Cd69, Gzmb, Prf1, Ccl5, Tbx21 (Tbet)*
nAg.PD-1^{+} TCF-7^{+} Cd8	**High:** *Tcf7, Slamf6, Tox, Lag3, Pdcd1, Tigit, Cxcr3* **Low:** *Ifng, Cd226, Gzmk, Prf1*
nAg.Cd8$_{iSTIM}$	**High:** *Ifng, Lag3, Pdcd1, Cd69, Gzmb, Cxcr3, Ccl5* **Low:** *Havcr2*
nAg.Cd8$_{Cycling_}$1	**High:** *Mki67, Ifng, Tox, Lag3, Pdcd1, Havcr2, Klrd1, Cd226, Gzmb, Gzmk, Prf1, Cxcr3* **Low:** *Tcf7, Slamf6*
nAg.Cd8$_{Cycling_}$2	**High:** *Mki67, Ifng, Lag3, Pdcd1, Havcr2, Tigit, Tnfrsf4 (OX40), Tnfrsf9 (41BB), Gzmb, Gzmk, Prf1* **Low:** *Tcf7, Slamf6*
nAg.Cd8$_{Cycling_}$3	**High:** *Mki67, Ifng, Tox, Lag3, Pdcd1, Havcr2, Gzmk, Prf1* **Low:** *Tcf7, Slamf6*
nAg.Cd8$_{Cycling_}$4	**High:** *Mki67, Ifng, Tox, Lag3, Pdcd1, Havcr2, Klrd1, Tnfrsf9, Gzmb, Gzmk, Prf1, Cxcr3, Ccl5* **Low:** *Tcf7, Slamf6*
nAg.Cd8$_{Cycling_}$5	**High:** *Mki67, Tox, Pdcd1, Havcr2, Prf1, Cxcr3* **Low:** *Lag3, Tcf7*
nAg.Cd8$_{Naive/Mem_}$1	**High:** *Tcf7, Tox, Il7r, Slamf6, Lef1, Ccr7, Klf2, Cd62l, Runx3*
nAg.Cd8$_{Naive/Mem_}$2	**High:** *Tcf7, Cd69, Il7r, Slamf6, Lef1, Ccr7, Klf2, Sell (Cd62l)*
nAg.Cd8_12	**High:** *Ifng, Tox, Lag3, Pdcd1, Tigit, Cd160, Nkg7, Tnfrsf4, Tnfrsf9, Tnfrsf18 (GITR), Gzmb, Ccl1, Ccl3* **Low:** *Tcf7, Slamf6*
nAg.Cd8_13	**High:** *Tox, Tigit, Cd39, Cd226, Runx3, Tbx21* **Low:** *Mki67, Lag3, Pdcd1, Havcr2*

Figure 4

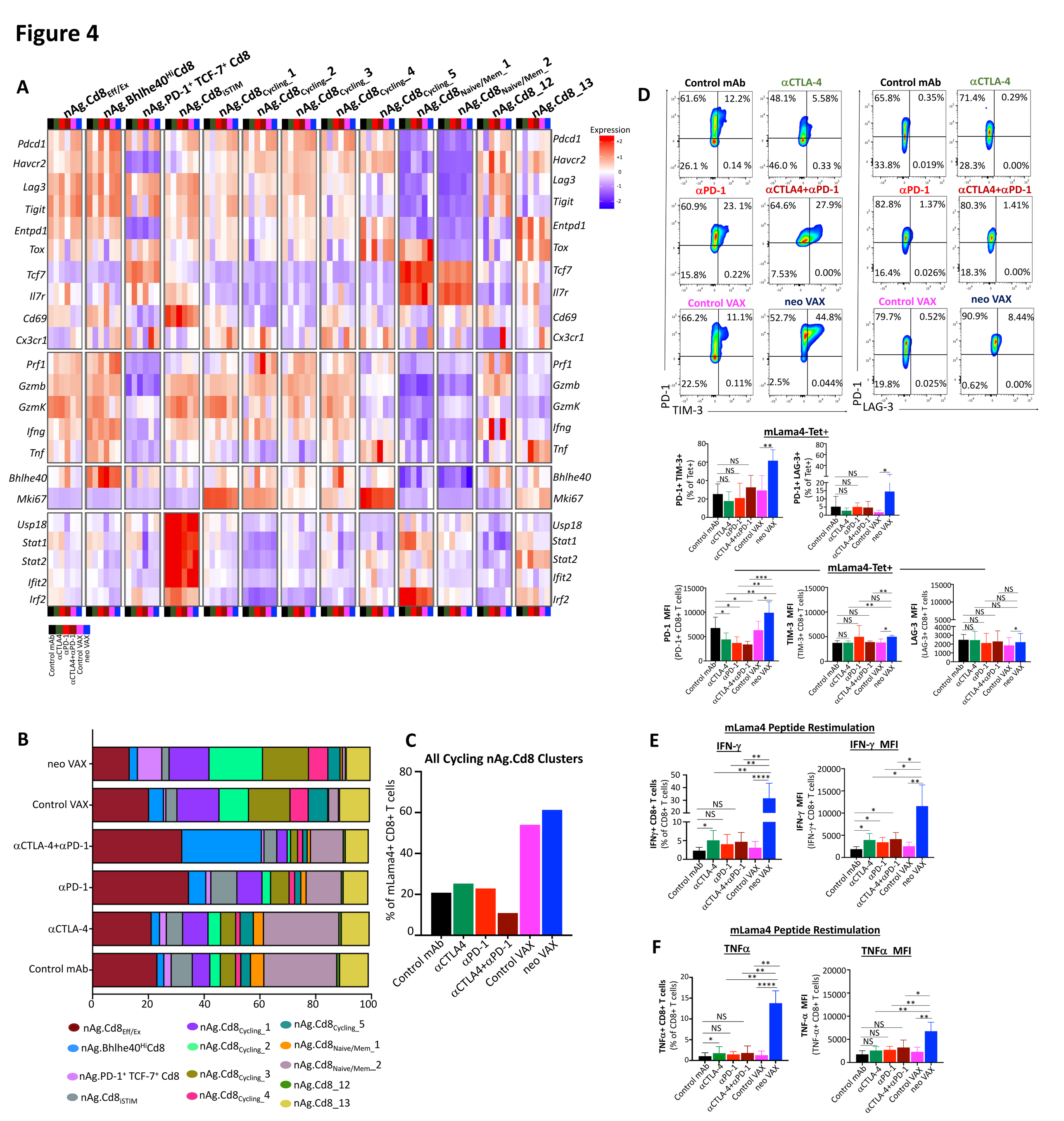
A
nAg.Cd8Eff/Ex
nAg.Bhlhe40HiCd8
nAg.PD-1+ TCF-7+ Cd8
nAg.Cd8iSTIM
nAg.Cd8Cycling_1
nAg.Cd8Cycling_2
nAg.Cd8Cycling_3
nAg.Cd8Cycling_4
nAg.Cd8Cycling_5
nAg.Cd8Naive/Mem_1
nAg.Cd8Naive/Mem_2
nAg.Cd8_12
nAg.Cd8_13
Pdcd1
Havcr2
Lag3
Tigit
Entpd1
Tox
Tcf7
Il7r
Cd69
Cx3cr1
Prf1
Gzmb
GzmK
Ifng
Tnf
Bhlhe40
Mki67
Usp18
Stat1
Stat2
Ifit2
Irf2
Expression
Control mAb
αCTLA4
αPD-1
αCTLA4+αPD-1
Control VAX
neo VAX
B
neo VAX
Control VAX
αCTLA-4+αPD-1
αPD-1
αCTLA-4
Control mAb
nAg.Cd8Eff/Ex
nAg.Bhlhe40HiCd8
nAg.PD-1+ TCF-7+ Cd8
nAg.Cd8iSTIM
nAg.Cd8Cycling_1
nAg.Cd8Cycling_2
nAg.Cd8Cycling_3
nAg.Cd8Cycling_4
nAg.Cd8Cycling_5
nAg.Cd8Naive/Mem_1
nAg.Cd8Naive/Mem_2
nAg.Cd8_12
nAg.Cd8_13
C
All Cycling nAg.Cd8 Clusters
% of mLama4+ CD8+ T cells
D
Control mAb
αCTLA-4
αPD-1
αCTLA4+αPD-1
Control VAX
neo VAX
PD-1
TIM-3
LAG-3
mLama4-Tet+
PD-1+ TIM-3+ (% of Tet+)
PD-1+ LAG-3+ (% of Tet+)
PD-1 MFI (PD-1+ CD8+ T cells)
TIM-3 MFI (TIM-3+ CD8+ T cells)
LAG-3 MFI (LAG-3+ CD8+ T cells)
E
mLama4 Peptide Restimulation
IFN-γ
IFN-γ MFI
IFNγ+ CD8+ T cells (% of CD8+ T cells)
IFN-γ MFI (IFN-γ+ CD8+ T cells)
F
TNFα
TNFα MFI
TNFα+ CD8+ T cells (% of CD8+ T cells)
TNF-α MFI (TNF-α+ CD8+ T cells)

Figure 5

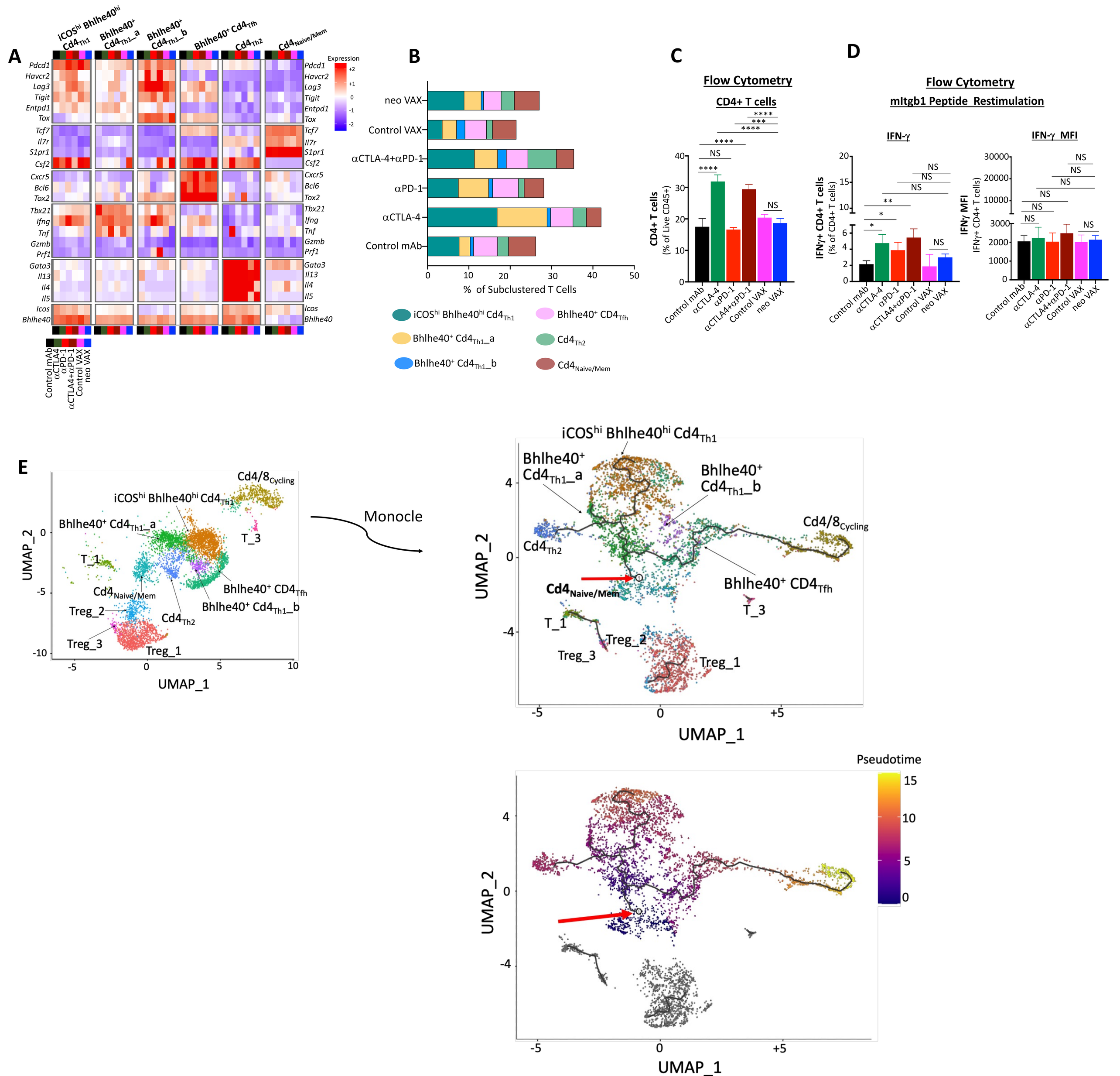
A
iCOS^hi Bhlhe40^hi Cd4_Th1
Bhlhe40^+ Cd4_Th1_a
Bhlhe40^+ Cd4_Th1_b
Bhlhe40^+ Cd4_Tfh
Cd4_Th2
Cd4_Naive/Mem
Expression
Pdcd1
Havcr2
Lag3
Tigit
Entpd1
Tox
Tcf7
Il7r
S1pr1
Csf2
Cxcr5
Bcl6
Tox2
Tbx21
Ifng
Tnf
Gzmb
Prf1
Gata3
Il13
Il4
Il5
Icos
Bhlhe40
Control mAb
αCTLA-4
αPD-1
αCTLA4+αPD-1
Control VAX
neo VAX
B
neo VAX
Control VAX
αCTLA-4+αPD-1
αPD-1
αCTLA-4
Control mAb
% of Subclustered T Cells
iCOS^hi Bhlhe40^hi Cd4_Th1
Bhlhe40^+ Cd4_Tfh
Bhlhe40^+ Cd4_Th1_a
Cd4_Th2
Bhlhe40^+ Cd4_Th1_b
Cd4_Naive/Mem
C
Flow Cytometry
CD4+ T cells
CD4+ T cells
(% of Live CD45+)
D
Flow Cytometry
mItgb1 Peptide Restimulation
IFN-γ
IFNγ+ CD4+ T cells
(% of CD4+ T cells)
IFN-γ MFI
IFNγ MFI
IFNγ+ CD4+ T cells)
NS
E
Cd4/8_Cycling
iCOS^hi Bhlhe40^hi Cd4_Th1
Bhlhe40^+ Cd4_Th1_a
T_3
T_1
Cd4_Naive/Mem
Bhlhe40^+ CD4_Tfh
Bhlhe40^+ Cd4_Th1_b
Treg_2
Cd4_Th2
Treg_3
Treg_1
UMAP_1
UMAP_2
Monocle
Pseudotime

Figure 6

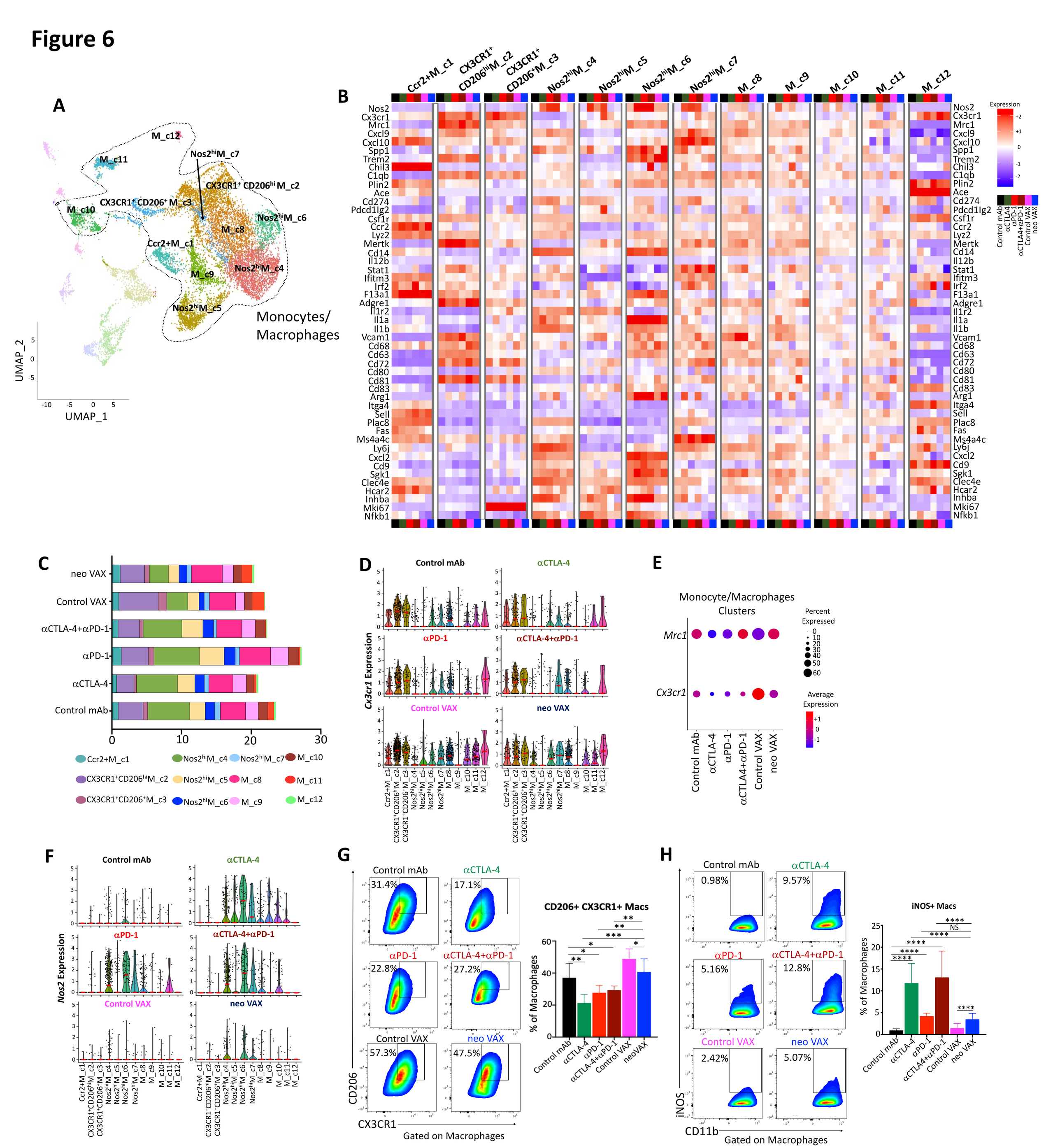
A
M_c12
M_c11
Nos2hiM_c7
CX3CR1+ CD206hi M_c2
CX3CR1+ CD206+ M_c3
M_c10
Nos2hiM_c6
M_c8
Ccr2+M_c1
Nos2hiM_c4
M_c9
Nos2hiM_c5
Monocytes/
Macrophages
UMAP_2
UMAP_1
B
Ccr2+M_c1
CX3CR1+ CD206hiM_c2
CX3CR1+ CD206+M_c3
Nos2hiM_c4
Nos2hiM_c5
Nos2hiM_c6
Nos2hiM_c7
M_c8
M_c9
M_c10
M_c11
M_c12
Nos2
Cx3cr1
Mrc1
Cxcl9
Cxcl10
Spp1
Trem2
Chil3
C1qb
Plin2
Ace
Cd274
Pdcd1lg2
Csf1r
Ccr2
Lyz2
Mertk
Cd14
Il12b
Stat1
Ifitm3
Irf2
F13a1
Adgre1
Il1r2
Il1a
Il1b
Vcam1
Cd68
Cd63
Cd72
Cd80
Cd81
Cd83
Arg1
Itga4
Sell
Plac8
Fas
Ms4a4c
Ly6j
Cxcl2
Cd9
Sgk1
Clec4e
Hcar2
Inhba
Mki67
Nfkb1
Expression
Control mAb
αCTLA4
αPD-1
αCTLA4+αPD-1
Control VAX
neo VAX
C
neo VAX
Control VAX
αCTLA-4+αPD-1
αPD-1
αCTLA-4
Control mAb
Ccr2+M_c1
Nos2hiM_c4
Nos2hiM_c7
M_c10
CX3CR1+CD206hiM_c2
Nos2hiM_c5
M_c8
M_c11
CX3CR1+CD206+M_c3
Nos2hiM_c6
M_c9
M_c12
D
Control mAb
αCTLA-4
αPD-1
αCTLA-4+αPD-1
Control VAX
neo VAX
Cx3cr1 Expression
E
Monocyte/Macrophages
Clusters
Mrc1
Cx3cr1
Control mAb
αCTLA-4
αPD-1
αCTLA4+αPD-1
Control VAX
neo VAX
Percent
Expressed
Average
Expression
F
Control mAb
αCTLA-4
αPD-1
αCTLA-4+αPD-1
Control VAX
neo VAX
Nos2 Expression
G
Control mAb
31.4%
αCTLA-4
17.1%
αPD-1
22.8%
αCTLA-4+αPD-1
27.2%
Control VAX
57.3%
neo VAX
47.5%
CD206
CX3CR1
Gated on Macrophages
CD206+ CX3CR1+ Macs
% of Macrophages
H
Control mAb
0.98%
αCTLA-4
9.57%
αPD-1
5.16%
αCTLA-4+αPD-1
12.8%
Control VAX
2.42%
neo VAX
5.07%
iNOS
CD11b
Gated on Macrophages
iNOS+ Macs
% of Macrophages

Figure 7

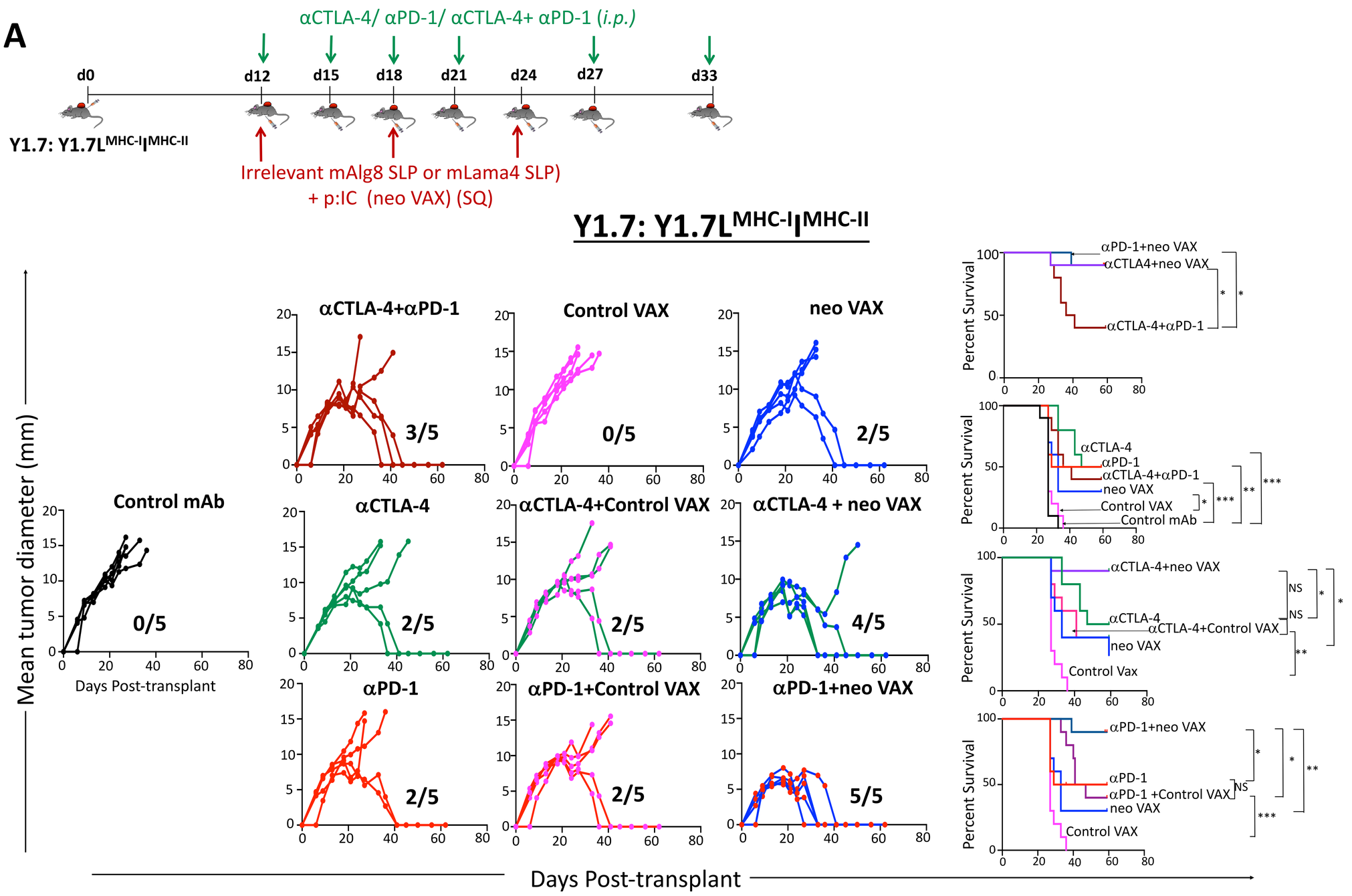
A
αCTLA-4/ αPD-1/ αCTLA-4+ αPD-1 (i.p.)
d0
d12
d15
d18
d21
d24
d27
d33
Y1.7: Y1.7L MHC-I MHC-II
Irrelevant mAlg8 SLP or mLama4 SLP)
+ p:IC (neo VAX) (SQ)
Y1.7: Y1.7L MHC-I MHC-II
Mean tumor diameter (mm)
Control mAb
0/5
αCTLA-4+αPD-1
3/5
Control VAX
0/5
neo VAX
2/5
αCTLA-4
2/5
αCTLA-4+Control VAX
2/5
αCTLA-4 + neo VAX
4/5
αPD-1
2/5
αPD-1+Control VAX
2/5
αPD-1+neo VAX
5/5
Days Post-transplant
Percent Survival
αPD-1+neo VAX
αCTLA4+neo VAX
αCTLA-4+αPD-1
αCTLA-4
αPD-1
αCTLA-4+αPD-1
neo VAX
Control VAX
Control mAb
αCTLA-4+neo VAX
αCTLA-4
αCTLA-4+Control VAX
neo VAX
Control Vax
αPD-1+neo VAX
αPD-1
αPD-1 +Control VAX
neo VAX
Control VAX
Days Post-transplant

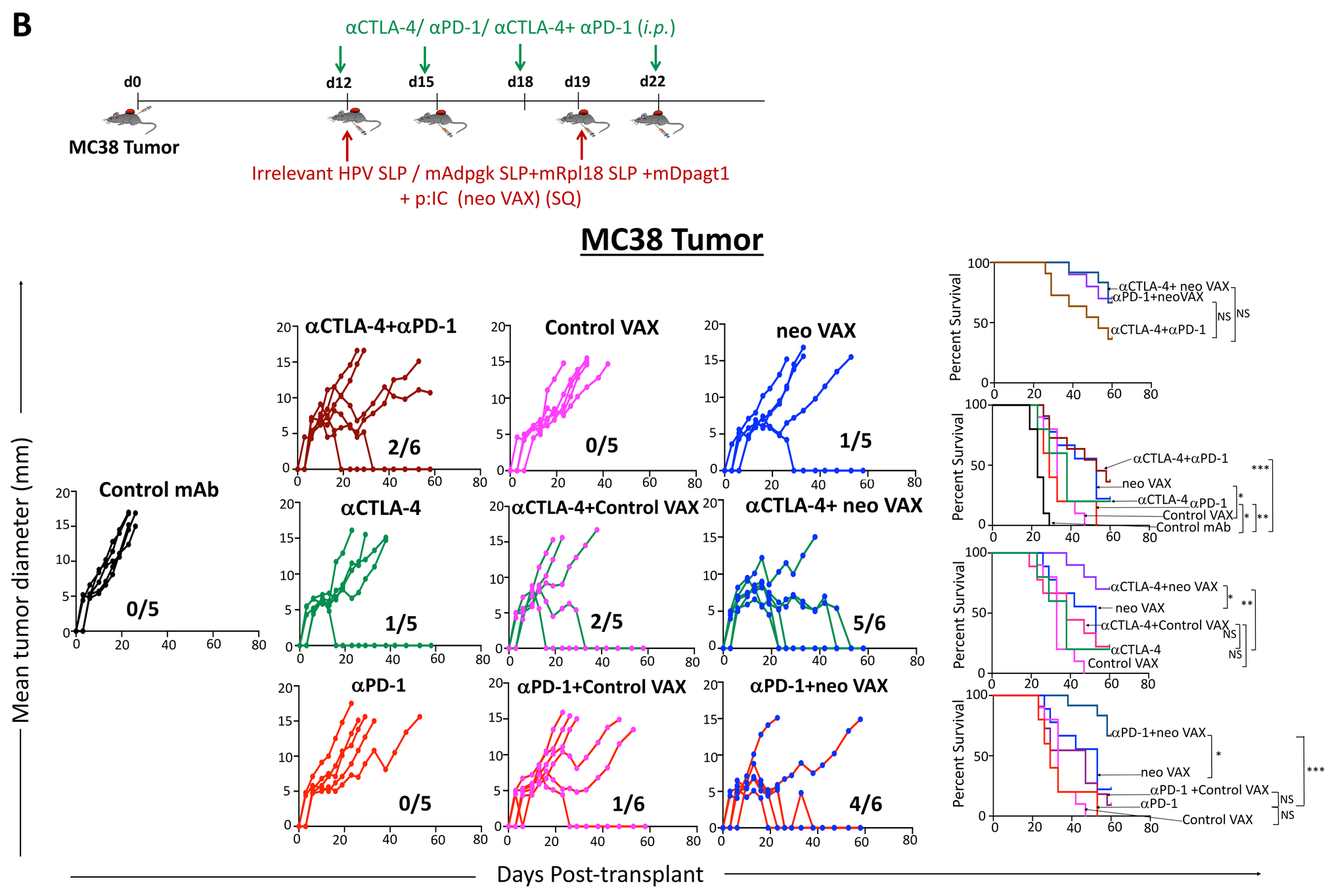
B
αCTLA-4/ αPD-1/ αCTLA-4+ αPD-1 (i.p.)
d0
d12
d15
d18
d19
d22
MC38 Tumor
Irrelevant HPV SLP / mAdpgk SLP+mRpl18 SLP +mDpagt1
+ p:IC (neo VAX) (SQ)
MC38 Tumor
Mean tumor diameter (mm)
Control mAb
0/5
αCTLA-4+αPD-1
2/6
Control VAX
0/5
neo VAX
1/5
αCTLA-4
1/5
αCTLA-4+Control VAX
2/5
αCTLA-4+ neo VAX
5/6
αPD-1
0/5
αPD-1+Control VAX
1/6
αPD-1+neo VAX
4/6
Days Post-transplant
Percent Survival
αCTLA-4+ neo VAX
αPD-1+neoVAX
αCTLA-4+αPD-1
αCTLA-4+αPD-1
neo VAX
αCTLA-4
αPD-1
Control VAX
Control mAb
αCTLA-4+neo VAX
neo VAX
αCTLA-4+Control VAX
αCTLA-4
Control VAX
αPD-1+neo VAX
neo VAX
αPD-1 +Control VAX
αPD-1
Control VAX